DISSERTATION

The fate of fucoidan in the ocean

zur Erlangung des Doktorgrades der Naturwissenschaften
-Dr. rer. Nat-
im Fachbereich Biologie/Chemie der Universität Bremen

Vorgelegt von
Inga Hellige

Bremen, Dezember 2024

The present work was done between November 2021 and December 2024 in the working group Carbon Sequestration and Glycobiochemistry at University of Bremen, MARUM Centre for Marine Environmental Sciences and Max Planck Institute for Marine Microbiology in Bremen, Germany. It was funded by sea4soCiety, CDRmare campaign in the German Marine Research Alliance.

SCIENTIFIC SUPERVISOR
Prof. Dr. Jan-Hendrik Hehemann

DISSERTATION REVIEWERS
Prof. Dr. Jan-Hendrik Hehemann
Prof. Dr. Thorsten Dittmar

EXAMINATION COMMITTEE
Prof. Dr. Kai Bischof (head)
Prof. Dr. Jan-Hendrik Hehemann
Prof. Dr. Kai-Uwe Hinrichs
Dr. Greta Reintjes
Linda Biehler
Nahja Busse

Date of colloquium: 19 February 2025

Contents

Abstract

Rising carbon dioxide levels and the need to achieve the goals of the Paris Agreement have led to a focus on solutions to actively remove atmospheric CO_2. Nature-based solutions, particularly blue carbon ecosystems such as mangroves, salt marshes, seagrass meadows and macroalgae, are of growing interest due to their ability to store large amounts of carbon in their biomass. Additionally, mangroves, salt marshes and seagrass exude organic carbon through their roots. In contrast, macroalgae do not have a root system, but exude dissolved organic carbon as a mucilage layer. Up to 50% of the dissolved organic carbon secreted by brown algae is fucoidan, an extracellular matrix polysaccharide. The exuded carbon is dispersed and thus challenging to trace in the environment. This results in macroalgae often being excluded from carbon budgets.

This thesis investigates the secretion rates and the fate of fucoidan in the ocean. The active release of fucoidan was confirmed in six tested brown algae species worldwide with rates ranging from 0.32 to 0.88 mg g^{-1} dry weight day^{-1}. Fucoidan was found to be resistant to immediate microbial hydrolysis. Its persistence in mesocosms and the increase of fucoidan in the particulate phase indicate aggregation and sedimentation.

Globally, brown algae release approximately 0.1 Gt of fucoidan carbon annually, equivalent to 0.367 Gt of CO_2, parts transported and stored in coastal vegetative ecosystems each year.

Fucoidan may be used as an indicator to trace algal-derived carbon from source to sink. This thesis emphasises that algal-derived polysaccharides such as fucoidan are promising candidates for carbon sequestration that is collectively stored in coastal vegetative ecosystems.

Zusammenfassung

Steigende Kohlendioxidwerte und die Notwendigkeit, die Ziele des Pariser Abkommens zu erreichen, haben dazu geführt, dass man sich auf Lösungen zur aktiven Entfernung von atmosphärischem CO_2 konzentriert. Naturbasierte Ansätze, insbesondere Blue-Carbon-Ökosysteme wie Mangroven, Salzwiesen, Seegraswiesen und Makroalgen, sind aufgrund ihrer Fähigkeit, große Mengen an Kohlenstoff in ihrer Biomasse zu speichern, von wachsendem Interesse. Außerdem geben Mangroven, Salzwiesen und Seegras organischen Kohlenstoff über ihre Wurzeln ab. Im Gegensatz dazu haben Makroalgen kein Wurzelsystem, sondern geben gelösten organischen Kohlenstoff in Form einer Schleimschicht ab. Braunalgen sekretieren bis zu 50% des ausgeschiedenen gelösten organischen Kohlenstoffs als extrazelluläres Matrixpolysaccharid Fucoidan. Der ausgeschiedene Kohlenstoff verteilt sich und ist daher in der Umwelt schwer nachzuweisen. Dies führt dazu, dass Makroalgen häufig aus den Kohlenstoffbudgets ausgeschlossen werden.

In dieser Thesis werden die Sekretionsraten und der Verbleib von Fucoidan im Meer untersucht. Die aktive Sekretion von Fucoidan wurde bei sechs getesteten Braunalgenarten mit Raten zwischen 0.32 und 0.88 mg g^{-1} Trockengewicht Tag^{-1} bestätigt. Fucoidan erwies sich als resistent gegen sofortige mikrobielle Hydrolyse. Seine Persistenz in Mesokosmen und die Zunahme von Fucoidan in der partikulären Phase deuten auf Aggregation

und Sedimentation hin.
Weltweit setzen Braunalgen jährlich etwa 0.1 Gt Fucoidan-Kohlenstoff frei, das entspricht 0.367 Gt CO_2, wobei Teile in vegetativen Ökosystemen in Küstengewässern transportiert und gespeichert werden könnten. Fucoidan kann als Indikator verwendet werden, um den aus Algen gewonnenen Kohlenstoff von der Quelle bis zur Senke zu verfolgen. Diese Doktorarbeit unterstreicht, dass aus Algen gewonnene Polysaccharide wie Fucoidan ein potenzieller Weg zur Kohlenstoffbindung sind, der in vegetativen Küstenökosystemen kollektiv gespeichert wird.

Abbreviations

AEX	anion exchange chromatography
C	carbon
CAZyme	carbohydrate active enzyme
CDR	carbon dioxide removal
CO_2	carbon dioxide
CVE	coastal vegetated ecosystem
DAPI	4',6-Diamidin-2-phenylindol
DIC	dissolved inorganic carbon
DOC	dissolved organic carbon
DOM	dissolved organic matter
dw	dry weight
EPS	extracellular polymeric substances
FCSP	fucose containing sulfated polysaccharide
GF/F	glass fibre filter (grade F)
HMW	high molecular weight
HPAEC	high-performance anion exchange chromatography
mCDR	marine carbon dioxide removal
MALDI	matrix-assisted laser desorption/ ionisation
NPP	net primary productivity
O_2	oxygen
PAD	pulsed amperometric detection
PAR	photosynthetically active radiation
PBS	phosphate buffered saline
POC	particulate organic carbon
POM	particulate organic matter
ppm	parts per million
RDOC	recalcitrant dissolved organic carbon
se	standard error
spp	species plural
TEP	transparent exopolymer particles
Tris	Tris(hydroxymethyl)aminomethane

List of Figures

List of Tables

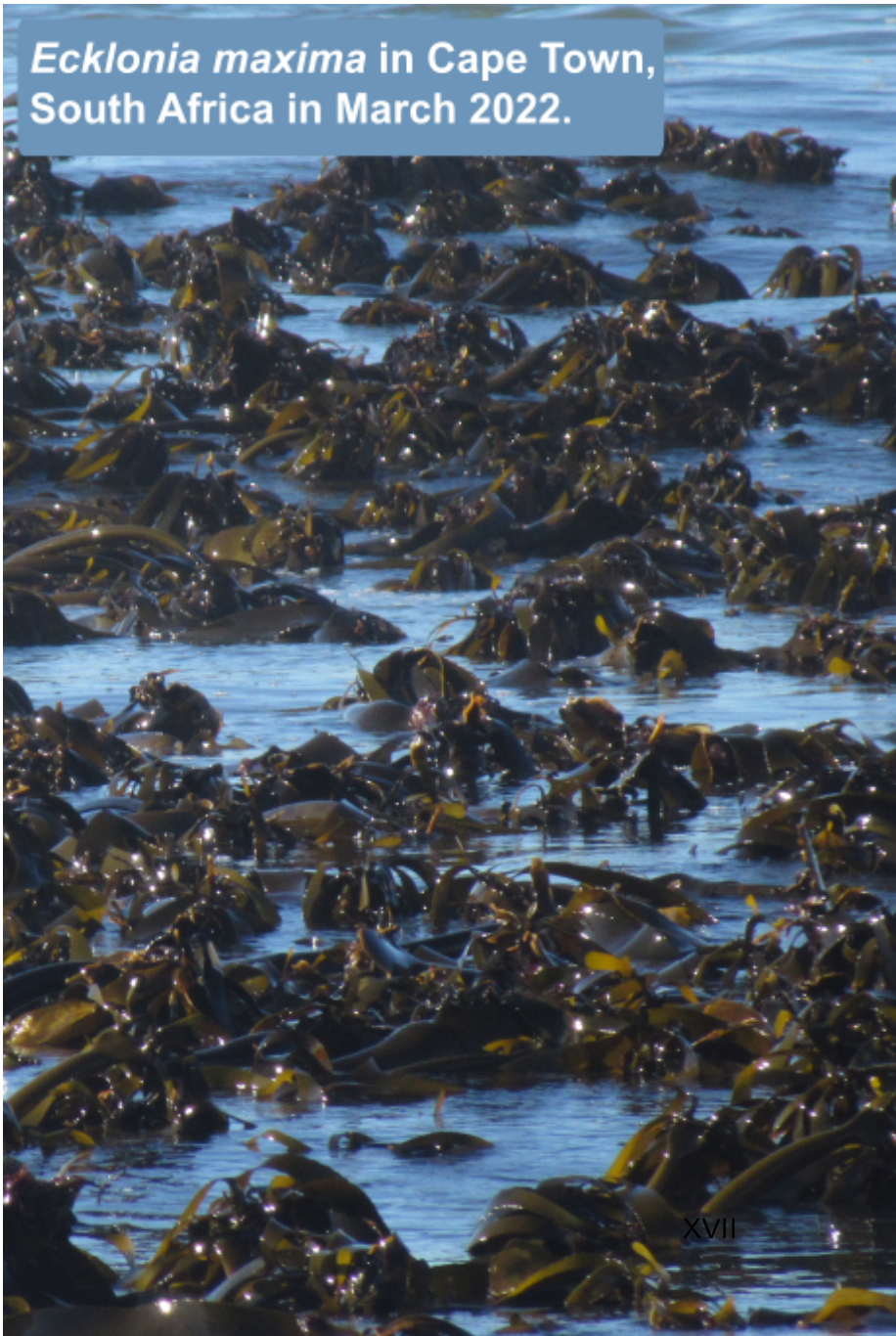

***Ecklonia maxima* in Cape Town, South Africa in March 2022.**

1 Introduction

1.1 Carbon dioxide removal by marine nature-based solutions

Atmospheric carbon dioxide (CO_2) levels have surged in recent decades from approximately 180-280 ppm to over 450 ppm, with a continuous rapid increase [Lüthi et al., 2008, Keeling et al., 1976, Friedlingstein et al., 2023]. This increase is primarily driven by anthropogenic CO_2 emissions, such as burning of fossil fuels, deforestation and industrial processes. Global warming is a result of this rapid atmospheric CO_2 increase compared to pre-industrial times [Matthews et al., 2009], which the Paris Agreement of 2016 aims to limit to $+1.5°C$, preferably below $+2°C$ [Fuss et al., Siegel et al., 2021, Rogelj et al., 2018]. Central to reaching the goals of the Paris Agreement is the concept of a finite carbon dioxide budget. Any additional emissions need to be balanced with removal into sinks [Fankhauser et al., 2022]. Current annual carbon dioxide emissions are estimated to range from 36 to 40 Gt [Gür, 2022]. To limit global warming to 1.5°C, between 400 to 800 Gt CO_2 remain as an estimated left total carbon budget [Fankhauser et al., 2022]. This requires emissions to peak before 2030 and reach net zero by around 2050 [Gür, 2022, Masson-Delmotte et al., 2018]. The main goal is the reduction of emissions. However, large-scale Carbon Dioxide Removal (CDR) strategies to buffer CO_2

emissions are gaining increasing interest as essential solutions [Fankhauser et al., 2022].

CDR strategies aim to actively extract CO_2 from the atmosphere and store it in various forms. Among these, ocean carbon sequestration has raised significant research interest [Mengis et al., 2023, Krause-Jensen et al., 2018, Macreadie et al., 2021]. Finding CDR options that are effective at permanently removing carbon, while being technologically and economically feasible remains challenging [Mengis et al., 2023, Laffoley, 2020, Hagger et al., 2022].

Marine CDR (mCDR) includes capturing carbon via biological processes and the sequestration in marine ecosystems. This concept is often referred to as "blue carbon", which spans from the storage potential of coastal vegetated ecosystems (CVEs) such as mangroves, salt marshes, seagrass meadows and macroalgae to phytoplankton in the open ocean [Mengis et al., 2023, Krause-Jensen and Duarte, 2016]. CVEs have demonstrated their importance as carbon sinks, although their potential, especially of macroalgae, remains largely underestimated [Krause-Jensen and Duarte, 2016].

Mangroves, salt marshes, seagrass meadows and peatlands only cover 1% of Earth's surface, but store approximately 20% of the global organic ecosystem carbon, stored within their soils, sediments, and plant material as part of the carbon cycle [Temmink et al., 2022]. Numbers of carbon storage are difficult to obtain as they are highly variable [Mcleod et al., 2011]. The bulk of

the organic carbon in the ocean is held in the dissolved form in the water layer and in living biomass. Wetlands store most as soil organic matter, e.g. salt marshes and seagrass and mangroves build their own organic-rich sediments [Macreadie et al., 2019, Watanabe et al., 2020]. Mangroves and salt marshes are estimated to sequester 200 and 250 g C m^{-2} $year^{-1}$, respectively, while seagrass meadows bury around 150 g C m^{-2} $year^{-1}$. In addition, around 100 g C m^{-2} $year^{-1}$ is estimated to orginate from external sources being trapped and buried. Globally, CVEs currently sequester 0.7 Pg C $year^{-1}$ [Temmink et al., 2022].
Not only biomass, but also secreted organic carbon contributes to the ecosystem's carbon storage potential. Seagrass meadow sediments were shown to be dominated by sugars, released through their root system [Sogin et al., 2022]. In contrast, macroalgae lack a root system and thus release most of their carbon as exudates [Abdullah and Fredriksen, 2004, Wada et al., 2007, Reed et al., 2015, Paine et al., 2021, Wada and Hama, 2013]. Often exudates by macroalgae are excluded from carbon storage estimates due to difficulties in tracking the secreted organic molecules in the environment [Krause-Jensen et al., 2018, Krause-Jensen and Duarte, 2016].

1.2 The ocean carbon pool

The ocean holds approximately 50 times more carbon than the atmosphere [Prentice et al., 2001]. An exchange of carbon between the atmosphere and the surface ocean occurs constantly, with an estimated annual gross exchange of about 90 Pg C $year^{-1}$ (Fig.1). Environmental factors such as temperature, wind speed, and water mixing depth influence the solubility of CO_2 in the ocean and play a significant role in this exchange [Prentice et al., 2001, Takahashi et al., 1997].
Organic matter in the ocean is categorized into dissolved organic matter (DOM) and particulate organic matter (POM). DOM is defined by its size, passing through a 0.7 µm glass fibre filter [Carlson and Hansell, 2015]. The ocean contains approximately 662 Pg of carbon as DOM, with dissolved inorganic carbon (DIC) being significantly higher, at about 38,100 Pg C. In comparison, particulate organic carbon (POC) is estimated to 3 Pg C [Carlson and Hansell, 2015] (Fig.1). Various processes determine the concentration of carbon in the ocean and its uptake of CO_2 from the atmosphere [Watanabe et al., 2020]. Primary producers, such as coastal vegetation and phytoplankton consume DIC through photosynthetic inorganic carbon fixation leading to increased CO_2 absorption from the atmosphere as surface waters re-equilibrate with air [Takahashi et al., 1997]. Further, some species float at or near to surface waters, enabling the direct uptake of CO_2 from the at-

mosphere [Flores-Moya and Fernández, 1998]. The consumed DIC can be used to build up their biomass [Pauly and Christensen, 1995], after which it can either enter the food web [Pauly and Christensen, 1995], or sink to the deep ocean and becomes sediment upon the death of primary producers [Turner, 2015]. Further, fixed carbon is exuded as dissolved organic carbon (DOC) [Watanabe et al., 2020, Barron et al., 2014, Chen et al., 2020].

A large portion of released DOC in the water is readily consumed by bacteria or degraded by ultraviolet radiation, returning to the DIC pool. This labile fraction accounts for around 25 Pg C $year^{-1}$ [Hansell, 2013]. However, significant fractions of DOC, constituting around 2 Pg C $year^{-1}$, can persist for centuries, forming a reservoir of sequestered carbon. The sources of carbon stored in the DOC reservoir are yet poorly resolved [Hansell, 2013, Jiao et al., 2014, Hansell and Carlson, 1998] (Fig.1).

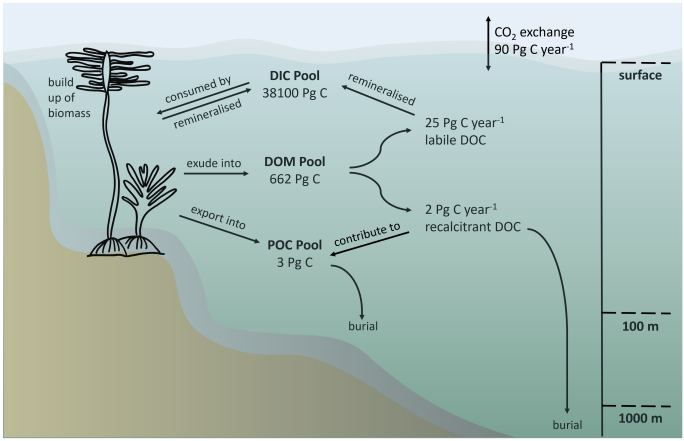

Figure 1: **Schematic view on carbon pools in the ocean**, including dissolved inorganic carbon (DIC), dissolved organic matter (DOM) and particulate organic matter (POC), adapted from [Krause-Jensen and Duarte, 2016, Prentice et al., 2001, Carlson and Hansell, 2015, Hansell, 2013].

1.3 Carbon storage potential of macroalgae

Macroalgae have been estimated to sequester approximately 173 Tg C year^{-1}, with values ranging from 61 to 268 Tg C year^{-1} [Krause-Jensen et al., 2018]. They contribute to carbon storage by building up their biomass and exporting about 43% of their production as dissolved and particulate organic carbon into the water column. Of this, approximately 52% can be accounted to DOC and around 11% is suggested to be POC, e.g. [Krause-

Jensen and Duarte, 2016, Wada et al., 2007, Reed et al., 2015, Sieburth, 1969, Buck-Wiese et al., 2023, Lucas et al., 1981].
For example, kelps are known to release 16-62% of their primary production as DOC [Abdullah and Fredriksen, 2004, Wada et al., 2007], while the macroalgae *Sargassum* exports between 5-20% of its net primary production as recalcitrant DOC, which can persist in the water column for up to 150 days [Watanabe et al., 2020]. The lability of organic matter produced by macroalgae varies, but macroalgae organic matter molecules contribution to carbon cycling is significant. In fact, macroalgae beds are considered the most extensive vegetated coastal habitats, having larger global net primary production than other CVEs [Krause-Jensen and Duarte, 2016, Watanabe et al., 2020, Raven, 2018].
Exudates can assemble into marine snow, including POM derived from macroalgae, such as phytodetritus and extracellular polymeric substances (EPS). Marine snow contributes to the vertical carbon flux by exporting up to 3% of the ocean's annual primary production from the surface to the deep sea [Legendre et al., 2015, Ducklow et al., 2001].
When macroalgae carbon sinks to the deep sea, it may remain sequestered for over 1000 years [Krause-Jensen et al., 2018, Ortega et al., 2019, Vidal-Melgosa et al., 2021]. At the seafloor, macroalgae biomass is partially consumed by benthic organisms and sediment microbes, with only a small fraction preserved in seafloor sediments for centuries. The consumption rates of

deep-sea carbon are particularly slow, further extending its sequestration [Cavan et al., 2017, Chen et al., 2022]. Even in the scenario where all biologically sequestered carbon is eventually returned to the DIC pool, ocean circulation patterns, driven by the thermohaline circulation, would retain carbon in the deep ocean for 500 to 1500 years. This long transit time ensures that approximately 70% of the DIC-enriched waters remain sequestered before they resurface and potentially exchange CO_2 with the atmosphere [Siegel et al., 2021, Wunsch, 2002].
Macroalgae carbon is not only transported to the deep sea, but may also influence coastal ecosystems. Evidence of macroalgal carbon contribution to other CVEs has been observed, with studies reporting up to 50% macroalgal carbon contributing to seagrass sediment and up to 60% to Red Sea mangrove sediment [Kennedy et al., 2010, Almahasheer et al., 2017]. This highlights the export of large fractions of macroalgal exudates to adjacent CVEs, continental shelves or the deep sea [Krause-Jensen et al., 2018, Krause-Jensen and Duarte, 2016, Watanabe et al., 2020]. However, the quantities and composition of macroalgal-derived compounds stored in CVEs remain unknown.

1.4 Glycan carbon sequestration

Glycans are a significant component of dissolved organic carbon, consituting roughly 5-15%, with concentrations peaking in proximity to photosynthesizing algae [Pakulski and Benner, 1992, McCarthy et al., 1996, Hung et al., 2003, Benner et al., 1992, Bligh et al., 2022]. These glycans are primarily derived from photosynthesis [Aluwihare et al., 1997, Myklestad, 1995, Granum et al., 2002] and influence atmospheric CO_2 levels [Hedges, 2002].

The main product of photosynthesis, glucose, serves as a fundamental building block for polysaccharides. Polysaccharides are diverse molecules characterized by their composition, connectivity, and configuration. Monosaccharides, the building blocks of polysaccharides, are linked by glycosidic bonds, resulting in stereoisomers with distinct configurations [Hofmann et al., 2015, Arnosti et al., 2021]. The variability in glycosidic bond positions and orientations results in a variety of structural arrangements. Additionally, substitutions with functional groups such as sulfate, amino, methyl, or acetate further complicate the structures [Arnosti et al., 2021]. The complexity of glycans is significantly higher compared to nucleic acids and proteins [Laine, 1994]. For example, laminarin and cellulose are both polymers of glucose that differ in their linkage positions and ramification. Laminarin functions as a storage polysaccharide, while cellulose serves as a structural polysaccharide that

provides stability to the cell wall [Becker et al., 2017, Bäumgen et al., 2021].

In contrast to intracellular storage glycans extracellular matrix glycans, such as fucoidan are highly complex [Bligh et al., 2022]. Their chemical complexity offers protection, as bacteria must express complex cascades of carbohydrate-active enzymes (CAZymes) to degrade them [Vidal-Melgosa et al., 2021, Hehemann et al., 2014, Hettle et al., 2022, Avcı et al., 2020, Krüger et al., 2019, Sichert and Cordero, 2021, Sidhu et al., 2023]. Microbial responses to glycans influence glycan turnover and shape microbial communities [Sichert and Cordero, 2021, Kloareg et al., 2021, Rogowski et al., 2015]. This interaction underscores the role of glycans in microbial community dynamics and carbon persistence in ecosystems.

In marine ecosystems, algal glycans such as laminarin and fucoidans vary in their enzyme requirements for depolymerization [Bligh et al., 2022, Becker et al., 2017, Huang et al., 2021, Steinke et al., 2022, Sichert et al., 2020]. Simpler glycans like laminarin require fewer enzymes for complete depolymerisation, while more complex glycans, such as fucoidans, necessitate a higher enzyme count [Bligh et al., 2022, Becker et al., 2017, Steinke et al., 2022, Sichert et al., 2020]. For example, specialized bacteria like Lentimonas CC4 use hundreds of enzymes to degrade fucoidans from six algal species [Sichert et al., 2020]. Anionic glycans against towards bacterial degradation have the potential to act as binding agents [Mopper et al., 1995], accu-

mulating and sinking to ocean depths, thus sequestering carbon for thousands of years [Vidal-Melgosa et al., 2022, Salmeán et al., 2022].

1.5 The complex polysaccharide fucoidan

Fucoidans, also referred to as fucose-containing sulfated polysaccharides (FCSP) or sulfated fucans, are a major cell wall component found predominantly in macroalgae and diatoms. It forms a dense network with proteins, minerals, phenolic compounds, and various polysaccharides [Deniaud-Bouët et al., 2014, 2017, Michel et al., 2010, Huang et al., 2021, Vidal-Melgosa et al., 2021, Buck-Wiese et al., 2023].
Fucoidan is predominantly composed of the monosaccharide fucose, though other monosaccharides can also be incorporated, and it is characterized by its high degree of sulfation [Deniaud-Bouët et al., 2017, Kopplin et al., 2018]. The structure of fucoidan varies significantly depending on its source [Sichert et al., 2020] and can fluctuate seasonaly [Fletcher et al., 2017]. Fucoidans can be classified into two main categories, the homofucans and heterofucans. Homofucans feature a backbone consisting solely of fucose, while heterofucans have a non-fucose backbone with fucose side branches. Different algae orders exhibit distinct fucoidan structures. Laminariales and Ectocarpales fucoidans are characterized by α-1,3 linked L-fucose with sulfate esters at C-4 [Kopplin et al., 2018, Nagaoka

et al., 1999]. Fucoidans from Fucales feature an alternating α-1,3/α-1,4 linked L-fucose backbone with sulfate at C-2 and C-4 [Chevolot et al., 2001]. Fucoidan structures range from linear with few branches to highly complex and extensively branched, often including other monosaccharides such as galactose, mannose, or glucuronic acid [Sichert et al., 2020, Kopplin et al., 2018].
The exact molecular structures of fucoidans remain challenging to fully characterize due to their complexity [Sichert et al., 2020, Kopplin et al., 2018]. Complexity and diversity of fucoidan not only play a crucial role in algal cell walls, but also suggest their potential as carbon sinks in the ocean.

1.6 Fucoidan as a global carbon sink

Brown algae and diatoms have been shown to secrete fucoidan [Buck-Wiese et al., 2023, Vidal-Melgosa et al., 2021, Huang et al., 2021], with fucoidan detected in century-old sediment, highlighting its potential as a carbon sink [Vidal-Melgosa et al., 2022, Salmeán et al., 2022].
The active secretion of fucoidan by *Fucus vesiculosus* has been demonstrated, estimating that up to 50% of the total dissolved organic carbon is fucoidan-derived [Buck-Wiese et al., 2023]. Additionally, diatoms have been observed to exude fucoidan that accumulates in POM during an algal bloom around the island of Heligoland [Vidal-Melgosa et al., 2021]. This constant

production and secretion of fucoidan, released in the mucilage, resembles immunological defense mechanisms against microbes [Bligh et al., 2022, Kloareg et al., 2021]. This resistance against microbial hydrolysis [Giljan et al., 2023] might be caused by its complex and variable structure. This necessitates the involvement of hundreds of enzymes for complete degradation [Sichert et al., 2020], being energy expensive [Arnosti, 2000, Orellana et al., 2022]. Fucoidan degradation might not occur completely, but enzymatic activity of microorganisms leads to the fragmentation into smaller oligosaccharides or reducing its strong negative charge by cleavage of sulfate groups [Arnosti et al., 2021, Sichert et al., 2020, Holtkamp et al., 2009, Qiu et al., 2022, Silchenko et al., 2013, Trang et al., 2022]. Fragmentation might make less abundant non-fucose monosaccharides in the polysaccharide more accessible to microorganisms. As catabolism of fucose proceeds through a complex cascade rare in bacteria, the non-fucose components of fucoidan are likely less persistant than the fucose components [Sichert et al., 2020, Orellana et al., 2022].

Washed off from the mucilage layer, fucoidan disperses in the dissolved phase, making enzymatic degradation even more unlikely [Arnosti et al., 2021, Arnosti, 2000]. Under certain conditions, including concentration-dependent scenarios, fucoidan may assemble into particles, as supported by increasing DOC concentrations being followed by increasing POC concentrations [Engel et al., 2004]. Surface active transparent exopoly-

mer particle (TEP) polysaccharides have been observed to be enriched in fucose [Mopper et al., 1995] and during an algal bloom up to 15% of fucose contributed to the POM 3 µM fraction [Vidal-Melgosa et al., 2021]. Evidence of fucose, which is the main monosaccharide of fucoidan, supports its presence of fucoidan in the particulate fraction. Aggregation often results in sinking [Engel et al., 2004, Iversen, 2023, Verdugo, 2012], ultimately contributing to the accumulation of fucoidan in sediment [Vidal-Melgosa et al., 2022, Salmeán et al., 2022]. This accumulation supports fucoidan being a possible carbon sink.
The dispersal and transportation of polysaccharides like fucoidan might influence various ecosystems. Tidal currents may flush glycans into environments like salt marshes, while other ecosystems may encounter overspill scenarios from sources such as seagrass sugars [Sogin et al., 2022]. Coastal vegetated areas have been found to harbour substantial amounts of carbon [Krause-Jensen and Duarte, 2016, Temmink et al., 2022, Mcleod et al., 2011]. The sources and sinks of carbon are important to understand the storage dynamics of algal polysaccharides across ecosystems.

1.7 Knowledge gap

The complex polysaccharide fucoidan has been shown to be secreted by diatoms and one brown algae, *Fucus vesiculosus* [Buck-Wiese et al., 2023, Vidal-Melgosa et al., 2021, Huang

et al., 2021]. Whether this is a common trait of brown algae remains unknown. The fate of fucoidan after secretion is hypothesized, as fucoidan might escape microbial hydrolysis and accumulate to form particles. These particles might sink to the sediments, forming a carbon sink in the ocean. The transportation, as well as its storage are understudied, as macroalgae might interact with further coastal vegetated ecosystems in carbon storage (Fig.2).

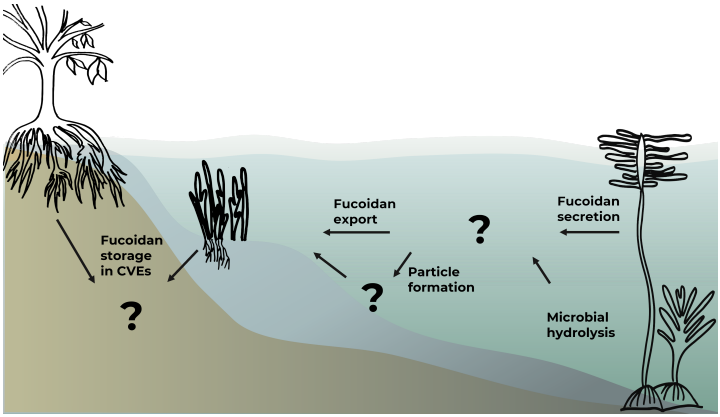

Figure 2: **Hypothetical fucoidan carbon sequestration pathway. Fucoidan might be exuded by macroalgae.** Secreted fucoidan might be removed through microbial hydrolysis or persists to assemble into particles. Persisting or aggregating fucoidan might be transported into coastal vegetated ecosystems (CVEs), where it might be stored in sediments for centuries.

1.8 Aim of thesis

This thesis aims to unravel the fate of fucoidan in the ocean. More specifically, the following aspects are examined:

1. **Fucoidan is actively secreted by brown algae around the globe**
   Here, six tested brown algae around the globe are studied in respect to their fucoidan secretion capability. Dissolved fucoidan concentrations are measured over multiple weeks in mesocosm experiments and aggregated with environmental data to prove natural fucoidan presence.

2. **Fucoidan has the potential to resist microbial hydrolysis**
   Complexity of fucoidan challenges microbial hydrolysis. Incubations with fluorescently labelled *Sargassum* fucoidan with tank water from *Sargassum fluitans* and control incubations are performed to test if the natural microbial community is able to hydrolyse fucoidan. The experiment should provide evidence for fucoidan being resistant against complete hydrolysis.

3. **Fucoidan forms a carbon sink by accumulation into particles and sinking to depths**
   The potential of fucoidan persisting in the dissolved phase,

transitioning to the particulate phase and its possibly sinking to the bottom of mesocosms is investigated. Environmental data is used to support fucoidan presence in dissolved and particulate organic carbon.

4. **Fucoidan is stored in coastal vegetated ecosystems, showing collaborative carbon storage potential of CVEs**

   Sediment sampled from coastal vegetated ecosystems is analysed to investigate their carbon storage potential. Specifically possible fucoidan presence stored in CVEs is studied to show the interaction of carbon storage between CVEs.


Lessonia spicata in Las Cruces,
Chile in January 2022.

2 Natural range of brown algae restricts carbon sequestration in secreted fucoidan to below one gigaton

2.1 Contribution to manuscript

Conceptualization: 40%
Field work: 50%; in detail: Chile, South Africa, United States of America and Finland (4 out of 6 mesocosm sites)
Laboratory work: 70%; in detail: sampling and sample preparation for transportation, fucoidan extraction from seawater and biomass, sequential extraction of polysaccharides, monosaccharide analysis of dissolved fraction before and after anion exchange chromatography, monosaccharide analysis of particulate fucoidan, quantification of particulate organic carbon, cell counts, immunolabelling, ELISA antibody tests, microscopy
Data analysis: 50%
Visualisation: 50%
Writing: 50%

Manuscript in preparation

Authors: Inga Hellige and Hagen Buck-Wiese, Margot Bligh, Timothy Thomson, Lydia White, Carol Arnosti, Dariya Baiko, Mar Fernández-Méndez, Sherif Ghobrial, Camilla Gustafsson, Mohammed Kajee, C. Chad Lloyd, Miriam Philippi, Dan Potin, Philippe Potin, Mark Rothman, Beatriz Salgado Murillo, Michael Seidel, Catharina Uth, Evie Wieters, Marie Magnusson and Jan-Hendrik Hehemann

Keywords: seaweed | carbohydrates | polysaccharides | aggregation | TEP particle | marine carbon cycle | biological carbon pump | carbon dioxide removal | carbon sequestration

2.2 Abstract

Brown algae may sequester significant quantities of carbon in the ocean. Enumeration requires a molecular tracer for brown algal carbon, such as the polysaccharide fucoidan. Here, we show fucoidan secretion by all six assessed brown algae species across the globe and trace this recalcitrant polysaccharide as it coagulated into particles. Based on quantification of fucose-hydrolyzed polymers prior and after the specific targeting of the negatively charged fraction of fucoidan, we showed brown algae investing 1.7-4.2% of their net primary production into an average secretion of 0.32-0.88 mg fucoidan per gram biomass (dry weight) per day, accounting for 20-50% of released or-

ganic carbon. This per-biomass rate suggests a global secretion of 0.04-0.1 gigatons fucoidan carbon. Fucoidan was traceable over months, resisted microbial consumption, and coagulated together with allochthonous material into microbial cells and fucoidan comprising particles, which persisted over an entire year of incubation in the dark. In situ measurements showed the environmental accumulation of fucoidan inside and coagulation downstream of a *Saccharina latissima* farm. Persistence and aggregation of fucoidan form a molecular pathway for long-term removal of algal and through coagulation also non-algal carbon from surface waters. Brown algae generally secrete fucoidan, which defuses the competition between biomass use and dumping for carbon sequestration by inducing an external pathway of carbon storage decoupled from the fate of the algal biomass. Preserving and increasing the abundance of brown algae can serve as a nature-based solution for carbon sequestration, with enhanced algae biomass increasing fucoidan-driven carbon storage.

2.3 Introduction

Brown algae have the potential for carbon sequestration at scale due to their efficient carbon dioxide fixation. Farming macroalgae at sea, not possible with microalgae, bears vast economic opportunity and in the process expands the macroalgal habitat range. Among macroalgae, brown algae contribute the most to

net carbon fixation and global biomass standing stocks [Duarte et al., 2022b, Watanabe et al., 2020, Pessarrodona et al., 2023], annually converting a gigaton (Gt) of carbon into dissolved organic molecules. Those molecules that resist immediate conversion back to carbon dioxide via heterotrophic reactions may be exported to below the carbon sequestration horizon in the ocean [Duarte et al., 2022b, Smith, 1981, Michel et al., 2010]. However, uncertainty about the pathways of the exported carbon has to date obscured any carbon sequestration enacted by brown algae.

While plants exude mucilage via their roots in the process of soil-carbon regulation [Baetz and Martinoia, 2014], brown algae interact via the entirety of their tissue-surface interface with the surrounding water and secrete carbon-rich mucilage directly into the ocean. This carbon must be traced with molecular specificity to measure carbon sequestration. Among the molecules that compose the algal mucilage layer, through which 1-35% of net primary production are released [Abdullah and Fredriksen, 2004, Wada et al., 2007, Wada and Hama, 2013, Reed et al., 2015, Paine et al., 2021], the anionic polysaccharides alginate and fucoidan dominate [Deniaud-Bouët et al., 2014, Bengtsson et al., 2011]. Fucoidan is not only a major component of biomass and mucilage, but also resists microbial degradation and persists in centuries-old sediments [Michel et al., 2010, Salmeán et al., 2022, Vidal-Melgosa et al., 2022]. These attributes render this complex polysaccharide a candi-

date molecule to trace brown algal carbon [Salmeán et al., 2022, Vidal-Melgosa et al., 2022] using recently developed techniques to detect and quantify fucoidan in seawater [Buck-Wiese et al., 2023] to evaluate the role of algae in climate change mitigation.

Here, we traced fucoidan in environments with wild and farmed brown algae, in mesocosm experiments to quantify fucoidan secretion for 6 brown algal species as a function of biomass, and over 12 months to monitor long-term persistence (Fig. 3, 7, table 2, 3). We hypothesized all tested brown algae to secrete fucoidan and measured fucoidan accumulation by liquid chromatography-based quantification of selectively concentrated fucoidan monosaccharides supported by structure-sensitive antibody binding. In the process, we were prompted to analyze particulate organic carbon and fucoidan in particles retained on glass fiber filters. To corroborate these chemical and biocatalytic analyses, we employed fluorescence microscopy to visualize aggregates, cells and fucoidan in mesocosm water.

2.4 Results

2.4.1 *Fucoidan in coastal surface waters produced by Laminariales and Fucales*

Sampling seawater along transects perpendicular to natural and farmed brown algae populations revealed that dissolved fucoidan exists in marine environments in quantifiable amounts

(Fig. 3, table 3). Dissolved fucoidan was quantified by fucose in hydrolysable polymers selected by >1 kDa size and its charge by targeting the negatively charged fucoidan fraction by binding to anion exchange chromatography. These measurements revealed dissolved fucoidan in surface waters of coastal environments globally (Fig. 7). Fucoidan concentrations in the algae-inhabited surface waters generally exceeded bottom water concentrations, which were often indistinguishable from processing blanks (Fig. 7A, C, D). Considering advective fluxes, elevated concentrations emerged in proximity to algae populations for sampled transects in South Africa, France and Mexico (7A, C, H). Surface fucoidan concentrations reached highest concentrations of 93.25 ±2.95 µg L^{-1} (mean ±s.e.m) inside one *Sargassum* patch in Mexico (Fig. 7G) and 75.26 ±14.61 µg L^{-1} in outgoing tidal surface waters downstream of beds of *L. digitata* in France (Fig. 7C). These results indicate that brown algae release fucoidan at rates and with stability sufficient to establish measurable gradients in coastal surface waters.

Mesocosm experiments with locally dominant brown algae demonstrated the secretion of fucoidan by all investigated species in six marine regions (Fig. 3, 8). A less specific analysis selecting fucoidan by size only to include fucoidan molecules with lower charge density complemented the size- and charge-selected fucoidan quantification. Both demonstrated fucoidan concentrations to increase over the incubation period in brown algae mesocosms, which exceeded mesocosms without brown algae

in a hierarchical Bayesian model (without brown algae effect: size-selected $\tilde{}N_{-0.52,\ 0.1,}$ $R^2 = 0.47$; size- and charge-selected $\tilde{}N_{-0.16,\ 0.02,}$ $R^2 = 0.39$) (Fig. 8G-R). To account for water exchanges and the resulting dilution of secreted molecules, we proceeded to calculate for each mesocosm independently a cumulative fucoidan value, which exacerbated the difference between mesocosms with and without brown algae (without brown algae effect: size-selected $\tilde{}N_{-0.88,\ 0.1,}$ $R^2 = 0.48$; size- and charge-selected $\tilde{}N_{-0.31,\ 0.02,}$ $R^2 = 0.60$). For all assessed species, except for *E. radiata*, the size-selected fucoidan accounted for 30-50% of accumulating dissolved organic carbon, decreasing to 15-25% for size and charge-selected fucoidan (Fig. 8, 9). Brown algae in mesocosms were, thus, drivers of fucoidan accumulation irrespective of their biomasses and removal processes.

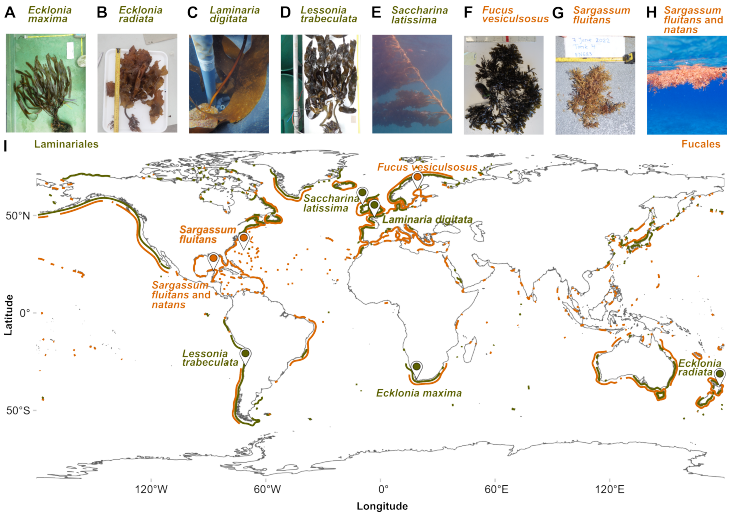

Figure 3: **Sampling representatives of a global taxon and their surroundings.** Images of assessed algae **A)** *E. maxima*, **B)** *E. radiata*, **C)** *L. digitata*, **D)** *L. trabeculata*, **E)** *S. latissima* (only transect sampling), **F)** *F. vesiculosus*, **G)** *S. fluitans*, and **H)** *S. spp.* (only transect sampling). **I)** Occurrence of brown algae based on a recent distribution dataset by Assis et al. [2020], and locations of transects and mesocosm incubations.

2.4.2 *Secretion and persistence of dissolved fucoidan*

To distinguish fucoidan secretion from removal, we calculated the change in concentration over time and simulated this change as a function of brown alga biomass and fucoidan concentration (Fig. 4A-D). *E. maxima* mesocosms were excluded due to light-limitation indoors (Fig. 10) and *L. digitata* mesocosms due to missing water replenishments on day 10 (Fig. 8). Cumulative concentrations peaked on day 12, before removal of brown algae, reaching 1.52 $\pm$0.32 mg L^{-1} size-selected and 0.64 $\pm$0.11 mg L^{-1} size and charge-selected fucoidan compared to control mesocosms at 0.29 $\pm$0.07 mg L^{-1} and 0.21 $\pm$0.08 mg L^{-1}, respectively (Fig. 4A, C). Our hierarchical Bayesian regression model trained exclusively on the concentration change isolated the effect of brown algae biomass for size- ($N_{0.28,\ 0.05}$, $R^2 = 0.18$), and size- and charge-selected fucoidan ($N_{0.09,\ 0.02}$, $R^2 = 0.19$) versus concentration-dependent removal (both size-selected and size- and charge-selected ~ $N_{-0.06,\ 0.02}$) (Fig. 4B, D).

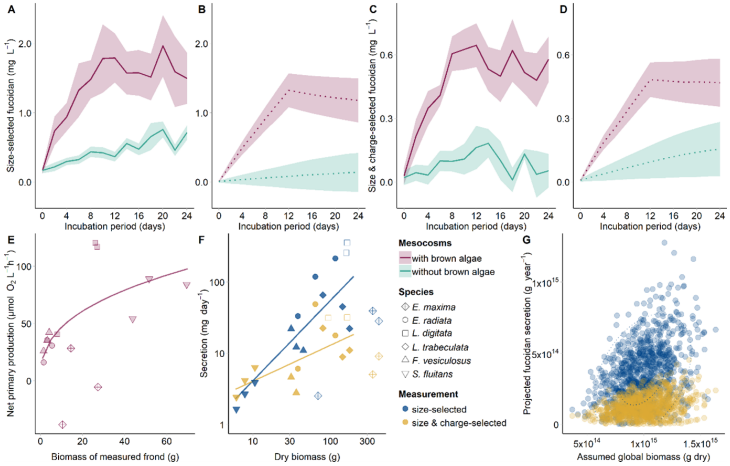

Figure 4: **Algal fucoidan secretion rates scale with biomass enabling a global projection. A-D)** show cumulative fucoidan concentrations in mesocosms with brown algae (red) and mesocosms without brown algae (teal), excluding *L. digitata* and *E. maxima* due to experimental flaws; size-selected fucoidan experimental data in **A)** and simulated based on a hierarchical Bayesian model in **B)**; size- and charge-selected fucoidan experimental data in **C)** and simulated in **D)**. **E)** Net primary production plotted against biomass of measured frond with regression based on log10-transformed values and excluding *E. maxima* due to insufficient light. No data available for *L. trabeculata*. **F)** Secretion of size-selected (blue) and size- and charge-selected fucoidan (yellow) during the first four days of incubation plotted against dry biomass of incubated algae. Regression models use log10-transformed values and exclude *E. maxima* and *L. digitata*.

Figure 4: **G)** Projected annual secretion based on biomass-secretion relationships for size-selected (blue) and size and charge-selected (yellow) fucoidan as function of global dry biomass estimates.

Estimated fucoidan secretion rates scaled with brown algae biomass and enabled projecting a global estimate. To minimize the simultaneous effect of fucoidan removal, fucoidan secretion was estimated from accumulation rates during the first four days of incubation (Table 1, Fig. 11). This approach was supported by accumulation rates of fucoidan in brown algae mesocosms invariably peaking during the first four days of incubations (Fig. 11). Secreted fucoidan carbon accounted for 1.7-4.2% of net primary productivity, which correlated with dry weight while showing inter-species differences (Table 1, Fig. 4E, 12, 13). The secretion of both size-selected fucoidan and size and charge-selected fucoidan scaled significantly with brown algal biomass (size-selected: $p < 0.001$, $R^2 = 0.67$; size-and charge-selected: $p = 0.034$, $R^2 = 0.35$) (Fig. 4F). Fucoidan secretion scaling with biomass, allows for modelling of global fucoidan estimates. With biomass estimated as ˜N(1Gt, 0.2Gt), we projected global fucoidan secretion with a mean of ˜0.321 Gt for size-selected estimates and ˜0.117 Gt for size-and charge-selected estimates (Fig. 4G).

Table 1: **Fucoidan secretion rates** based on accumulation during the first four days of incubation in size-selected and size- and charge-selected fraction. Reported values include secretion per volume and time, per unit brown algae biomass and time normalized by mesocosm volumes, and percentage of net primary production (NPP) detected as secreted fucoidan carbon.

	brown algae	*E. maxima*	*E. radiata*	*L. digitata*	*L. trabeculata*	*F. vesiculosus*	*S. fluitans*	Mean
incubation	dry weight (g)	280.8 ± 68.0	79.5 ± 15.5	139.5 ± 14.4	133.4 ± 17.9	37.4 ± 2.5	8.2 ± 0.8	
	volume (L)	220	220	250	250	57	40	
by size	accumulation (mg L^{-1} d^{-1})	0.17 ± 0.04	0.58 ± 0.24	1.43 ± 0.34	0.33 ± 0.15	0.36 ± 0.06	0.09 ± 0.01	0.49 ± 0.20
	accumulation (mg g_{dw}^{-1} d^{-1})	0.13 ± 0.01	1.63 ± 0.29	2.27 ± 0.47	0.89 ± 0.50	0.58 ± 0.12	0.42 ± 0.04	0.98 ± 0.33
	% of NPP	negative NPP	9.85 ± 3.69	5.94 ± 1.22	no NPP measured	0.57 ± 0.13	2.46 ± 0.17	4.23 ± 1.05
by size and charge	accumulation (mg L^{-1} d^{-1})	0.04 ± 0.02	0.12 ± 0.06	0.18 ± 0.07	0.04 ± 0.02	0.06 ± 0.02	0.17 ± 0.03	0.10 ± 0.03
	accumulation (mg g_{dw}^{-1} d^{-1})	0.02 ± 0.01	0.32 ± 0.19	0.36 ± 0.19	0.11 ± 0.06	0.11 ± 0.04	0.75 ± 0.05	0.28 ± 0.11
	% of NPP	negative NPP	2.41 ± 1.81	0.95 ± 0.46	no NPP measured	0.11 ± 0.04	4.45 ± 0.52	1.78 ± 0.52

Continued assessment of dissolved fucoidan concentrations over 12 months of laboratory incubations supported the notion of fucoidan recalcitrance under environmental conditions (Fig. 4A,C, Fig. 15, 14, 16). Fucoidan-specific monoclonal antibody binding confirmed the persistence of dissolved fucoidan in *L. trabeculata* mesocosms (Fig. 17A), while the other incubations did not show antibody binding to fucoidan standards or dissolved fucoidan in incubations (Fig. 17B-F, M). The non-specific antibody BAM7, which primarily binds to alginate, but also cross-binds with fucoidan or pectin, showed signals in tanks with macroalgae for *E. radiata* and *F. vesiculosus* incubations, as well as in mesocosms without brown algae for *L. trabeculata* and *L. digitata* incubations (Fig. 17G-L, N). Sampling after one year of incubation at 4°C in the dark revealed more size-selected fucoidan in water from algae mesocosms (0.38 $\pm$0.27 mg L^{-1}) compared to controls (0.14 $\pm$0.05 mg L^{-1}). Notably, close to no size- and charge- selected fucoidan remained (with brown algae: 0.0008 $\pm$0.0003 mg L^{-1} v. without brown algae: 0.0005 $\pm$0.0003 mg L^{-1}), suggesting charge density to promote removal of dissolved fucoidan (Fig. 16C). Thus, our results document that fucose polymers could survive months in incubations under oceanic conditions, while strongly anionic fucoidan disappeared from the dissolved fraction.

2.4.3 *Brown algae fucoidan aggregates*

In mesocosms with brown algae, particulate organic carbon and specifically particulate fucoidan accumulated, which continued after removing algae specimens. Particulate organic carbon increased significantly over time in mesocosms with brown algae, including after algae were removed (log10-transformed, $p = 0.028$, $R^2 = 0.07$), but not in mesocosms without brown algae (log10-transformed, $p = 0.934$) (Fig. 5A). Fucose released by acid hydrolysis from material retained on glass fiber filters provided a semiquantitative estimate of particulate fucoidan (Fig. 18A-F). Particulate fucoidan concentrations increased in brown algae mesocosms (log10-transformed, $p < 0.001$, $R^2 = 0.27$), but not mesocosms without brown algae (log10-transformed, $p = 0.959$) (Fig. 5B). This accumulation was confirmed by structure-sensitive BAM1 antibody labeling of extracts from filter sections (Fig. 19). These results revealed the aggregation of dissolved brown algal fucoidan into particles, a process which would at least contribute to the observed removal from the dissolved fraction.

Location-specific differences were evident: Oligotrophic Sargasso Sea incubations only showed particulate fucoidan in brown algae mesocosms (Fig. 18F). In contrast, the nutrient-rich upwelling regions inhabited by *E. maxima* (Fig. 18A) and *L. trabeculata* (Fig. 18D) saw control mesocosms initially exceed brown algae mesocosms in particulate fucoidan. In *L. digitata*

mesocosms, freshly added seawater with particulate fucoidan concentrations of up to 0.17 mg L^{-1} may have resulted in equal particulate fucoidan concentrations for mesocosms with and without algae (Fig. 18C). After 24 days, we collected sedimented particles from these incubations, providing evidence for fucoidan removal and indicating its potential role as a carbon sink (Fig. 20). Fucose comprising only 3-12% of monosaccharides in this sedimented matter indicates the coagulation with and precipitation of allochthonous carbon including microbial cells (Fig. 20A-B).

To test whether fucoidan aggregation is an environmentally relevant process, we analyzed both the size- and charge-selected and the particulate fucoidan fraction of samples from a transect through a kelp farm. We found elevated concentrations of particulate fucoidan downstream (3.55 $\pm$0.97 mg L^{-1}) of the *Saccharina latissima* farm in Northern Ireland compared to upstream (0.95 $\pm$0.44 mg L^{-1}) and within the kelp farm (0.91 $\pm$0.21 mg L^{-1}) (Fig. 5C). Size- and charge-selected fucoidan concentrations were elevated both within the kelp farm (2.32 $\pm$0.79 mg L^{-1}) and downstream (2.11 $\pm$0.41 mg L^{-1}) compared to upstream (1.62 $\pm$0.48 mg L^{-1}) of the farm. These findings indicate that fucoidan particle formation occurs under environmental conditions and draws down carbon (Fig. 5C).

Microscopy of BAM1 antibody-stained filters confirmed the aggregation of fucoidan into recalcitrant particles and suggested coagulation with DAPI-stained microbial cells. *F. vesiculosus*

incubations were enriched in BAM1-stained particles after 8 days compared to day 0 (Fig. 5D-E). Screening filters for particles after 9 months of incubation in the dark showed that fucoidan aggregation had apparently continued and revealed the persistence of fucoidan particles (Fig. 5F). Microbial cells bound to aggregates with a matrix of fucoidan may indicate the removal of bacteria by coagulation from the surface ocean, as potentially indicated by declines in cell counts during brown algae mesocosm incubations (Fig. 18G-L). The formation and months-long persistence of fucoidan particles under environmental conditions in the dark delineates a carbon sequestration pathway that extends beyond the carbon in fucoidan itself.

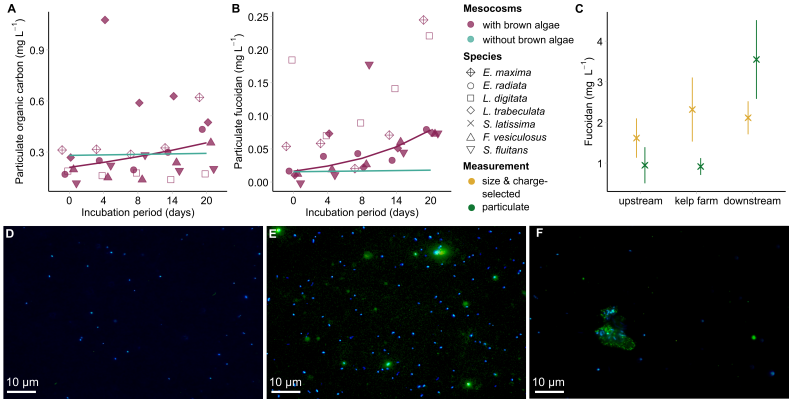

Figure 5: **Brown algal fucoidan aggregates into particles that persist for months.** Brown algal fucoidan aggregates into particles that persist for months. **A)** Particulate organic carbon in mesocosms with brown algae (red) and without brown algae (teal), with lines indicating linear models of log10-transformed concentrations. **B)** Particulate fucoidan estimated from acid-released fucose in mesocosms with brown algae (red) and without brown algae (teal), with lines indicating linear models of log10-transformed concentrations. In both **A)** and **B)**, calculations exclude *E. maxima* and *L. digitata*. **C)** Size- and charge-selected (yellow) and particulate (dark green) fucoidan measured along a transect of a *S. latissima* farm in Northern Ireland. **D-F)** filters from *F. vesiculosus* mesocosms showing DAPI-stained cells (blue) and BAM1 immunolabeled fucoidan (green) for **D)** day 0, **E)** day 8 and **F)** day 270 in the dark.

2.5 Discussion

Here, we report for the first time the presence of the complex mucilage polysaccharide fucoidan in coastal surface waters around the world and trace it to adjacent brown algae populations. All tested brown algae species from the orders Laminariales (4 species) and Fucales (2 species) secreted fucoidan. Secretion rates scaled with algae biomass and bulk DOC exudation. Extrapolated, our mesocosms results suggest that current global brown algae populations secrete annually 0.12-0.32 Gt fucoidan. Both in-situ and mesocosm observations indicate environmental persistence of brown algal fucoidan for months to years. Moreover, our results demonstrate the coagulation of brown algae-secreted fucoidan with allochthonous material into particles that can potentially sink to the deep ocean, reaching the carbon sequestration horizon and potentially enable long-term carbon storage [Krause-Jensen and Duarte, 2016].
Through the secretion of recalcitrant fucoidan, brown algae farms have the potential to emerge as an economy-driven carbon sink. Using floatation organs and during exposure in the intertidal zone, brown algae directly access atmospheric carbon dioxide zone for photosynthesis [Flores-Moya and Fernández, 1998] (Fig. 21). The controversial strategy of bailing and sinking of algae, but also harvesting seaweed for food or other products upend photosynthesis and thereby terminate fucoidan secretion [Ricart et al., 2022]. We identified 20-50% of

exudates, accounting for 1-35% of net primary production as fucoidan, in line with previously reported 13-47% for *Fucus vesiculosus* [Abdullah and Fredriksen, 2004, Wada and Hama, 2013, Wada et al., 2007, Reed et al., 2015, Paine et al., 2021, Buck-Wiese et al., 2023]. Increases in dissolved organic carbon and to some extend fucose across mesocosms suggest the simultaneous secretion of extracellular polysaccharides by microalgae. This highlights the need for specific quantification and even higher specificity could be achieved e.g. through enzymatic hydrolysis [Buck-Wiese et al., 2023, Bligh et al., 2022, Steinke et al., 2022, Becker et al., 2017] (Fig. 8A-F). Assuming 30% of carbon in fucoidan [Buck-Wiese et al., 2023], our results scale to an annual secretion of 0.04 to 0.1 Gt fucoidan carbon, using a reported global brown seaweed forest area of 1,965,227 km^2, excluding holopelagic seaweed biomass such as Sargassum that can account to 20 Mill. tons floating biomass per year [Filbee-Dexter et al., 2024, Wang et al., 2019]. Global seaweed farming produces about 3.2 $megatons_{dw}$ annually across all phyla, an almost negligible amount compared to the natural standing stock. Nonetheless seaweed farming has enormous potential for expansion and, as shown here, sustains carbon removal as ecosystem service through the environmental persistence and coagulation of secreted fucoidan [Duarte et al., 2022a].

Persisting secreted fucoidan aggregated into particles, which resembled transparent extracellular polymers (TEP), captured

microbial cells and other allochthonous material [Busch et al., 2017, Engel, 2004, Alldredge et al., 1993], and likely induced sedimentation (Fig. 5, 18). Fucoidan degradation is rare and enzymatically costly in the environment [Arnosti, 2000, Holtkamp et al., 2009, Silchenko et al., 2013, Sichert et al., 2020, Qiu et al., 2022, Trang et al., 2022, Orellana et al., 2022], in line with its hypothesized protective, surface cleaning physiological role, but when it does occur, it is often observed inside particles [Arnosti et al., 2012, Lloyd et al., 2022, Reintjes et al., 2023]. We observed year-long persistence of fucose in dissolved polymers from brown algae (Fig. 8, 14, 15, 16), diminishing removal over time from the dissolved phase (Fig. 4, 16). To which extend the aggregation into recalcitrant particles accounted for this removal from the dissolved phase could not be determined due to uncertainty about sinking rates, which may have differed between mesocosm systems (Fig. 5, 6). The discovery that brown algae fucoidan aggregates into particles is pivotal as it reveals a driver of long-term carbon removal through export from the surface ocean [Engel et al., 2004, Verdugo, 2012, Iversen, 2023]. Our observations, supported by reported accumulation and aggregation of microalgal fucoidan-like polysaccharides with microbial cells [Vidal-Melgosa et al., 2021, Huang et al., 2021], document enhanced sedimentation in brown algae mesocosms (Fig. 5, 20). Increasing particulate fucoidan and microscopy images of particles show that fucoidan coagulation can give rise to long-lived TEP and thereby fuel the biological

carbon pump [Engel, 2004, Verdugo, 2012], supporting the idea that fucoidan contributes to the drawdown of organic matter. This finding that secreted fucoidan coagulates and sinks both autochthonous and allochthonous carbon provides evidence for a direct pathway of carbon sequestration.

In conclusion, all six tested brown algae secreted fucoidan supporting the assumption that it is a common trait of brown algae. The observed correlation between biomass and secretion rate enables extrapolation with a global biomass estimate projecting an annual secretion of 0.04–0.1 Gt fucoidan carbon. Hinging on biomass, humanity can influence global secretion rates by protecting and restoring threatened kelp forests, through afforestation and via commercial farming. Secreted brown algae fucoidan persisted for months in the dissolved phase, triggering particles to assemble. Aggregation enabled sinking, which can lead to fucoidan crossing the carbon sequestration horizon in the ocean [Salmeán et al., 2022, Vidal-Melgosa et al., 2022]. This aggregation does not only affect the fate of fucoidan carbon but extends the drawdown effect to allochthonous carbon involved in aggregate formation including cells. Secreted fucoidan, thus, embodies a molecular tracer for exported brown algae carbon, sequestering carbon directly due to its recalcitrant, carbon-rich chemistry and indirectly by aggregating with other carbon-containing matter into sinking particles.

2.6 Methods summary

The accumulation and removal of dissolved organic molecules including the complex polysaccharide fucoidan was investigated in mesocosm experiments with brown algae across the globe (Fig. 3). Six mesocosm experiments with specimens of either Laminariales (4) or Fucales (2) were conducted over 24 days, followed by year-long monitoring of incubation water (Fig. 22A). For the first 12 days, brown algae specimens attached to their original substratum were kept in mesocosms next to control mesocosms without algae. Sampling of 1 L of mesocosm water occurred every second day followed by an exchange of half the mesocosm water with fresh seawater, while recording environmental conditions as well as primary productivity of specimens. After 12 days, specimens were taken out and sampling continued for another 12 days without water exchange. After 24 days of incubation, long-term incubations featuring quarter-yearly sampling started with 6-10 L of water from each mesocosm: one set under a regulated light cycle at 20°C, another set in darkness at 4°C with added nutrients of 40 µM NO_3^- and 3 µM PO_4^{3-}, mimicking surface versus deep sea conditions, not considering differences in pressure. Additional water samples were taken along transects perpendicular to near-shore brown algae populations to track fucoidan concentrations in the environment.

The analysis of obtained water and particulate samples con-

sisted of specific quantification of an organic carbon or carbohydrate fraction accompanied by visual analyses of stained cells and carbohydrates (Fig. 22B-C). Dissolved organic carbon was derived from total organic carbon measurements on glass fiber filtered water. Polysaccharide concentrations and composition of dissolved, anionic and particulate fractions were determined by quantifying monosaccharides after acid-mediated depolymerization. Intact polysaccharides were specifically detected using structure-sensitive monoclonal antibodies, which also semi-quantitatively stained particulate fucoidan. Microbial cells were stained on fixed polycarbonate filters and counted. A detailed description of the materials and experimental procedures can be found below.

2.7 Extended materials and methods

Experimental set-up Algae incubations were carried out at six locations across the world with an abundant local species of the order Laminariales or Fucales (table 2). *Lessonia trabeculata*, *Ecklonia maxima*, *Sargassum fluitans*, *Ecklonia radiata*, *Laminaria digitata* and *Fucus vesiculosus* were incubated in local ambient seawater (Fig. 21A). Incubation volumes ranged between 40 and 250 L. Seawater was pre-filtered at 80 µm for *Lessonia trabeculata* and *Ecklonia maxima* incubations. *Ecklonia radiata* incubations started with unfiltered seawater and were topped up from day two onwards with seawater pre-filtered

at 10 µm and UV treated, except on day ten when new, unfiltered seawater was used. For *Sargassum fluitans*, *Laminaria digitata* and *Fucus vesiculosus* incubations, unfiltered ambient seawater was used. *Lessonia trabeculata*, *Sargassum fluitans*, *Ecklonia radiata* and *Laminaria digitata* were incubated outdoors under ambient light conditions, in the case of *Lessonia trabeculata* and *Ecklonia radiata* under a transparent roof, and 50% shade cloth for *Ecklonia radiata*, whereas *Ecklonia maxima* and *Fucus vesiculosus* incubations were conducted indoors under artificial light conditions. Each mesocosm experiment consisted of six individual tanks, supplied with air and an aquarium pump for water circulation. Water temperatures were kept constant ± 2°C by placing the incubation tanks of *Lessonia trabeculata* (17°C), *Ecklonia maxima* (18°C) and *Ecklonia radiata* (18°C) into a constantly running and cooling water bath. *Laminaria digitata* incubations were cooled to around 17°C using chillers (TECO TK500 G2, France), and *Sargassum fluitans* incubations were heated to 23°C using a heating rod (Eheim Thermocontrol 300, Germany) in the surrounding water bath, with a higher temperature deviation to 16°C on day 8. Fucus vesiculosus was incubated at 14°C in a temperature-controlled room.

Algae biomass Total wet weight of individual algae was taken after the 12-day incubation. In addition, algae were separated into holdfast, stripe, and fronds and weighed independently.

Biomass of *Sargassum fluitans* in the Sargasso Sea experiment was freeze dried, whereas all the other algae were dried at 60°C in an oven to determine dry biomass.

Primary productivity Primary productivity was measured using PyroScience FireSting oxygen probes (Pyroscience GmbH, Germany) during all incubations, except for *Lessonia trabeculata*. For each species and replicate, a single algal frond was incubated for a minimum of 20 min inside a separate 2 L bottle filled with tank water and measuring probes. In the case of *Sargassum fluitans* mesocosms, whole algae were fit into the 2 L bottle. The water was stirred using an underwater propeller (Tamyia, Japan). Temperature and oxygen were measured during each separate incubation. Based on measurement of oxygen production and respiration, we calculated the net primary productivity in µmol O_2 per dry biomass per day. This data was used to calculate the fixed carbon and the ratio of % NPP of mg fucoidan carbon g^{-1} d^{-1} to mg carbon g^{-1} d^{-1}.

PAR measurements The light conditions were determined using the radiation data during the *Lessonia trabeculata* incubation from the Centro de Estudios Avanzados en Zonas Áridas (CEAZA) approximated based on a study [Tsubo and Walker, 2005]. Mesocosms in the *Ecklonia maxima* experiment were each irradiated with a Osram Power Star hqi-e 440W/D

lamp located centrally above mesocosms with a nominal flux of 40000 lumen for 14 hours daily. The PAR data during the *Sargassum fluitans* incubation was recorded by the R/V *Endeavor*. Estimates for PAR during the *Laminaria digitata* incubation experiment at Roscoff, France, were calculated from NASA POWER (https://power.larc.nasa.gov/). PAR measurements were conducted using Hobo logger during *Ecklonia radiata* incubations and RBRsolo logger with an attached PAR sensor (LI-192 Underwater Quantum Sensor) during *Fucus vesiculosus* incubations with a 12/12 light cycle, including two hours of dusk and dawn.

Transects Water samples were taken along transects moving away from seaweed beds at all local mesocosm sites. In Chile, two transects were sampled starting from Algarrobo and Las Cruces. Sampling was performed at 15 m depth at station, 5 m below surface and 30 m at station 2, 5 m below surface and 60 m at station 3 and 5 m below surface and 90 m at station 4. In South Africa, station 1 was sampled at 15 m depths, station 2 at 5 m below surface and 30 m, station 3 at 5 m below surface and 45 m, and station 4 at 5 m and 60 m depth. On cruise R/V *Endeavor* EN683, sampling was conducted at three stations, station 21 to 23, covering depths of 5 m below surface, the deep chlorophyll maximum (DCM), minimum dissolved oxygen (O_2min), and the bottom depth. In Roscoff, France, samples were collected during incoming and outgoing

tides at four distinct stations at 5m below surface and 30 m. In New Zeland, surface and deep samples were taken at four stations. In Finland surface water samples were sampled at five stations moving away from *Fucus vesiculosus* beds. Additionally, sampling included inside and outside assessments of Sargassum patches in Mexico. Sampling activities were conducted at a *Saccharina latissima* farm in Northern Ireland upstream, inside and downstream of the algae farm at 5 m below surface. At each station 3 replicates from the same niskin cast were analysed. Detailed information on sampling locations can be found in supplementary table 3.

Sample analysis Every second day for the first 24 days of incubation 1 L of water was sampled from each tank (Fig. 22B). Afterwards every 3 months 1 L of water was taken from the long-term incubations. 800 mL of the sample was filtered through a pre-combusted (450°C, 4.5 h) 47 mm glass fiber filter (0.7 µm pore size). 20 mL of filtered water were acidified for analysis of dissolved organic carbon. Anionic polysaccharides were extracted and purified from 400 mL of the filtered seawater using anion exchange chromatography (AEX) and eluted with 4 M NaCl. 7.5 mL of unfiltered water for bacterial cell numbers was fixed in a final concentration of 3% formaldehyde solution for 1 h at room temperature. The solution was filtered onto a 47 mm polycarbonate filter with a pore size of 0.22 µm, dried and frozen at -20°C. After 24-days of incu-

bation, tank water was separated into long-term incubations before emptying tanks. Sedimented particles were scooped out from the bottom of the tanks in Chile, South Africa and France (Fig. 22C). Particles were frozen at -20°C until further analysis. Samples were transported frozen to the Max Planck Institute for Marine Microbiology in Bremen, Germany, for further purifications, monosaccharide quantification, antibody binding and cell counting.

DOC Dissolved organic carbon (DOC) was measured at Tvärminne Zoological Station, Hanko, Finland for *Fucus vesiculosus* incubations. Samples were acidified to pH2 using HCL (25%, p.a., Carl Roth, Germany) in pre-combusted glass vials with acid-washed lids. For all other incubations, DOC was measured at the Institute for Chemistry and Biology of the Marine Environment, University of Oldenburg, Germany. Samples were acidified as mentioned above in HDPE-vials. All samples were stored at 4°C in the dark until analysis. Concentrations of DOC were determined using a Shimadzu TOC-V_{CPH}-analyzer. DOC deep sea reference material (DSR; Hansell Biogeochemistry Laboratory, University of Miami, USA) was used for quality control, with accuracy and precision $< 5\%$.

Dialysis To desalt samples, 10 mL of filtered seawater or AEX fractions were transferred to pre-rinsed 1-kDa membranes (Spec-

traPor Biotech CE Dialysis Membrane, Carl Roth, Germany) and dialyzed three times against MilliQ-water at 4°C for a minimum of 12 hours in total. Dialyzed samples were transferred to 15 mL tubes, freeze dried (Labogene, Scanvac Coolsafe, Denmark) and resuspended in 2 mL MilliQ water.

Acid hydrolysis To convert polysaccharides into quantifiable monosaccharides, 500 µL of the dialysed, resuspended samples were combined with 500 µL 2 M HCL in pre-combusted glass vials (450°C, 4.5 h), which were sealed. Polysaccharides were hydrolysed at 100°C for 24 h. After hydrolysis, the samples were transferred to microtubes and dried in an acid-resistant vacuum concentrator (Martin Christ Gefriertrocknungsanlagen GmbH, Germany). Samples were resuspended in 500 µL MilliQ-water.

Monosaccharide quantification Monosaccharides were quantified using anion exchange chromatography with pulsed amperometric detection (HPAEC-PAD), as previously described [Engel and Händel, 2011, Vidal-Melgosa et al., 2021]. Samples were analyzed using a Dionex ICS-5000+ system equipped with a CarboPac PA10 analytical column (2 x 250 mm) and a CarboPac PA10 guard column (2 x 50 mm). Neutral and amino sugars were separated during an isocratic phase with 18 mM NaOH followed by a gradient reaching up to 200 mM

NaCH3COO to resolve acidic monosaccharides.

Carbohydrate microarray analysis Monoclonal antibodies targeting brown algae polysaccharides were employed to screen mesocosm samples for dissolved carbohydrates. Filtered and dialysed samples were concentrated by a factor of 20 prior to analysis with carbohydrate microarrays by printing aliquots onto nitrocellulose membrane and measuring antibody binding via colorimetric signal [Torode et al., 2015, Vidal-Melgosa et al., 2021]. Extracted fucoidan from the incubated algal biomass, alginate (Sigma), laminarin (Carbosynth) and mixed-linked glucan (Megazyme) were used as standards at concentrations of 2.5, 5, 10 and 20 mg L^{-1}. The printed microarrays were blocked in MPBS for 1 h and incubated individually for 2 h with the monoclonal antibodies BAM1, BAM2, BAM7, LM21, BS400-2, BS400-4 and the anti-rat control at a concentration of 10 µg mL^{-1} [Torode et al., 2015, 2016]. The arrays were washed with PBS and incubated with secondary antibodies in MPBS for 2 h, then washed again in PBS and deionised water. The arrays were developed in 5-bromo-4-chloro-3-indolyl phosphate and nitroblue tetrazolium in alkaline phosphatase buffer (100 mM NaCl, 5 mM MgCl2, 100 mM Tris-HCl, pH 9.5) and analyzed with the software Arrray-Pro Analyzer 6.3 (Media Cybernetics).

Fucoidan extraction Fucoidan was extracted from seawater

using anion exchange columns. 400 mL of GF/F filtered seawater samples passed through 5 mL HiTrap ANX high sub FF columns (Cytiva), which had been conditioned with 25 mL of 0.5 M NaCl and 20 mM Tris-HCl (pH=8), 25 mL of 4 M NaCl and 20 mM Tris-HCl (pH=8) and again with 25 mL of 0.5 M NaCl and 20 mM Tris-HCl (pH=8), all at 5 mL min-1 flow rate. For washing, 30 mL of 0.5 M NaCl and 20 mM Tris-HCl (pH=8) was applied after the sample and combined with the sample flow through. To elute anionic fucoidan, 12 mL of 4 M NaCl and 20 mM Tris-HCl (pH=8) was passed over the columns at 5 mL min^{-1} and collected in a 15-mL tube. The 15-mL tubes were stored at 4°C until further processing. The columns were cleaned with 25 ml MilliQ at 5 mL min^{-1} flow rate, 20 mL 1 M NaOH at 1 mL min^{-1} flow rate and 25 ml MilliQ at 5 mL min^{-1} flow rate.

Fucoidan extraction from biomass Biomass was dried at 60°C in an oven or in case of Sargassum biomass freeze-dried. Dried biomass was processed and fucoidan extracted as described in a recent study [Thobor et al., 2024]. The obtained fucoidan powder was used at different concentrations to prepare fucoidan standards.

Particulate organic carbon GF/F filters were cut, with 20-35% of the total cut filters weighed and placed in an acid

desiccator overnight. The filter pieces were dried in an oven at 60°C for 2 hours, packed into tin cups, and compressed. Particulate organic carbon (POC) was quantified using a Vario Micro Cube (Elementar Analysensysteme) calibrated with sulfanilamide standards.

Particulate fucoidan GF/F filters were cut and weighed. 15% of the cut GF/F filters were directly acid hydrolysed in 600 µL of 1M HCl at 100°C for 24hrs in glass vials. The supernatant was transferred, dried and resuspended in the same amount. Monosaccharides were quantified using HPAEC-PAD (see above).

Sequential extraction and ELISA BAM1 Approximately from 20% of the cut GF/F filters, polysaccharides were sequentially extracted using MilliQ-water and 0.3 M EDTA. Filter pieces were mixed with 1.8 mL of MilliQ-water, vortexed and kept in an ultrasonic water bath for 1 hour. Filters were centrifuged at 6000G for 15 min. Supernatant was transferred into a new vial and filter pieces were mixed with 1.8 mL of 0.3 M EDTA, vortexed and kept in an ultrasonic water bath for 1 hour. Filters were centrifuged at 6000G for 15 min and supernatant was again transferred into a new vial. Extracts of MilliQ and EDTA were combined for further analysis by pipetting 50 µl of each into a pre-coated 96 well plate to settle overnight at 4°C. Solu-

tion in each well was removed the next day, 200 µL of 5% skim milk in PBS was added to each well and incubated for 2 hours. After incubation skim milk was removed, wells were washed 9 times with deionized water and 100 µL of antibody BAM1 in skim milk PBS solution at a concentration of 1:10 was added into each well and incubated for 1.5 hours. Antibody-mix was removed afterwards and wells were washed 6 times with deionized water and 100 µL of secondary antibody anti-rat in skim milk PBS solution at a concentration of 1:10000 was added into each well and incubated for 1.5 hours. Antibody-mix was removed afterwards and wells were washed 6 times with deionized water. Development solution was added and stopped after 15 min with 1M HCl. Absorption was measured at 450 nm using Spectramax Id3 plate reader (Molecular Devices).

Immunolabeling on filters Frozen filters were cut into pieces and filter sections were incubated in 400 µl 5% skim milk in PBS for 1 hour inside tubes. After blocking, solution was replaced with 200 µl of primary antibody BAM1 at 1:5 dilution in skim milk PBS for 1.5 hours. After incubation filter sections were washed 4 times with 1 mL of PBS. 200 µl of secondary antibody anti-rat FITC conjugated at 1:100 dilution were added to filters inside the tube and incubated for 1.5 hours in darkness. Filter sections were afterwards washed 4 times with 1 mL of PBS. Afterwards filter sections were stained with DAPI (see below).

Cell counts Frozen filters were cut into pieces and filter sections were mounted on glass slides with premixed 4',6-Diamidino-2-phenylindole (DAPI) 1:1000 diluted in the antifading reagents Citifluor:Vectashield as 4:1 (v/v).

Microscopy Slides were covered and stored at 4°C in the dark. Cells were counted and immunolabeled filter sections for BAM1 fucoidan binding were visualized using Nikon 50i with Zeiss AxioCam MRc at 100 x magnification (Plan Apo VC objective). Sedimented particles were imaged using Thermo Scientific Invitrogen EVOS FL Auto Imaging System at 20x magnification Brightfield.

Data analysis Fucoidan concentrations were calculated from fucose HPAEC-PAD data based on fucose concentrations in acid-hydrolysed fucoidan standards. Fucoidan was extracted from algae biomass and added to seawater at different concentrations. The dissolved fucoidan in seawater was then processed with mesocosm and transect samples. Fucoidan standards were added to GF/F filter pieces and processed together with samples. In this way, specific fucoidan standard series were generated for samples before and after charge-selection and particulate samples for each algal species. The calibrated dissolved fucoidan concentrations served to calculate a cumu-

lative fucoidan value by accounting for water exchanges during the incubation of brown algae. For each independent mesocosm until day 12, half the concentration measured during the previous sampling prior to the water exchange was added to calculate the cumulative value. The cumulative values were used to calculate the change in fucoidan concentrations between two sampling events. As this value was highly susceptible to measurement error, we also calculated a sliding window-change in fucoidan concentrations which spanned four sampling events. All values were calculated separately for fucoidan selected based on size and fucoidan selected based on size and charge.

To assess the drivers of fucoidan accumulation and removal in mesocosms, a series of hierarchical Bayesian models was computed using the package Rstantools in R version 4.3.3 (R core team, [R Core Team, 2020, Gabry et al., 2024]). Mesocosm incubations with *Ecklonia maxima* (Cape Town, South Africa) and *Laminaria digitata* (Roscoff, France) were excluded from the analysis due to the experimental flaws stated in the results section. First, two models that included wither the actual concentrations of size-selected and size- and charge-selected fucoidan or the cumulative concentrations as dependent variables were constructed, with presence/absence of brown algae and incubation period as fixed factors and location and day of incubation as random factors. Fucoidan concentrations were assumed to be normally distributed. Over 3000 iterations, posterior distributions were calculated and recorded after 1000 warm

up iterations. Second, a model that used the sliding window-changes in size-selected and size- and charge-selected fucoidan concentrations dependent on brown algae biomass scaled to mesocosm volume and fucoidan concentration during the previous sampling event was computed. Sliding window changes were assumed to be normally distributed. This model had no intercept and included location and mesocosm nested within location as random factors. Over 5000 iterations, posterior distributions were calculated and recorded after 1000 warm up iterations with a thinning factor of 2. The posterior distributions of the effect of brown algae biomass and previous fucoidan concentration were analyzed by simulating mesocosm incubations at 20 locations. Random effects of location and mesocosm were included in the simulation. As during the actual experiments, water exchanges were simulated to account for the diluting effect on fucoidan concentrations. Biomass per volume ratios were drawn from the physical mesocosm experiments. To estimate the global secretion of fucoidan, 500 simulations based on the posterior distribution of the brown algae biomass effect were performed. Global biomass estimates were sourced from a normal distribution with a mean of 1015 kg and a standard deviation of 2x1014 kg [Filbee-Dexter et al., 2024]. These simulations were run for both size-selected and size- and charge-selected fucoidan and accounted for the posterior distribution of the random effect of location.

Persistence of fucoidan concentrations in all incubations com-

bined was tested using paired statistical tests. Normality was tested using Shapiro-Wilk test. Differences between mesocosms with brown algae and mesocosms without brown algae were tested for normally distributed data with paired t-tests. Due to predominantly non-normally distributed data, Wilcoxon tests were employed. Correlation of particulate organic carbon and particulate fucoidan concentrations over time for all incubations combined were determined using linear correlation.
The occurrence map (Fig. 3) was plotted using R packages 'marmap' [Pante and Simon-Bouhet, 2013] and 'sf' [Bivand, 2021].

2.8 Acknowledgements

The authors thank technicians at Max-Planck Institute for Marine Microbiology and Marum Centre for Environmental Research, University of Bremen, namely Tina Horstmann for carbohydrate microarray analysis, Alek Bolte and Katharina Föll for HPAEC-PAD measurements and Gabriele Klockgether for particulate organic carbon measurements, as well as Fernanda Vargas Acevedo, Ricardo Calderón from Estación Costera de Investigaciones Marinas, Chile, Alistair Busby, Chris JT Boothroyd, Derek Kemp, John Boton and Andrea Plos from the Department of Forestry, Fisheries and the Environment and the Department of Biological Sciences, University of Cape Town, South Africa, Lynne Butler, Bonny Clarke, the chief engineer, the cap-

tain and the crew of the R/V *Endeavor* during cruise EN683, Ari Brandenburg and Chris Blake with the University of Waikato at Sulphur Point, Tauranga, New Zealand, M. Guadalupe Barba-Santos and Evelyn Raquel Salas-Acosta in the reef systems research unit at Puerto Morelos, Universidad Nacional Autónoma de México, Lena Eggers, Katherine Jones and Philipp Hach with the Alfred-Wegener Institute in Bremerhaven, Germany, the crew of R/V *Neomysis* and the Roscoff Aquarium Services platform part of EMBRC-France supported by the Investments of the Future program (ANR-10-INSB-02), for its technical assistance and support at the Station Biologique de Roscoff, France, and Joanna Norkko, Jaana Koistinen, Eva Rohlfer from Tvärminne Zoological Station for their assistance in field and lab work, and Islander Kelp in Northern Ireland for support with water sampling inside their kelp farm. The authors thank Hussein Awwad, Mohammed Shahin, Carla Knappik and Daria Gulenko for their support with sample processing. Funding: The authors acknowledge invaluable support from the Max-Planck-Society, the DFG Heisenberg grant for Glyco-Carbon Cycling in the Ocean and the Cluster of Excellence initiative (EXC-2077–390741603), Simons Collaboration on Principles of Microbial Ecosystems, European Research Council grant for project C-Quest, the sea4SoCiety, CDRmare campaign in the German Marine Research Alliance (for funding incubations in Finland), the Entrepreneurial Universities Macroalgal Biotechnologies Programme supported by the Tertiary Education Com-

mission (TEC) and the University of Waikato, New Zealand, the CoastClim, Coastal Ecosystem and Climate Research project, Finland, and funding from the U.S. National Science Foundation (OCE-1736772 and OCE-2022952 to CA).

2.9 Supplementary information

Table 2 to 3
Fig. 21 to 22

2.9.1 Supplementary tables

Table 2: Overview of species, sampling time, location and incubation volume of all different experiments.

Species	Sampling time	Location	Coordinates	Incubation volume
Ecklonia maxima	March 2022	South Africa, Southern Atlantic	-33.9296, 18.3807	220 L
Ecklonia radiata	May 2022	New Zealand, Southern Pacific	-37.6711, 176.1672	220 L
Laminaria digitata	August 2022	France, The English Channel	48.7272, -3.9873	250 L
Lessonia trabeculata	January 2022	Chile, Southern Pacific	-33.5021, -71.6337	250 L
Fucus vesiculosus	October 2022	Finland, Baltic Sea	59.8445, 23.2494	57 L
Sargassum fluitans	May 2022	United States of America, Sargasso Sea	35.1961, -70.0048	40 L

Table 3: Overview of transect sampling, including country, location, station, species, longitude and latitude.

Species	Country	Location	Station	Distance to algae	Longitude	Latitude
Ecklonia maxima	South Africa	Seapoint	Stn1	0.4km	33°55.200'S	18°22.405'E
Ecklonia maxima	South Africa	Seapoint	Stn2	1.8km	33°54.830'S	18°21.613'E
Ecklonia maxima	South Africa	Seapoint	Stn3	3.7km	33°54.033'S	18°20.783'E
Ecklonia maxima	South Africa	Seapoint	Stn4	4.8km	33°54.025'S	18°19.889'E
Ecklonia radidata	New Zealand	Tauranga	Stn1	4.5km	37°37'40.73"S	176°21'46.84"E
Ecklonia radidata	New Zealand	Tauranga	Stn2	0km	37°39'2.29"S	176°24'35.08"E
Ecklonia radidata	New Zealand	Tauranga	Stn3	1.3km	37°39'3.97"S	176°25'24.94"E
Ecklonia radidata	New Zealand	Tauranga	Stn4	1.9km	37°39'8.80"S	176°25'53.90"E

Species	Country	Location	Station	Distance to algae	Longitude	Latitude
Laminaria digitata	France	Roscoff	Stn1-incoming	0km	48°42.878'N	3°57.355'W
Laminaria digitata	France	Roscoff	Stn2-incoming	1.5km	48°43.637'N	3°57.091'W
Laminaria digitata	France	Roscoff	Stn3-incoming	3.3km	48°44.635'N	3°56.722'W
Laminaria digitata	France	Roscoff	Stn4-incoming	4km	48°45.023'N	3°56.593'W
Laminaria digitata	France	Roscoff	Stn1-outgoing	0km	48°42.896'N	3°57.353'W
Laminaria digitata	France	Roscoff	Stn2-outgoing	1.5km	48°43.641'N	3°57.079'W
Laminaria digitata	France	Roscoff	Stn3-outgoing	3.3km	48°44.661'N	3°56.716'W

Species	Country	Location	Station	Distance to algae	Longitude	Latitude
Laminaria digitata	France	Roscoff	Stn4-outgoing	4km	48°45.047'N	3°56.641'W
Lessonia trabeculata	Chile	Las Cruces	Stn1	0.7km	33°29'24.64"S	71°39'4.47"W
Lessonia trabeculata	Chile	Las Cruces	Stn2	2km	33°29'21.45"S	71°39'53.85"W
Lessonia trabeculata	Chile	Las Cruces	Stn3	3km	33°29'26.20"S	71°40'39.35"W
Lessonia trabeculata	Chile	Las Cruces	Stn4	4.8km	33°29'6.41"S	71°41'41.07"W
Lessonia trabeculata	Chile	Algarrobo	Stn1	0.5km	33°21'22.13"S	71°41'34.32"W
Lessonia trabeculata	Chile	Algarrobo	Stn2	1.5km	33°20'56.05"S	71°42'4.82"W

Species	Country	Location	Station	Distance to algae	Longitude	Latitude
Lessonia trabeculata	Chile	Algarrobo	Stn3	2km	33°21'31.73"S	71°42'38.74"W
Lessonia trabeculata	Chile	Algarrobo	Stn4	3.3km	33°22'5.80"S	71°43'25.40"W
Saccharina latissima	Northern Ireland	Rathlin	upstream	0.1km	55°17.225'N	6°13.555'W
Saccharina latissima	Northern Ireland	Rathlin	upstream	0.1km	55°17.345'N	6°13.551'W
Saccharina latissima	Northern Ireland	Rathlin	kelp farm	0km	55°17.364'N	6°13.481'W
Saccharina latissima	Northern Ireland	Rathlin	kelp farm	0km	55°17.368'N	6°13.460'W
Saccharina latissima	Northern Ireland	Rathlin	kelp farm	0km	55°17.371'N	6°13.412'W
Saccharina latissima	Northern Ireland	Rathlin	downstream	0.2km	55°17.375'N	6°13.346'W
Saccharina latissima	Northern Ireland	Rathlin	downstream	0.2km	55°17.389'N	6°13.305'W
Saccharina latissima	Northern Ireland	Rathlin	downstream	0.2km	55°17.396'N	6°13.281'W

Species	Country	Location	Station	Distance to algae	Longitude	Latitude
Saccharina latissima	Northern Ireland	Rathlin	down-stream	0.2km	55°17.406'N	6°13.256'W
Fucus vesiculosus	Finland	Tvärminne	Stn1	0km	59°48.849'N	23°14.802'E
Fucus vesiculosus	Finland	Tvärminne	Stn2	1km	59°48.643'N	23°13.835'E
Fucus vesiculosus	Finland	Tvärminne	Stn3	2.3km	59°48.327'N	23°12.529'E
Fucus vesiculosus	Finland	Tvärminne	Stn4	3.4km	59°48.107'N	23°11.502'E
Fucus vesiculosus	Finland	Tvärminne	Stn5	5km	59°47.745'N	23°9.907'E
Sargassum fluitans	United States	Western North Atlantic	Stn21	0km	33.740°N	75.291°W
Sargassum fluitans	United States	Western North Atlantic	Stn22	2100km	42.86173°N	53.86997°W

Species	Country	Location	Station	Distance to algae	Longitude	Latitude
Sargassum fluitans	United States	Western North Atlantic	Stn23	500km	34°04'59.0"N	70°05'52.0"W
Sargassum fluitans	Mexico	Puerto Morales	Patch	inside	20°49'56.89"N	86°52'15.41"W
Sargassum fluitans	Mexico	Puerto Morales	Patch	outside -50m away	20°49'56.89"N	86°52'15.41"W

2.9.2 Supplementary figures

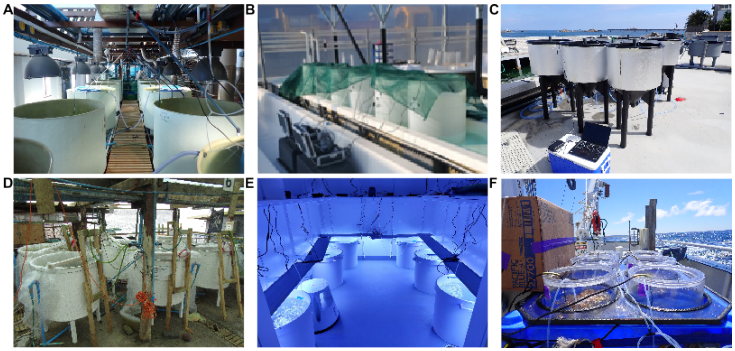

Figure 6: **Tank systems of algae incubations. A)** *Ecklonia maxima* in South Africa, **B)** *Ecklonia radiata* in New Zealand, **C)** *Laminaria digitata* in France, **D)** *Lessonia trabeculata* in Chile, **E)** *Fucus vesiculosus* in Finland and **F)** *Sargassum fluitans* in the Western North Atlantic.

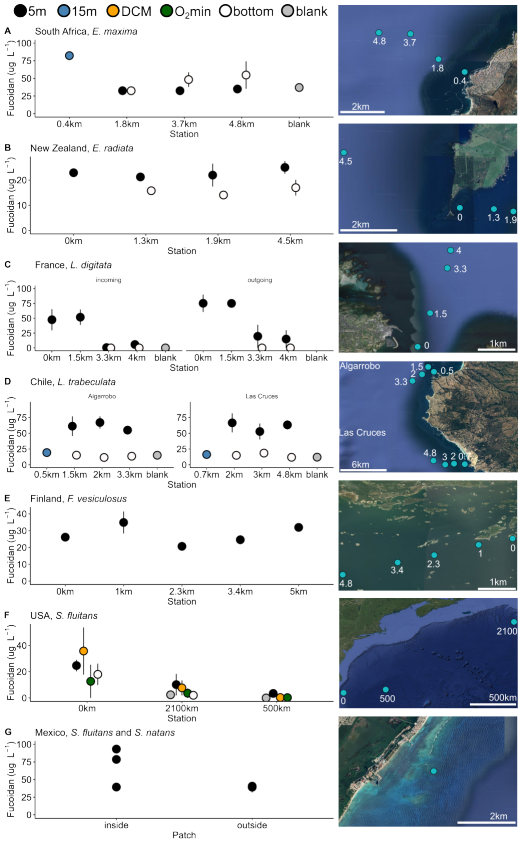

Figure 7: **Fucoidan concentrations (ug L^{-1}) after purification via anion exchange purification (AEX) in surface and bottom waters moving away from coastline.**.Water samples taken at depths of 5m (black), 15m (blue), deep chlorophyll maximum (yellow), O_2 minimum zone (green), bottom (white)

Figure 7: and MilliQ blank samples processed with samples (grey) on the right plus sample maps on the left. **A)** South Africa, *E. maxima*, 0.4km away from coast sampled at 15m, 1.8km: 5m and 30m, 3.7km: 5m and 45m, 4.8km: 5m and 60m; **B)** New Zealand, *E. radiata* sampled at surface and bottom 0 to 4.8km away from algae bed; **C)** France, *L. digitata*, sampled during incoming and outgoing tides at four different stations in 5m and 30m depths (0 to 4km away from algae bed); **D)** Chile, *L. trabeculata*, Las Cruces, sampled at 0.5km away from coast at 15m, 1.5km away at 5m and 30m, 2 km away at 5m and 60m and 3.3 km away at 5m and 90m. In Algarrobo sampled at 15m 0.7km away from coast, at 5m and 30m 2km away, at 5m and 60m 3km away and at 5m and 90m 4.8km away from algae bed; **E)** Finland surface water sampling moving away up to 5 km from *Fucus vesiculosus* bed; **F)** USA, *S. fluitans*, on board R/V *Endeavor*, stations 21 -23, sampled 5m, DCM, O2 min and bottom. Station 21 is closest to coastline, around *S. fluitans* (0km), station 22 around 2100 km away and station 23 around 500km away from *S. fluitans*; **G)** Mexico, *S. fluitans* and *S. natans*, surface water samples taken inside and outside (around 50m away) of *Sargassum* patches. Fucoidan concentrations based on fucose concentrations of fucoidan standards extracted from biomass, except for *S. latissima* concentrations, which are calculated based on 30% of fucose.

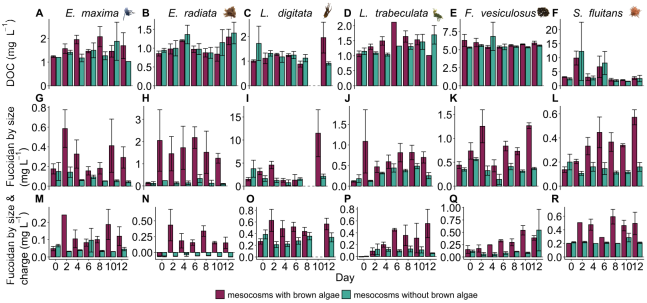

Figure 8: **Fucoidan concentrations by all tested brown algae over 12 days of incubation. A-F)** DOC concentrations (µM), **G-L)** fucoidan selected by size, **M-R)** and fucoidan concentrations selected by size and charge during 12-day incubations in mesocosms with brown algae (red bars) and without brown algae (teal bars). Bars represent the mean of three mesocosm replicates with error bars indicating standard errors.

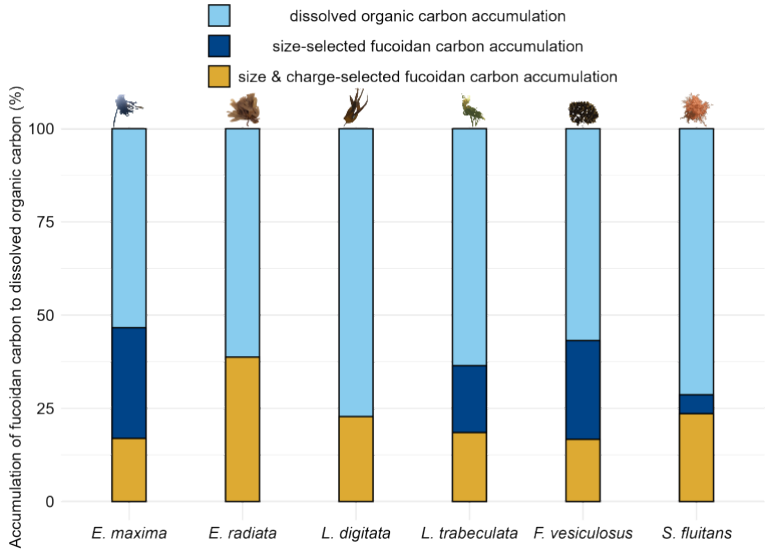

Figure 9: **Up to 50% of total dissolved organic carbon (DOC) can be attributed to fucoidan carbon. Up to 30% confirmed by anionic fucoidan fraction after size and charge selection.** DOC concentrations were set to 100% to calculate relative fucoidan carbon accumulation. Without and with charge-selection refers to the quantified fucose in bulk hydrolysable polymers $>$ 1kDa without and with specific anion exchange chromatography, targeting the negatively charged fucoidan fraction. Fucoidan carbon to DOC revealed the following values: *E. maxima*: 47% by size, 17% by size and charge; *L. digitata*: 23% by size and charge; *E. radiata*: 39% by size (estimated by size were excluded from this graph, due to more fucoidan being present in estimates than quantified DOC); *L. trabeculata*: 36% by size, 18% by size and charge;

Figure 9: *F. vesiculosus*: 43% by size, 16% by size and charge; *S. fluitans*: 29% by size, 24% by size and charge (DOC concentrations above 500 µM were excluded for *S. fluitans* incubations due to contamination).

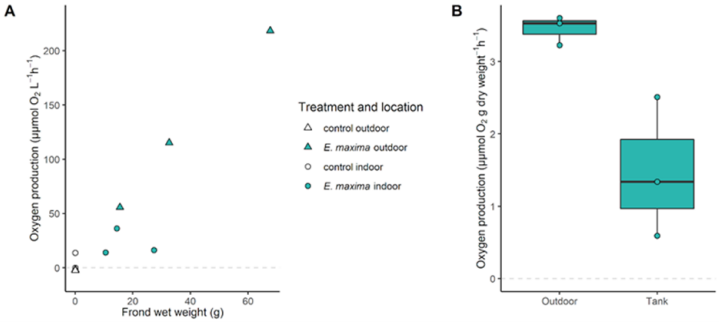

Figure 10: **Substantially higher oxygen production of *in situ E. maxima* specimens compared to specimens kept indoor in tanks. A)** Oxygen production scaled with wet weight of incubated fronds for outdoor algae (teal triangles) but not for indoor algae (teal circles) with control incubations in white. **B)** Oxygen production for outdoor algae in natural light exceeded oxygen production for tank algae under artificial light.

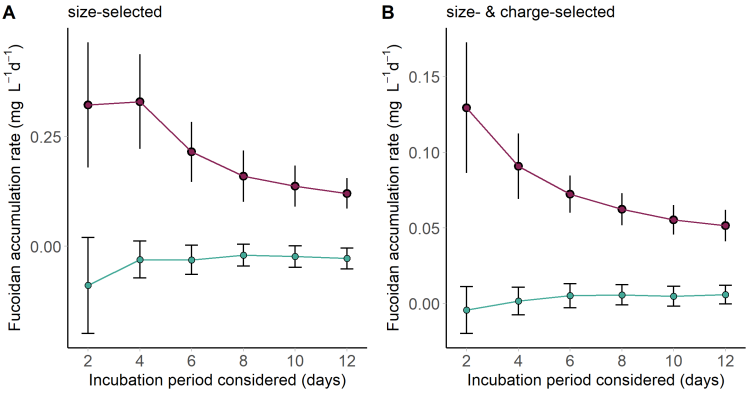

Figure 11: **Fucoidan accumulation rates peak during the first four days of incubation.** Fucoidan accumulation rate in mesocosms with brown algae (red) and mesocosms without brown algae (teal) in mg L^{-1} d^{-1} over 12 days of incubation **A)** size-selected estimates and **B)** size- and charge-selected estimates.

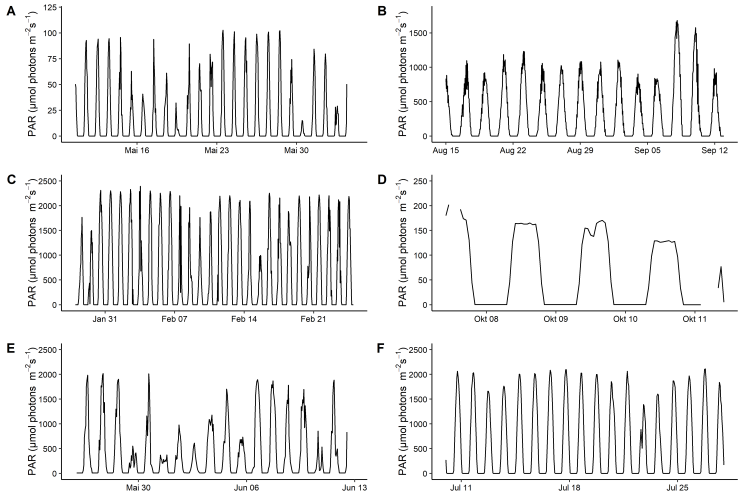

Figure 12: **Hourly means of photosynthetically active radiation (PAR) during brown algae incubations. A)** PAR measurements were conducted using Hobo loggers in each tank during *Ecklonia radiata* incubations, with tank 3 depicted in red to visualize lower PAR due to shading by a large algae specimen until taken out on May 22. **B)** Estimates for PAR during the *Laminaria digitata* incubation experiment at Roscoff, France, were calculated from NASA POWER (https://power.larc.nasa.gov/) all sky surface total PAR. **C)** Radiation data for the *Lessonia trabeculata* incubation from the meteorological station of the Centro de Estudios Avanzados en Zonas Áridas (CEAZA) at Las Cruces, Chile. **D)** A RBRsolo logger with an attached PAR-sensor (LI-192 Underwater Quantum Sensor) was used to measure PAR in one tank during *Fucus vesiculosus* incubations. **E)** The PAR data during the *Sargassum fluitans* incubation was recorded by R/V *Endeavor*.

Figure 12: **F)** Estimates for PAR during *Sargassum fluitans* bottle incubations at Puerto Morelos, Mexico, were calculated from NASA POWER (https://power.larc.nasa.gov/) all sky surface total PAR. No PAR data is available for *Saccharina latissima* algae farm sampling and for *Ecklonia maxima* mesocosms experiment irradiated with a Osram Power Star hqi-e 440W/D lamp located centrally above mesocosms with a nominal flux of 40000 lumen for 14 hours daily.

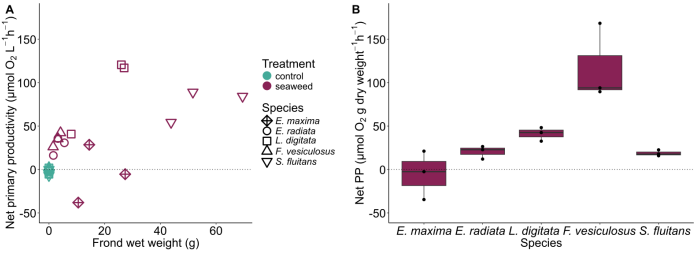

Figure 13: **Net primary production calculated and scaled with incubated biomass. A)** Oxygen production in light and respiration in dark converted to net primary productivity and plotted against wet weight of the frond incubated to measure oxygen evolution. Data points at zero-intercept of x-axis mark control mesocosms without brown algae. **B)** Net primary production per g dry weight of the incubated frond plotted by species. No data on oxygen production or consumption data are available for the incubation of *Lessonia trabeculata*.

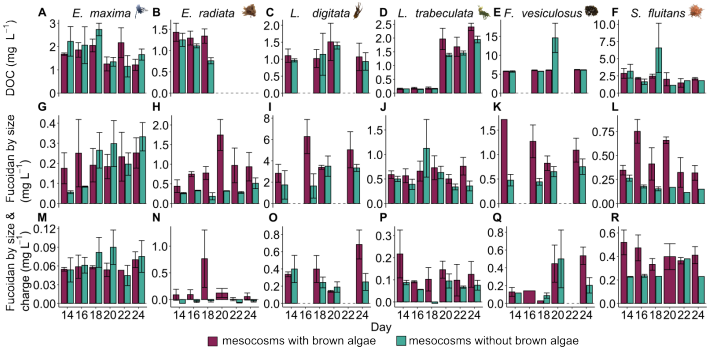

Figure 14: **Fucoidan concentrations by all tested brown algae over 12 days of incubation after removal of brown algae (day 14 to 24). A-F)** DOC concentrations (mg L^{-1}), **G-L)** size-selected fucoidan, **M-R)** and size and charge-selected fucoidan concentrations during 12-day incubations after removal of brown algae in mesocosms with (red bars) and without brown algae (teal bars). Bars represent the mean of three mesocosm replicates with error bars indicating standard errors.

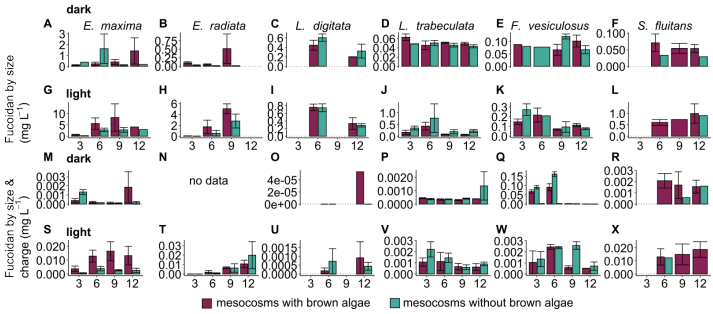

Figure 15: **Fucoidan concentrations (mg L^{-1}) by all tested brown algae over year long incubation (3-12 months)**. **A-F)** Size-selected fucoidan during dark incubations and **G-L)** light incubations and **M-R)** size and charge-selected fucoidan concentrations during dark and **S-X)** light incubations in mesocosms with brown algae (red bars) and without brown algae (teal bars). Bars represent the mean of three mesocosm replicates with error bars indicating standard errors. **N)** No data available for *E. radiata* incubation, quantified based on size and charge-selected fucoidan.

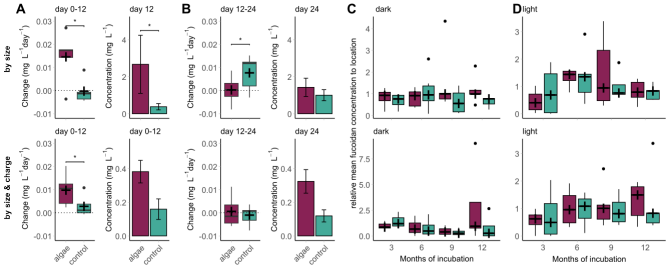

Figure 16: **Secreted fucoidan persists. A-D)** Fucoidan estimates selected by size. **A)** Significant change in fucoidan concentrations (mg L^{-1} d^{-1}) between algae and controls from day 0 to day 12 (p=0.03125, Wilcoxon-Test). Significantly higher fucoidan concentrations ±s.e.m (mg L^{-1}) between algae and controls on day 12 (algae: p=0.03125 vs. controls: p= 0.07278, Wilcoxon-Test). **B)** Change in fucoidan concentrations (mg L^{-1} d^{-1}) between algae and control tanks after brown algae were removed, from day 12 to day 24. Significant increase in fucoidan concentrations ±s.e.m (mg L^{-1}) in control mesocosm (p= 0.03125, Wilcoxon-Test). No significant differences in concentrations between algae and control tanks on day 24 (p=0.0625, Wilcoxon-Test). **C)** Relative mean fucoidan concentrations to each location in dark-incubated mesocosm water, sampled every 3 months for 1 year. No significant differences, based on Wilcoxon-Test. **D)** Relative mean fucoidan concentrations to each location in light-incubated mesocosm water, sampled every 3 months for 1 year. No significant differences, based on Wilcoxon-Test.

Figure 16: **E-H)** Fucoidan estimates selected by size and charge. **E)** Significant change in fucoidan concentrations (mg L^{-1} d^{-1}) between algae and controls from day 0 to day 12 (p=0.03125, Wilcoxon-Test). No significant difference in fucoidan concentrations $\pm$s.e.m (mg L^{-1}) between algae and controls on day 12 (p= 0.07278, Wilcoxon-Test). **F)** No significant change in fucoidan concentrations between algae and control tanks after brown algae were removed, from day 12 to day 24 (p=0.8438, Wilcoxon-Test) and no significant differences in concentrations $\pm$s.e.m (mg L^{-1}) between algae and control tanks on day 24 (p= 0.05072, Wilcoxon-Test). **G)** Relative mean fucoidan concentrations to each location in dark-incubated mesocosm water, sampled every 3 months for 1 year. No significant differences, based on Wilcoxon-Test. **H)** Relative mean fucoidan concentrations to each location in light-incubated mesocosm water, sampled every 3 months for 1 year. No significant differences, based on Wilcoxon-Test.

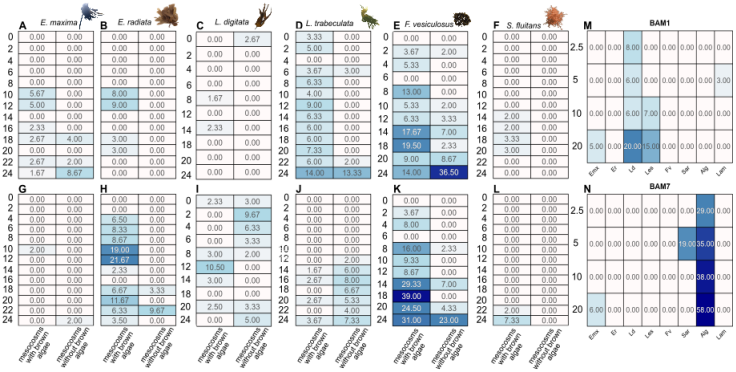

Figure 17: **Fucoidan-specific monoclonal antibody BAM1 confirmed persistence of dissolved fucoidan in *L. trabeculata* mesocosms. A-F, M)** Signals of fucoidan-specific BAM1 and **G-L, N)** alginate- and pectin-specific BAM7 in triplicate mesocosms with and without brown algae over 24 days. Each signal represents mean values of **A, G)** *E. maxima*, **B, H)** *E. radiata*, **(C, I)**, *L.digitata*, **D, J)** *L. trabeculata*, **E, K)**, *F. vesiculosus*, **F, L)** *S. fluitans*, **M)** BAM1 and **N)** BAM7 binding to standard series of fucoidans (concentrations in mg L^{-1} on left) extracted from biomass (Emx: *E. maxima* fucoidan, Er: *E. radiata* fucoidan, L.d: *L. digitata* fucoidan, Les: *L. trabeculata* fucoidan, F.v.: *F. vesiculosus* fucoidan, Sar: *S. fluitans* fucoidan) and alginate (ALG) and laminarin (LAM) indicate antibody specificity and detection ranges. Boxes are coloured according to antibody signals.

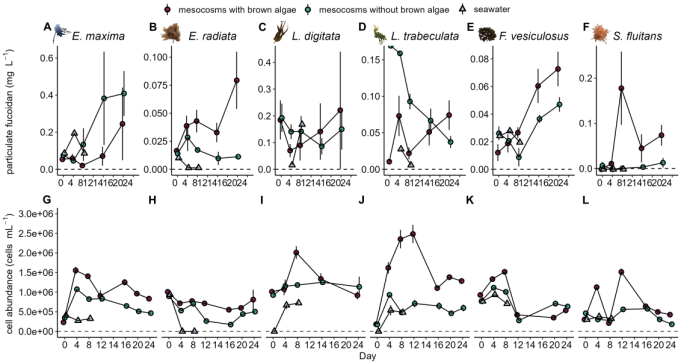

Figure 18: **Fucoidan aggregates with microbial cells. A-F)** Particulate fucoidan concentrations during incubations in brown algae (red circle) and control mesocosms (teal circle) fresh seawater (blue triangle). **G-L)** Microbial cell abundance estimated from DAPI-stained 0.2 µm polycarbonate filters for brown algae (red circle) and control mesocosms (teal circle), as well as fresh seawater (blue triangle).

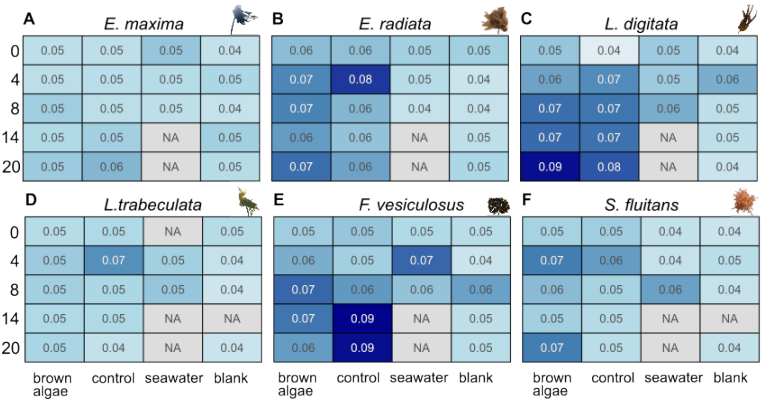

Figure 19: **Fucoidan specific BAM1 antibody signal in particulate fraction in brown algae and control incubations.** BAM1 signal in particulate fraction increases from day 0 to day 4 of all incubations, and is stable after day 4, measured for day 8, 14 and 20. No difference in signal between brown algae and control tanks of the following incubations **A)** *E. maxima*, **B)** *E. radiata*, **C)** *L. digitata*, **D)** *L. trabeculata*, **E)** *F. vesiculosus* and **F)** *S. fluitans*.

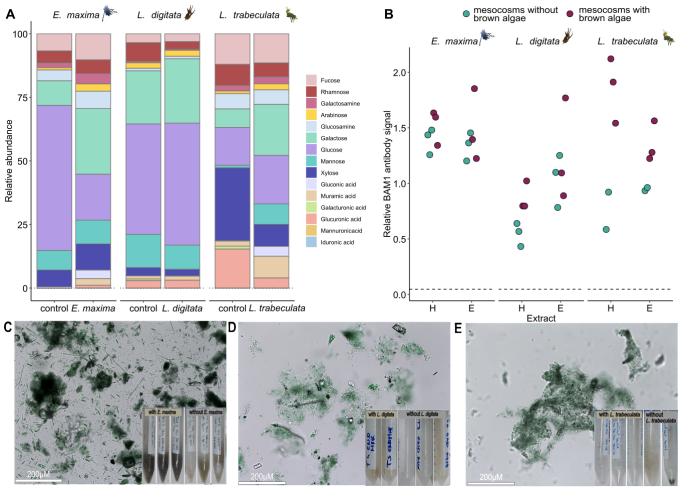

Figure 20: **Fucoidan presence confirmed in sedimented particles.** Sedimented particles of *Ecklonia maxima*, *Laminaria digitata*, *Lessonia trabeculata* and control (without brown algae) mesocosms sampled on day 24 of incubations. **A)** Relative abundance of monosaccharide of particles, dominated by glucose and galactose. **B)** BAM1 specific antibody binding to water (H) and EDTA (E) extracts of particles in brown algae tanks, as well as tanks without brown algae showing presence of fucoidan in sedimented particles originating from macro- and microalgae. **C-E)** Brightfield image of sedimented particles and particulate sampled in **C)** *E. maxima*, **D)** *L. digitata* and **E)** *L. trabeculata* incubations.

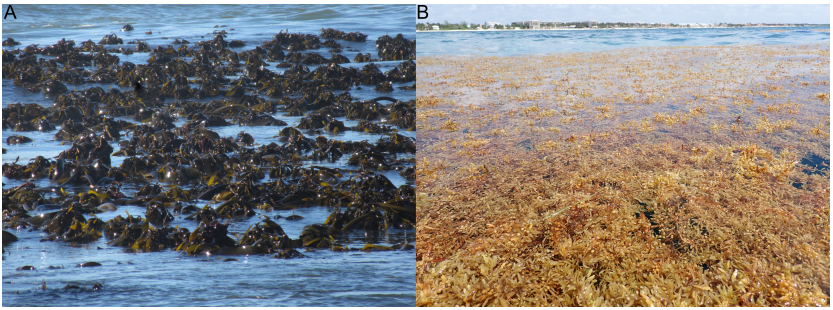

Figure 21: **Emerged algae of A) Laminariales and B) Fucales**. Photos showing some of the incubated algal species **A)** *Ecklonia maxima* in South Africa, **B)** *Sargassum fluitans* and *natans* in Mexico.

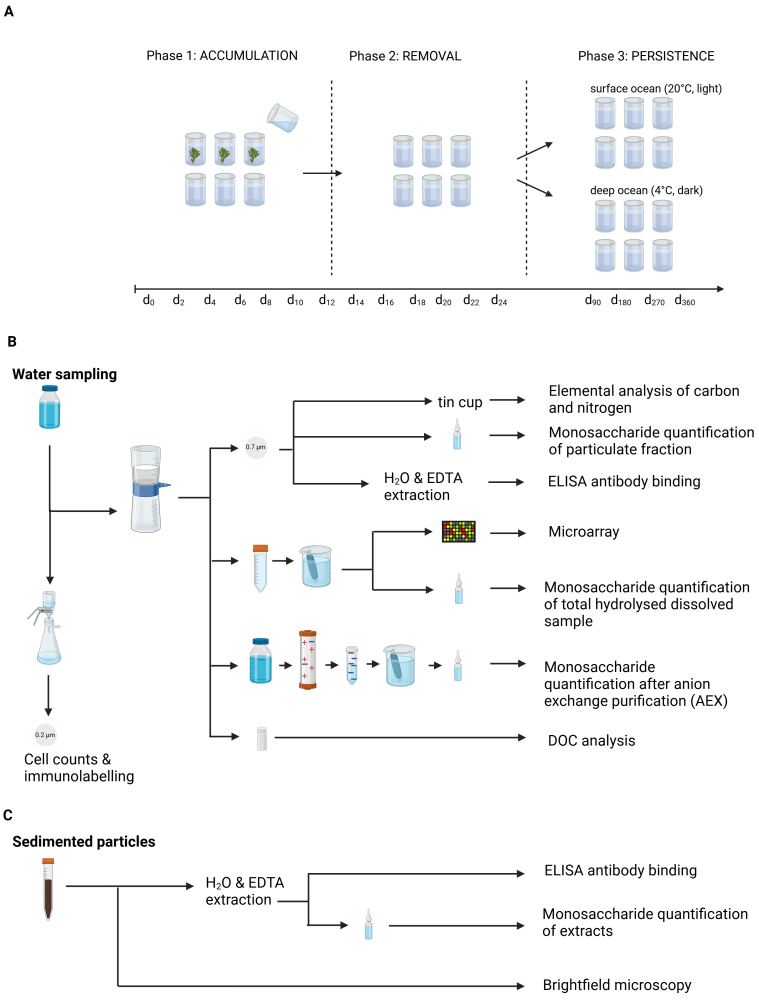

Figure 22: **Sampling scheme of algae incubations.** Created in BioRender. Hellige, I. (n.d.) BioRender.com/c28i208. **A)** Tank set-up consisting of six tanks. In phase 1 of experiment (Accumulation) three tanks were incubated with algae and three tanks served as controls for 12 days.

Figure 22: Water was sampled every second day starting at day 0. After every water sampling half of the water was replenished. After 12 days algae were removed, starting phase 2 of experiment (Removal), in which water of algae and control tanks was kept for another 12 days. Water was sampled every second day. After 24 days, in phase 3 of experiment (Persistence) remaining water inside the tank was split up into two separate incubations for each tank. First set was incubated at room temperature under a regulated light cycle, the second set was incubated at 4°C in the dark with the addition of nutrients. Samples were taken every 3 months for one year. **B)** At each sampling time 1 L of water was taken from each tank, filtered over a pre-combusted 0.7 µm GFF filter. Filter was cut and prepared for elemental analysis, for monosaccharide quantification of particulate fraction and specific antibody BAM1 ELISA binding. Filtered water was dialysed and monosaccharides were quantified with HPAEC-PAD after acid hydrolysis. Polysaccharides were detected via antibody microarray binding. Negatively charged fucoidan fraction was purified via AEX, dialysed, acid hydrolysed and monosaccharides quantified with HPAEC-PAD. DOC analysis was performed on acidified filtered water. Water was filtered over 0.2 µm PC filter for DAPI cell counts and BAM1 immunolabeling. **C)** Sedimented particles were scooped from bottom of the tanks after 24 days of incubation of *L. trabeculata*, *E. maxima* and *L. digitata* and sequentially extracted using MilliQ-water and 0.3M EDTA, monosaccharide quantification and specific antibody BAM1 ELISA binding was performed on extracts. Particles were imaged using a stereo microscope.


Sargassum fluitans
incubation in
May 2022
onboard
R/V *Endeavor.*

3 Environmental nutrients and microbial community govern the accumulation of fucoidan secreted by holopelagic *Sargassum*

3.1 Contribution to manuscript

Conceptualization: 30%
Field work: 30%; in detail: R/V *Endeavor*, United States of America, incubation of *Sargassum* 2022
Laboratory work: 25%; in detail: performed fucoidan extraction, monosaccharide quantification
Data analysis: 30%
Visualisation: 30%
Writing: 30%

Manuscript in preparation

Authors: Inga Hellige and Hagen Buck-Wiese and Margot Bligh, Silvia Vidal-Melgosa, C. Chad Lloyd, Miriam Philippi, Eden Magaña-Gallegos, Dariya Baiko, Mar Fernández-Méndez, Sherif Ghobrial, Thorben Otto, Jutta Niggemann, Michael Seidel, Mikkel Schultz-Johansen, Brigitta I. van Tussenbroek, Carol Arnosti and Jan-Hendrik Hehemann

Keywords: brown algae | seaweed | carbohydrates | polysaccharides | CAZymes | marine carbon cycle | carbon dioxide removal | Great Atlantic Sargassum Belt

3.2 Abstract

Holopelagic *Sargassum natans* and *fluitans* (*Sargassum*) recently invaded the equatorial Atlantic leading to the annual build-up of millions of tons of carbon-rich seaweed biomass. Brown algae including *Sargassum* secrete up to 35% of net primary production as dissolved organic carbon (DOC) such as phlorotannins and carbohydrates. A lack of structural resolution of secreted carbohydrates has limited our understanding of their ecological function and effect on the marine carbon cycle. Here, we report how holopelagic *Sargassum* modulates the rate of secretion of the complex extracellular polysaccharide fucoidan under different environmental conditions. Monosaccharide composition and monoclonal antibody binding revealed

that fucoidan constituted ˜11% of the dissolved organic carbon fraction of *Sargassum* incubated in filtered seawater. Seawater microbial communities showed no degradative activity on fucoidan from two tested macroalgae of the order Fucales. Specific *Sargassum* fucoidan degradative capabilities emerged in the microbiome of seawater incubated with *Sargassum* within 6 days, reducing fucoidan accumulation. During 24 hrs incubations under a range of nutrient and temperature scenarios, we show that *Sargassum* enhances fucoidan secretion by up to 200% in response to nutrient enrichment. This response suggests that fucoidan secretion is an active, adjustable process. The recent expansion of *Sargassum* into the equatorial Atlantic has most likely triggered an increase in fucoidan secretion into the ocean. Our results suggest that quantification of the accumulating carbon requires accounting for variability in secretion rates and potential adaptation of microbial communities.

3.3 Introduction

Since the beginning of the 21st century, carbon cycling by floating or holopelagic *Sargassum* species has surged 2-5 fold due to invasion of the equatorial Atlantic [Hu et al., 2021]. The "Great Atlantic *Sargassum* Belt" blooms in the subtropical Atlantic, receiving nutrients through equatorial upwelling and riverine inputs from the Congo and Amazon [Wang et al., 2019]. Since their expansion, holopelagic *Sargassum* annually fixes approx-

imately 3.6 Mill. tons CO_2 into biomass through photosynthesis [Wang et al., 2019]. CO_2 converted into exudates rivals the amount fixed into biomass [Paine et al., 2021, Powers et al., 2019]. However, most of the exuded compounds remain unknown, obscuring their ecological role and fate. Brown algae exude 15-35% of fixed carbon in the form of mannitol, phlorotannins, polysaccharides, and other forms of dissolved organic matter (DOM) [Abdullah and Fredriksen, 2004, Wada et al., 2007, 2008, Hatcher et al., 1977]. DOM has been defined as organic matter passing through glass fiber filters (pore size of 0.7 µm), with high molecular weight DOM being greater than 1 kDA [Carlson and Hansell, 2015]. Exudates may function as an 'overflow' mechanism for surplus fixed carbon, to shape the algae's microbiome and mediate interactions, or to protect from radiation [Paine et al., 2021, Bligh et al., 2022]. Brown algal polyphenols (phlorotannins) constitute approximately 5% of exuded *Sargassum* carbon and absorb UV radiation, during which they undergo degradation [Powers et al., 2019, Swanson and Druehl, 2002]. Mannitol provides energy transport and contributes 1-10% to brown algal exudates, and microbial consumption depletes dissolved concentrations [Lucas et al., 1981, Newell et al., 1980, Reed and Wright, 1986, Hall et al., 2022]. Polysaccharides in brown algae form cell walls as cellulose, the extracellular matrix as viscous alginate, and the readily-soluble fucoidan, which contributes 20-50% to exudates of *Fucus vesiculosus* [Buck-Wiese et al., 2023, Bligh

et al., 2022, Michel et al., 2010]. Whether *Sargassum* secretes fucoidan and if so, for what purpose, remains unknown.
Polysaccharides vary in complexity, from laminarin, a simple storage compound to fucoidan, a highly-branched complex extracellular matrix polysaccharide [Bligh et al., 2022, Sichert et al., 2020, Becker et al., 2020]. They constitute the majority of algal biomass, and are subject to microbial attack. Eukaryotes employ complex polysaccharides that show considerable stability to regulate surface microbial communities [Bligh et al., 2022, Ostrem Loss et al., 2023, Wang et al., 2021]. Microbes access carbon in polysaccharides with carbohydrate-active enzymes (CAZymes). Degradation effort scales with polysaccharide complexity [Bligh et al., 2022]. For example, laminarin contains beta-1,3 and beta-1,6 linkages and degradation requires only two CAZymes, occurring rapidly throughout the ocean. Degradation of complex polysaccharides, which often dominate the surface of algae, requires coordinated cascades of CAZymes [Becker et al., 2017, Sichert et al., 2020, Ndeh et al., 2017, Ficko-Blean et al., 2017, Reisky et al., 2019]. Fucoidan degradation involves potentially hundreds of CAZymes and proceeds slower than laminarin degradation, if at all [Arnosti et al., 2021, Becker et al., 2017, Krüger et al., 2019, Sichert et al., 2020, Alderkamp et al., 2007, Lloyd et al., 2023]. Fucoidan can resist microbial degradation under certain environmental conditions and can persist in the water column to be exported to sediments [Vidal-Melgosa et al., 2021, 2022, Salmeán et al.,

2022]. Here, we examined the accumulation of fucoidan exuded by *Sargassum* and the microbial communities' ability to hydrolyse this complex polysaccharide during three incubation experiments.

3.4 Methods

Study sites and sampling schemes Exudate accumulation was first investigated during shipboard tank incubations of *Sargassum* in filtered deep sea water in May 2019. *Sargassum* was collected by hand net aboard the R/V *Endeavor* in the Sargasso Sea at 37.50265°N and 72.0021°W. Three specimens of similar size were each incubated in 8 L of 0.7 µM pre-filtered (glass fiber filter, pre-combusted at 450°C, 4.5 hours, 0.7 µm pore size) seawater from 3190 m depth on deck under ambient light conditions (Fig. 23A). An additional incubation without *Sargassum* served as control. These incubations were initially placed on the fantail, but were moved to an upper deck after observing waves near the stern that splashed the fantail. Prior to a gale, the container holding the four incubation buckets was covered; after the gale, we uncovered the incubations again and discovered that some of the water had spilled due to the ship's motion, and one piece of *Sargassum* had gotten into the control bucket. This *Sargassum* was promptly removed. Every two days, 450 mL of water were sampled from each bucket over a period of 14 days. Seawater samples from the incubations were

filtered through a pre-combusted glass fiber filter.

Microbial degradation of accumulating exudates was monitored during shipboard incubations of *Sargassum* in unfiltered surface seawater in May 2022. *Sargassum* was collected by hand net aboard the R/V *Endeavor* in the Sargasso Sea at 35.1961°N and 70.0048°W. Three *Sargassum fluitans* specimens were incubated in 40L of unfiltered, surface seawater on deck under ambient light conditions (Fig. 25A). Three 40 L incubations without algae served as control incubations. Water mixing was ensured by supplied air and current pumps in each incubation. The water temperature in the incubations was regulated by placement in an approximately 500 L water bath heated using a heating rod (Eheim Thermocontrol 300, Germany) set to 23°C. However, due to the vessel's trajectory and locally adverse weather conditions, the water bath underwent temperature deviations down to 16°C on day 8 of the incubation. Every two days until day 12, half of the incubation water was replaced with fresh surface seawater to keep the algae and the microbial community under more natural conditions. After day 12 the algae were removed, and the water was incubated for a further 12 days. Water samples were taken for bacterial productivity and FLAPS measurements on days 0, 2, 4, 8, 12 and 22.

Environmental accumulation rates of exuded fucoidan were assessed in 24 hour incubations of *Sargassum* in natural seawater in July 2022. *Sargassum* was collected off the Caribbean coast of Puerto Morelos, Mexico at 20.8681°N and 86.8668°W.

Sargassum fluitans sections were incubated in 2.4 L of ambient Caribbean seawater under different temperature and nutrient conditions for 24 hours (Fig. 26A). Temperature conditions were kept stable using temperature controlled water baths [Magaña-Gallegos et al., 2023]. Prior to the nutrient incubations, *Sargassum fluitans* acclimated for 24 hours inside 18 L *ex situ* incubation systems with the according conditions before transfer to bottles. One control incubation without seaweed complemented triplicate algae incubations for each condition. Temperatures of 22, 25, 28 and 31°C covered the range of ambient seawater conditions of holopelagic *Sargassum* species throughout the Great Atlantic *Sargassum* Belt. Nutrient conditions ranged from ambient to deep sea levels, with the highest concentrations at 35 µM NO_3^- and 2.1875 µM PO_4^{3-}. Water samples were taken at the start and after 24 hours. 800 mL of the sample were filtered through a pre-combusted 47 mm glass fiber filter for exudate analysis. Fucoidan was immediately extracted using anion exchange chromatography (AEX).

Dissolved organic carbon (DOC) concentrations were quantified at the Institute for Chemistry and Biology of the Marine Environment, University of Oldenburg, Germany. Filtered seawater samples for DOC analysis were acidified to pH 2 using HCl (25%, p.a., Carl Roth, Germany) in HDPE bottles and kept at 4°C in the dark until analysis. DOC concentrations were analyzed using Shimadzu TOC-VCPH-analyzer via high-

temperature catalytic oxidation. For quality control, DOC deep sea reference material (DSR; Hansell Biogeochemistry Laboratory, University of Miami, USA) was used, ensuring trueness and precision within $< 10\%$.

Dialysis 5 mL of filtered water from the 2019 incubations and 10 mL of filtered seawater or AEX fractions from the 2022 Mexico incubations were dialysed in pre-rinsed 1 kDa membranes (SpectraPor® Biotech CE Dialysis Membrane, Carl Roth, Germany) three times against ultrapure water (MilliQ) at 4°C for a minimum of 12 hours in total. After dialysis samples were transferred to 15 mL tubes, prior to freeze drying (Labogene, Scanvac Coolsafe, Denmark). Dried samples were resuspended in 500 µL MilliQ water for the 2019 incubations and 2 mL MilliQ water for the 2022 incubations.

Total carbohydrate quantification Total carbohydrates were quantified in high molecular weight dissolved organic matter after dialysis (> 1 kDa) from 2019 incubations by phenol sulphuric acid assays against a glucose standard curve [Dubois et al., 1951].

Acid hydrolysis Polysaccharides were converted into quantifiable monosaccharides by combining 500 µL of the dialysed, resuspended samples with 500 µL 2 M HCL in pre-combusted

glass vials (450°C, 4.5 hours). Glass vials were sealed and the samples were hydrolysed at 100°C for 24 hours, prior to transfer into microtubes. Hydrolysed samples were dried in an acid resistant vacuum concentrator (Martin Christ Gefriertrocknungsanlagen GmbH, Germany) and resuspended in 500 µL MilliQ water for the 2019 incubations and in 1 mL MilliQ water for the 2022 incubations.

Monosaccharide quantification As previously described [Vidal-Melgosa et al., 2021, Engel and Händel, 2011], monosaccharides were quantified using anion exchange chromatography with pulsed amperometric detection (HPAEC-PAD). Samples were analyzed using a Dionex ICS-5000+ system fitted with a CarboPac PA10 analytical column (2 x 250 mm) and a CarboPac PA10 guard column (2 x 50 mm). Isocratic conditions of 18 mM NaOH resolved neutral and amino sugars, followed by a gradient of up to 200 mM $NaCH_3COO$ to separate acidic monosaccharides.

Carbohydrate microarray analysis Monoclonal antibodies specific to brown algae polysaccharides were utilized to screen 2019 mesocosm samples for dissolved carbohydrates. Sample aliquots after dialysis were printed onto nitrocellulose membranes, followed by detection of antibody binding through colorimetric signal [Vidal-Melgosa et al., 2021, Torode et al., 2015].

For analysis, the printed microarrays were blocked in MPBS for 1 hour and afterwards individually incubated for 2 hours. Monoclonal antibodies BAM1, BAM2, INRA-RU1, BAM7, BAM10 and the anti-rat control were used at a concentration of 10 µg mL^{-1} [Torode et al., 2015, 2016]. After incubation, the arrays were washed with PBS and treated with secondary antibodies in MPBS for 2 hours, then washed again with PBS and deionised water. The arrays were subsequently developed using 5-bromo-4-chloro-3-indolyl phosphate and nitroblue tetrazolium in alkaline phosphatase buffer (100 mM NaCl, 5 mM $MgCl_2$, 100 mM Tris-HCl, pH 9.5). Developed arrays were analyzed using Array-Pro Analyzer 6.3 software (Media Cybernetics).

Fucoidan extraction Fucoidan was extracted from 400 mL of filtered seawater from 2022 Mexico incubations based on Manuscript I. The elution was stored at 4°C until further processing.

Fucoidan extraction from biomass *Sargassum* biomass was freeze dried and ground to powder using a tissue lyser at 30/s for 45 sec. 10 g of the biomass powder was resuspended at a final concentration of 50 mM EDTA (pH= 8) in 1 L of MilliQ water. The further processing to extract fucoidan was performed as described in [Thobor et al., 2024]. The final solution was freeze dried to obtain fucoidan powder for preparation of

different concentrations of fucoidan standards, as well as for FLA-PS incubations.

Calculation of fucoidan concentrations. Fucoidan concentrations were calculated based on fucose concentrations calibrated with a fucoidan standard purified from *Sargassum* biomass and processed in the same way as the samples (Fig. S5).

Community productivity Community protein productivity was measured after [Kirchman, 2001]. Herefore, water sampled from *Sargassum* tanks (2022, *Endeavor*) on days 0, 2,4, 8,12 and 22, and in addition ambient seawater from the deep chlorophyll maximum zone was sampled as a control on day 0. Water was incubated with 20 nM ^{3}H-Leu at temperatures between 16.5 and 22.5°C according to the tank conditions for 6 to 12 hours. The average ^{3}H-Leu incorporation was measured and ^{3}H-Leu pM hour^{-1} was calculated for each tank.

FLA-PS Water was collected from all three algae tanks and one control tank on day 0, 6, 12 and 22 during the *Sargassum* incubation conducted aboard R/V *Endeavor* in 2022. To obtain polysaccharide hydrolysis rates, the following fluorescently labeled polysaccharides were added at concentration of 3.5 µM monosaccharide equivalent concentration for all polysaccharides other than fucoidan, which was added at a concentration

of 5 µM monomer equivalent, and incubated for 29 days: FLA-chondroitin-sulfate, FLA-arabinogalactan, FLA-laminarin, FLA-fucoidan from *Sargassum fluitans*, FLA-fucoidan from *Fucus vesiculosus*, FLA-pullulan and FLA-xylan, according to the study by Arnosti [2003]. The separate incubations were subsampled initially (t0) and on days 5, 10, 15 and 29; the subsamples were filtered through a 0.2 µM filter and stored at -20°C until analysis. Rates of polysaccharide hydrolase activities were determined via gel permeation chromatography with fluorescence detection, as described in detail in Arnosti [2003]. Hydrolysis rates were calculated as a change in the molecular weight distribution over time.

Statistical tests All data was analysed using R version 4.3.3 (R core team, [R Core Team, 2020]). Only in the Mexico bottle experiments were statistical tests of significance possible, due to the replication in other experiments. One-way ANOVAs were performed for fucoidan and DOC exudation rates with temperature and nutrient conditions as factors. Homogeneity of variance and normality were checked with Levene and Shapiro-Wilk tests respectively.

3.5 Results

3.5.1 *Identification of fucoidan in Sargassum exudates*

Dissolved organic carbon (DOC), including carbohydrates, accumulated steadily in *Sargassum* buckets during two weeks of incubation (Fig. 23). In 2019, onboard bucket incubations with or without *Sargassum* contained filtered bottom water to minimize any effects of bacterial degradation (Fig 23A). The DOC concentration exceeded 5 mg L^{-1} in two out of three *Sargassum* buckets after 1 day of incubation. Over the course of the two weeks, DOC concentrations increased 4 fold in the three *Sargassum* buckets, with no increase in the control bucket (Fig. 23B). Dissolved carbohydrates concurrently increased 9 fold in *Sargassum* incubations, from 0.9 mg L^{-1} to 7.9 mg L^{-1} (Fig. 23C) as estimated by phenol sulfuric acid assays. Based on the phenol sulfuric acid estimate and assuming carbohydrates comprise 40% carbon by weight, they constituted 5 to 15% of the accumulating DOC.

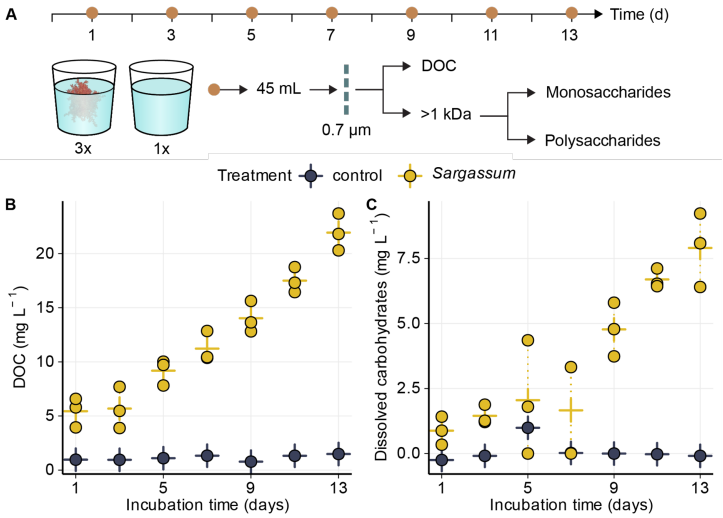

Figure 23: **Dissolved organic carbon (DOC) and carbohydrates accumulated in *Sargassum fluitans* bucket incubations.** Bucket incubations with algae (triplicate *Sargassum*, single control) over 13 days during a 2019 research cruise to the Sargasso Sea. Buckets were filled with 0.7 µm filtered bottom water from a depth of 3190 m; three buckets had *Sargassum*, one (control) did not. **(A)** Every two days (orange circles), 45 mL were subsampled and filtered (0.7 µm). **(B)** Dissolved organic carbon (DOC) was quantified in filtrates. **(C)** Monosaccharides were quantified after hydrolysis of the >1 kDa fraction (phenol sulfuric acid). Dark blue and yellow points represent control and *Sargassum* buckets respectively. Crosses indicate the mean and dotted lines the 95% confidence interval.

Monosaccharide quantification after acid hydrolysis (HCl) identified fucose, galactose, glucose and glucuronic acid increasing at comparable rates of 0.7 mg L^{-1} d^{-1} during the first 7 days of *Sargassum* incubations (Fig. 24A). These monosaccharides stem from polysaccharides in the 1 kDa to 0.7 µm size fraction of dialyzed samples from incubations. Following day 7, a marked increase in the rates of monosaccharide accumulation occurred uniformly across these four monosaccharides. At the end of the incubations fucose, galactose, glucose and glucuronic acid together accumulated to ~6 mg L^{-1}, constituting ~11% of the DOC (Fig. 23B). Monosaccharides in the control incubation without *Sargassum* remained at environmental concentrations (Fig. 24A). Carbohydrate polyacrylamide gel electrophoresis (C-PAGE) analysis indicated accumulation of anionic polysaccharides over the incubation period (Fig. 27).
The monosaccharides that accumulated in *Sargassum* incubations and the overall monosaccharide composition approximately matched fucoidan purified by anion exchange chromatography from *Sargassum* biomass. Fucose constituted 46%, galactose 18%, mannose/ xylose 14%, glucose 5%, uronic acids 15% and glucosamine 1% of monosaccharides in fucoidan purified from *Sargassum* (Fig. 24C). On day 13, polysaccharides in *Sargassum* buckets had a similar composition but with a five fold higher contribution of glucose (24%). The simultaneous increase of fucose, galactose, glucose, glucuronic acid (Fig. 24A) and glucosamine (Fig. 28) and the monosaccharide com-

position in the *Sargassum* buckets (Fig. 24B) point toward fucoidan exudation into the surrounding water. Structure specific monoclonal antibodies confirmed the exudation and accumulation of fucoidan during the 2019 *Sargassum* incubations (Fig. 24D-H). Signals of the fucoidan specific monoclonal antibody BAM1 [Torode et al., 2015] emerged on day 9 of incubations and increased subsequently in filtered water from *Sargassum* incubations, but not in the control. In addition, signals of BAM7, which binds various polysaccharides including fucoidan, alginate and pectin [Torode et al., 2016], BAM10, which binds alginate, and INRA-RUI, which binds rhamnogalacturonan I, emerged for *Sargassum* incubations on day 7. This timing aligned with the marked increase in accumulation rates of monosaccharides in polysaccharides (Fig. 24A).

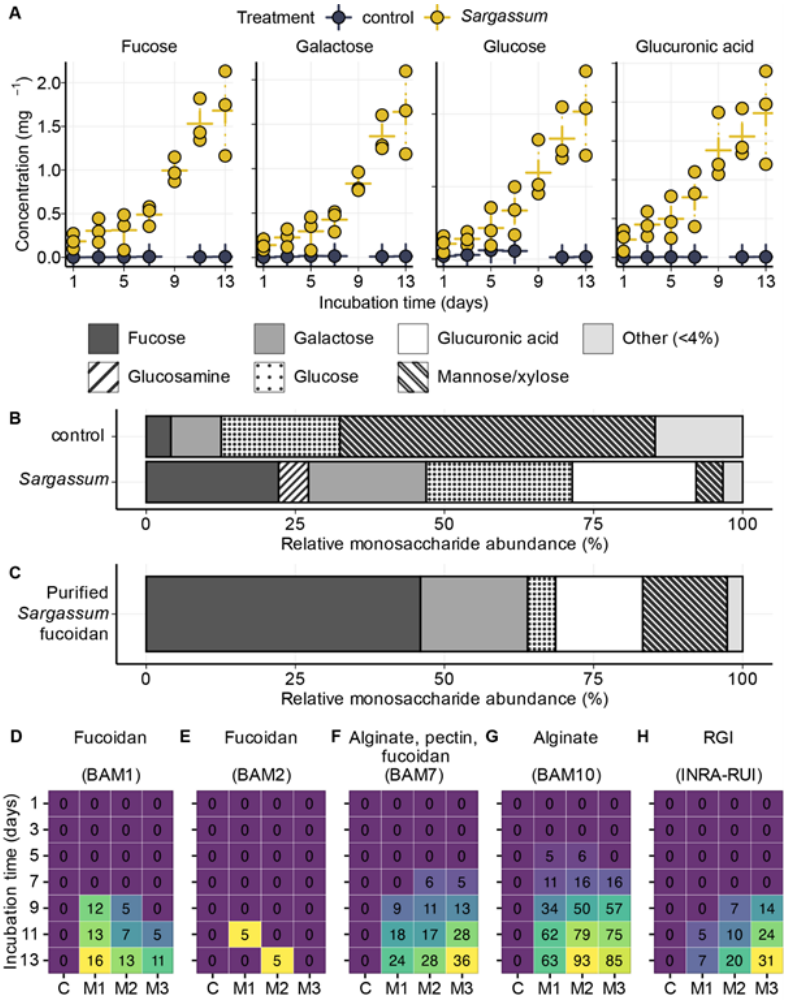

Figure 24: **Fucoidan-typical monosaccharides accumulated in algae mesocosms, confirmed with specific monoclonal antibody binding.**

Figure 24: **(A)** Monosaccharide components of dissolved molecules were quantified using high performance liquid chromatography after dialysis using a 1 kDa membrane and acid hydrolysis. Dark blue and yellow points represent control and *Sargassum* mesocosms respectively. Crosses indicate the mean and dotted lines the 95% confidence interval. The four depicted monosaccharides exhibited the most pronounced accumulation in algae mesocosms. Other quantified monosaccharides are shown in Fig. 28B-C. Monosaccharide composition (% by molarity) on day 13 in control and *Sargassum* buckets **(B)** and for *Sargassum* fucoidan purified from biomass **(C)**. The control represents a single replicate and *Sargassum* the mean of three replicates. Fucoidan purified from *Sargassum* biomass was acid hydrolyzed, and monosaccharides quantified using high performance liquid chromatography. Monosaccharides with relative abundances less than 4% were summed and denoted as 'other'. **(D-H)** Relative signal intensity of fucoidan specific BAM1 and BAM2, alginate, fucoidan and pectin specific BAM7, alginate specific BAM10, and rhamnogalacturonan I-specific INRA-RUI antibodies in triplicate mesocosms with *S. fluitans* (M1-M3) and control mesocosm (C) over 13 days.

3.5.2 *Microbial communities hydrolyze Sargassum fucoidan after six days of incubation*

A second onboard *Sargassum* incubation in 2022 with unfiltered surface water was performed to quantify exuded *Sargassum* fucoidan under closer to natural conditions, as well as its removal by microbial hydrolysis (Fig. 25A). No difference was found in microbial protein productivity from ^{3}H-Leucine uptake rates in *Sargassum* and control tanks (Fig. 25B), while *Sargassum* fucoidan was hydrolyzed after acclimation of mesocosm communities (Fig. 25D). The application of statistical tests was not possible as two replicates were measured for control mesocosms. Despite regulation of water temperature, the research vessel's course and locally adverse weather conditions resulted in mesocosm temperature fluctuations. ^{3}H-Leucine incubations were performed at the same temperature as the mesocosms at sampling (Fig. 25C), directly affecting uptake rates. Bulk assessment via community protein productivity failed to detect the microbial community benefiting from *Sargassum* carbon fixation. Seawater was subsampled from *Sargassum* and control tanks with unfiltered seawater on days 0, 6, 12 and 22 (Fig. 25A). At the four timepoints, separate incubations of 29 days each were established with fluorescently labeled polysaccharides (FLA-PS) for measurement of polysaccharide hydrolysis rates [Arnosti, 2003].

Day 0 incubations, which contained environmental microbial

communities, did not show measurable fucoidan hydrolysis over the 29 days (Fig. 25D). Fucoidan concentrations in *Sargassum* and control tanks accounted for 0.17 $\pm$0.03 mg L^{-1} (based on concentrations before AEX purification, shown in Manuscript I). However, simpler polysaccharides, including laminarin (Fig. 25 F), xylan, and pullulan (Fig. 29) were hydrolyzed. Communities in *Sargassum* tanks sampled on day 6, 12 and 22 hydrolyzed *Sargassum* fucoidan with maximum rates around 50 nM monomer hr^{-1} (Fig. 25D). Fucoidan accumulated inside the *Sargassum* tanks to 0.45 $\pm$0.16 mg L-1 by day 6 and to 0.57 $\pm$0.08 mg L^{-1} by day 12, while the controls showed consistent concentrations of 0.15 $\pm$0.05 and 0.16 $\pm$0.04 mg L^{-1} on day 6 and 12, respectively. On day 22, fucoidan concentrations declined to 0.32 $\pm$0.22 mg L^{-1} inside *Sargassum* incubations and 0.11 $\pm$0.00 mg L^{-1} inside controls (based on concentrations before AEX purification, shown in Manuscript I). The maximum hydrolysis rate (63 nM monomer hr^{-1}) of *Sargassum* fucoidan exceeded that of laminarin (37 nM monomer hr^{-1}). Control communities subsampled on the same days from tanks without *Sargassum* had lower ability to hydrolyze *Sargassum* fucoidan, with maximum hydrolysis rates ˜5 fold lower than *Sargassum* tank communities. All maximum hydrolysis rates were lower in incubations started with control tank communities subsampled on day 22 compared to incubations started at previous timepoints, including laminarin. Communities either did not degrade fucoidan from *Fucus vesiculosus* (i.e., day 6), or de-

graded it with 2 to 5 fold lower maximum hydrolysis rates than *Sargassum* fucoidan (i.e., days 12 and 22) (Fig. 25E).

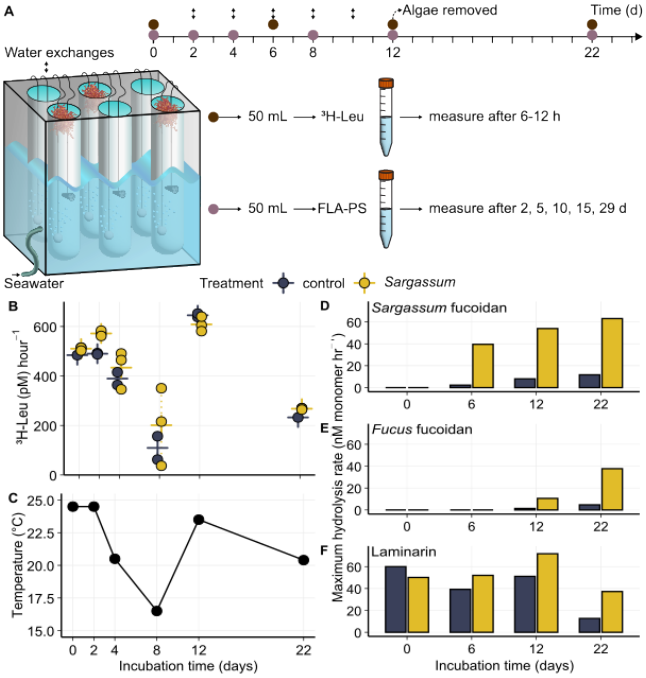

Figure 25: **No difference of community protein productivity between control and *Sargassum* tanks, while *Sargassum* fucoidan was hydrolyzed only after acclimation of mesocosm communities during incubations in May 2022. (A)** Tank incubations with macroalgae (triplicate *Sargassum* and duplicate control) aboard a 2022 research cruise over 12 days, with water exchanges every 2 days.

Figure 25: After 12 days, macroalgae were removed and tanks were incubated for a further 12 days. An outer water bath, air bubblers, and submerged pumps maintained temperatures and circulation, although adverse weather conditions resulted in temperature fluctuations **(C)**. Tanks were sub-sampled on days 0, 2, 4, 8, 12 and 22 (pink circles) and were incubated with ^{3}H-Leucine for 6-12 hours to measure productivity. Sub-samples of tanks from days 0, 6, 12 and 22 (brown circles) to set up new incubations with fluorescently-labeled polysaccharides (FLA-PS). Hydrolysis rates were measured periodically in the FLA-PS incubations over 29 days (Arnosti, 2003). **(B)** Community protein productivity was similar in control and *Sargassum* tanks. Dark blue and yellow points represent control (n = 2) and *Sargassum* (n = 3) mesocosm protein productivity rates respectively. Crosses indicate the mean and dotted lines the 95% confidence interval. **(C)** Temperature profile of ^{3}H-Leucine incubations. Productivity measurement incubations were run at the temperature of the tanks when subsampled. **(D-F)** Fucoidan was stable under environmental conditions and was hydrolyzed after specific acclimation of mesocosm communities. Maximum hydrolysis rates (nM monomer hr^{-1}) of fluorescently labeled polysaccharides (FLA-PS), *Sargassum* fucoidan **(D)**, *Fucus* fucoidan **(E)** and laminarin **(F)**, measured in incubation time series inoculated with seawater taken at specific time points (0, 6, 12 and 22 days) from tanks without (dark blue) and with (yellow) *Sargassum fluitans*. Time series ran for 29 days.

3.5.3 *Enhanced fucoidan secretion under nutrient enrichment*

Bottle incubations in Mexico with *Sargassum fluitans* assessed rates of bulk DOC and fucoidan release over 24 h under different temperature and nutrient regimes (Fig. 26A). Assuming carbon accounts for 30% of the weight of sulfated fucoidan [Buck-Wiese et al., 2023], fucoidan accounted for 63.4±12.5% of accumulating DOC based on filtered water (FW) measurements and 25.4±2.9% based on AEX results. The accumulation of *Sargassum* dissolved fucoidan in seawater increased in response to nutrient enrichment. Despite an apparent upward trend in fucoidan concentrations after AEX (Fig. 26F), there was no significant difference in fucoidan exudation across temperatures from 22°C to 31°C in FW (Fig. 26D) or AEX samples (Fig. 26F) (One-way ANOVAs, $p = 0.613$ and 0.131, respectively). Only single DOC samples were measured in the temperature experiment so statistical tests were not possible, but there was also no apparent trend across temperatures (Fig 4B). DOC concentrations increased from ~1.6 to ~2 mg L^{-1} from the lowest (0 µM NO_{3-} and PO_4^{3-}) to the highest (35 µM NO_{3-} and 2.18 µM PO_4^{3-}) nutrient amendment levels (Fig. 26D), but not significantly (One-way ANOVA, $p = 0.149$). Addition of nutrients did significantly increase fucoidan concentrations in FW (One-way ANOVA, $p = 0.017$, Fig. 26F). Concentrations of AEX purified fucoidans supported this trend, increasing

from 0.4 to 0.8 mg L^{-1} (Fig. 26H), although the increase was not statistically significant (One-way ANOVA, $p = 0.118$).

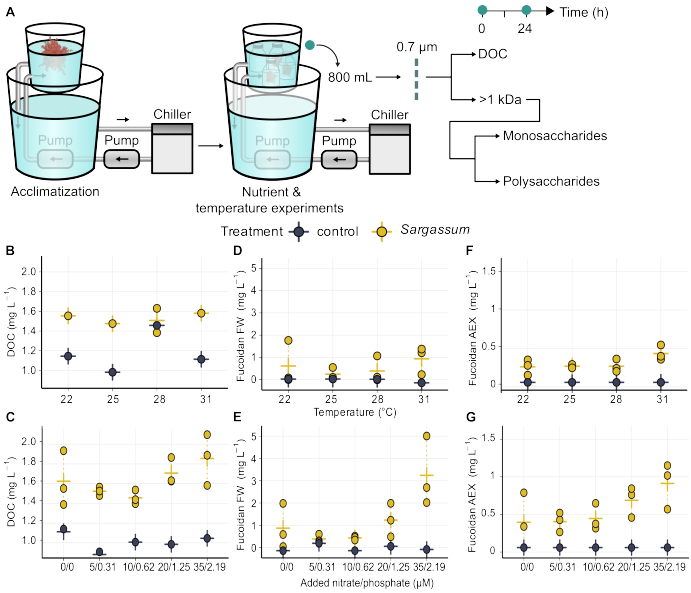

Figure 26: **Elevated temperature and nutrients enhance *Sargassum fluitans* fucoidan accumulation. (A)** Bottle incubations in 2022 at the Mexican Caribbean Coast. *Sargassum* were acclimatized in buckets for 24 h, then incubated in bottles (triplicate *Sargassum*, single control) under different temperature **(B, D, F)** and nutrient **(C, E, G)** conditions. Temperatures were maintained using an *ex situ* culture system [Magaña-Gallegos et al., 2023].

Figure 26: Initial and final samples were taken to establish DOC **(B-C)** and fucoidan exudation rates over 24 hours. Upper fucoidan concentrations were estimated by hydrolysis of dissolved polysaccharides in filtered water (FW, **D,E**). Lower estimates were established after purification from the >1 kDa fraction by anion exchange chromatography and calibrated with a standard extracted and purified from biomass (AEX, **F,G**). Dark blue points indicate the control mesocosm values. Yellow points show the three Sargassum incubations. Crosses indicate the mean and dotted lines the 95% confidence interval.

3.6 Discussion

Our study demonstrated the accumulation of fucoidan by three independent techniques, based on increasing concentrations of monosaccharides that constitute fucoidan from *Sargassum* exudates accompanied by an increase of specific monoclonal antibody binding to fucoidan (Fig. 24). Using the negative charge of fucoidan's sulfate groups, about half of the DOM monosaccharide signal could be specifically confirmed by extracting fucoidan using anion exchange chromatography (AEX) prior to hydrolysis. Enhanced nutrients appeared to increase fucoidan secretion (Fig. 26). This study suggests *Sargassum* releasing fucoidan into their extracellular matrix, which includes channels leading to the brown algae surface, as previously shown for

other brown algae [Sieburth, 1969, Buck-Wiese et al., 2023]. Further, we showed that microbial communities can adapt to degrade specific fucoidan structures (Fig. 25). The three experiments document the secretion of fucoidan by *Sargassum*, specific induction of fucoidan degradation, and modulation of secretion rates in response to environmental conditions.

Our findings place the contribution of exuded carbohydrates of *Sargassum* to DOC within the documented range for brown algae. Exudation of up to 35% of fixed carbon has been described for brown algae including *Sargassum*, with variable fractions of DOC comprising carbohydrates (3.7 to 71%) and no current estimates available for *Sargassum* [Abdullah and Fredriksen, 2004, Wada et al., 2007, 2008, Reed et al., 2015, Powers et al., 2019, Paine et al., 2021]. The two week bucket incubations suggested an ~11% contribution of fucose, galactose, glucose and glucuronic acid (Fig. 24A), typical *Sargassum* fucoidan monosaccharides (Fig. 24C), to DOC accumulation (Fig. 23B). Notably, the harsh extraction method to purify *Sargassum* fucoidan from biomass may have altered its structure (Fig. 24C). However, the monosaccharide profile aligns with the monosaccharide abundances of the secreted dissolved carbohydrates (Fig. 24B). The stagnant conditions without water exchange possibly led to leakage of fucoidan over the course of the experiment due to visually deteriorating health of the incubated algae and brown coloration of incubation water. This was supported by increasing BAM7 and BAM10 signals (Fig. 24D-

H), targeting mainly alginate [Torode et al., 2016], potentially indicative for release of the major structural component of the extracellular matrix of brown algae [Percival, 1979]. In bottle incubations, fucoidan from filtered water samples amounted to 64.1±12.5% of DOC, surpassing AEX estimates of 25.4±2.9% (Fig. 26, Fig. 31). As microbes continue to degrade the exuded DOC, non-degraded fucoidan may accumulate. For a range of environmental conditions (Fig. 26), we can report that fucoidan comprised up to two thirds of the accumulating *Sargassum* DOC, and at a minimum one quarter, as confirmed by AEX (Fig. 26).

Tank incubations in 2022 revealed no clear change in microbial community protein productivity in response to *Sargassum* (Fig. 25A-C). Although more algal exudates were available as a source of substrates than in control tanks, the unfiltered surface seawater used in incubations may have contained microalgae as an alternate source of algal exudates. Substrate specific assessments revealed that the environmental microbial community in seawater was unable to degrade fucoidan over a period of 29 days (Fig. 25D-F). Fucoidan concentrations were estimated to 0.17 ±0.03 mg L^{-1} on day 0 inside *Sargassum* tanks, ranging higher compared to environmental surface measurements of maximum 0.075 mg L^{-1} across the globe (Manuscript I). Resistance of fucoidan to degradation by environmental microbial communities aligns with other observations of slow or absent fucoidan hydrolysis in a range of seawater and sedimentary lo-

cations [Arnosti, 2000, Arnosti et al., 2021] (see discussion below). Microbial communities in *Sargassum* tanks later adapted to hydrolyse *Sargassum* fucoidan, while fucoidan accumulated by around 3- fold (0.45 $\pm$0.16 mg L^{-1} by day 6 and 0.57 $\pm$0.08 mg L^{-1} by day 12) in *Sargassum* tanks (Manuscript I). These high dissolved fucoidan concentrations can be reached inside algae farms (e.g. up to 1 mg L^{-1} inside *S. latissima* farm in Northern Ireland, shown by Manuscript I). Maximum hydrolysis rates higher for fucoidan than the simple polysaccharide laminarin after 22 days of incubation with *Sargassum*. Using two different types of fucoidan, our results indicate that the adaptation in community capabilities was specific to *Sargassum* fucoidan (Fig. 25D-F). Algae associated microorganisms frequently possess CAZymes to degrade the host's polysaccharides, and may have detached and proliferated in tanks [Bengtsson et al., 2011, Ficko-Blean et al., 2017, Arnosti et al., 2021, Schwartzman et al., 2022, Pontrelli et al., 2022, Thomas et al., 2017, Song et al., 2021]. Alternatively, initially rare seawater community members may have increased sufficiently in numbers to hydrolyze fucoidan at detectable rates, or some of the pathways to degrade fucoidan were induced by tank conditions. This potential shift or adaptation in microbial community becomes evident when comparing algae incubations to the control setups, wherein moderate *Sargassum* fucoidan hydrolysis emerged over time. We cannot distinguish whether a change in community composition or a change in activity among a

compositionally stable community specifically induced *Sargassum* fucoidan hydrolysis. Fucoidan from another brown algae, *Fucus vesiculosus*, was either not degraded or hydrolysed with ~2 to 5 fold lower maximum rates by tank communities than *Sargassum* fucoidan (Fig. 25D-E), underlining the importance of structure specific analyses. *Sargassum* fucoidan differs substantially in monosaccharide composition (Fig. 24B) from other brown algae fucoidan [Sichert et al., 2020].

The 2022 tank incubations show that the ability to degrade fucoidan, while not an inherent capability of seawater communities, can be gained by microbial communities exposed to a source. Bottle incubations of *Sargassum fluitans* under enhanced nutrient or temperature conditions apparently responded to nutrient enrichment with enhanced fucoidan secretion. Notably, the experiment suffered from minimum replication, resulting in low statistical power. Seaweeds respond to stress including air exposure and possible desiccation with increased secretion [Schramm et al., 1983, Sieburth, 1969, Paine et al., 2021]. Organic carbon exudation has been suggested to compensate for carbon fixation exceeding nutrient uptake, predicting a decrease in exudation as more nitrogen and phosphorus become available to algae [Carlson and Hansell, 2015]. Fucoidan consists predominantly of carbohydrates and sulfate groups, containing carbon but virtually no nutrients such as nitrogen and phosphorus [Buck-Wiese et al., 2023]. Surprisingly, enhancing nutrient availability to levels observed in the

deep sea, boosted fucoidan exudation, suggesting a different purpose than compensation (Fig. 26). One possible role could involve defense against biofouling on its surface, as enhanced growth of epiphytes under higher nutrient availability might occur [Kloareg et al., 2021, Luthuli et al., 2019, Jeong et al., 2018, Cho et al., 2022]. Environmental conditions modulating fucoidan exudation call for closer examination and *in situ* assessments to account for dissolved fucoidan carbon.

3.7 Conclusion

Sargassum exuded fucoidan accounted for 25 to 64% of net DOC accumulation in natural seawater. Temperature did not affect the rate of fucoidan secretion, while nutrient enrichment enhanced fucoidan secretion, suggesting an active modulation by the algae. Regulated secretion may serve as a defense mechanism, forming a protective slime against harmful epibionts. The environmental microbial community initially did not hydrolyze fucoidan, but during incubations in tanks microbes adapted to degrade fucoidan. The acquisition of specific *Sargassum* fucoidan hydrolytic capabilities by these microbes seems to result from a combination of priming through *Sargassum's* fucoidan exudation, as well as a community tank effect. Our results further suggest that *Sargassum* fucoidan is recalcitrant on timescales of weeks to months, indicating its poten-

tial contribution to semi labile oceanic DOM [Hansell, 2013]. Secreted fucoidan accumulated and prevailing environmental microbial communities showed apparently no degradative capabilities. Thus, the annual 20 Mt *Sargassum* proliferating in the Atlantic [Wang et al., 2019] secretes fucoidan carbon at roughly 0.27 to 0.85 Mt per year into the marine organic carbon reservoir (based on secretion rates in Manuscript I). The ultimate fate of this secreted fucoidan depends on the environmental conditions and potential adaptation of the microbial communities in the invaded regions.

3.8 Acknowledgements

The authors thank technicians at Max-Planck Institute for Marine Microbiology and Marum Centre for Environmental Research, University of Bremen, namely Tina Horstmann for carbohydrate microarray analysis, Alek Bolte and Katharina Föll for HPAEC-PAD measurements, as well as Matthias Friebe and Ina Ulber from the Institute for Chemistry and Biology of the Marine Environment, University of Oldenburg for DOC analyses, Lynne Butler, Bonny Clarke, the chief engineer, and the captain and the crew of the R/V *Endeavor* during cruises EN638 and EN683, M. Guadalupe Barba-Santos and Evelyn Raquel Salas-Acosta in the reef systems research unit at Puerto Morelos, Universidad Nacional Autónoma de México, Lena Eg-

gers, Katherine Jones and Philipp Hach with the Alfred-Wegener Institute in Bremerhaven, Germany for their assistance in field and lab work. The authors thank Hussein Awwad, Carla Knappik and Mohammad Shahin for their support with sample processing and acknowledge invaluable support from the Max-Planck-Society, the DFG Heisenberg grant for Glyco-Carbon Cycling in the Ocean and the Cluster of Excellence initiative (EXC-2077–390741603), the Simons Collaboration on Principles of Microbial Ecosystems, the European Research Council grant for project C-Quest and the sea4soCiety, CDRmare campaign in the German Marine Research Alliance, and funding from the U.S. National Science Foundation (OCE-1736772 and OCE-2022952 to CA).

3.9 Supplementary information

Fig 27 to Fig. 31

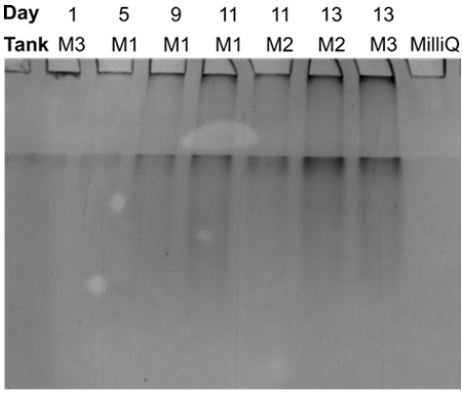

Figure 27: **Accumulation of anionic polysaccharides in *Sargassum* mesocosms from 2019.** Anionic polysaccharides were separated by carbohydrate polyacrylamide gel electrophoresis (C-PAGE). Results for mesocosms with *S. fluitans* (M1-M3) over 13 days of incubation, MilliQ was used as negative control.

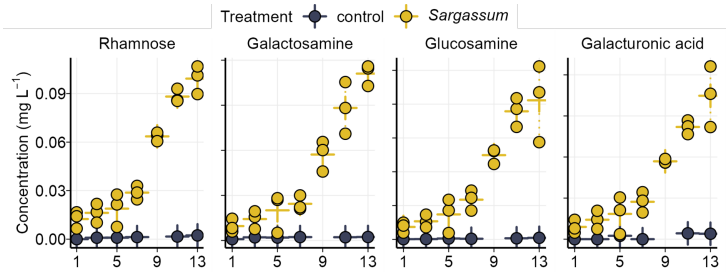

Figure 28: **Accumulation of further monosaccharides in *Sargassum* mesocosms from 2019.** Accumulation of dissolved monosaccharides, after acid hydrolysis of filtered and dialyzed seawater. Yellow and dark blue points represent *Sargassum* and control mesocosms respectively. Crosses indicate the mean and dotted lines the 95% confidence interval.

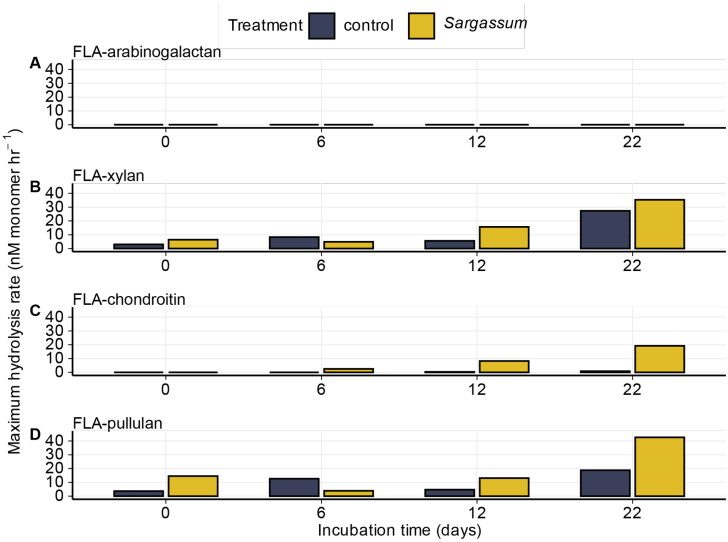

Figure 29: **Hydrolysis of polysaccharides by microbial communities in tanks with and without *Sargassum*.** Maximum hydrolysis rates (nM monomer hr-1) of fluorescently-labeled polysaccharides (FLA-PS), arabinogalactan **(A)**, xylan **(B)**, chondroitin **(C)** and pullulan **(D)**, measured in incubation time series inoculated with seawater taken at specific time points (0, 6, 12, 22 d) from tanks without (dark blue) and with (yellow) *Sargassum fluitans*. Time series ran for 29 days.

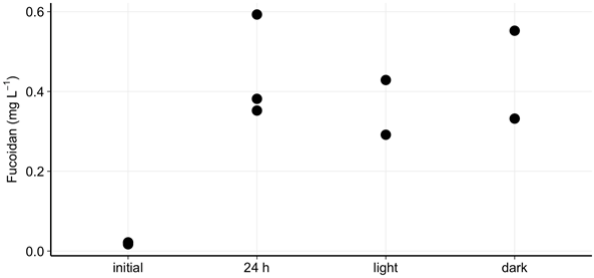

Figure 30: **Limited degradation of *Sargassum* fucoidan over 24 h.** Degradation experiment performed in Mexico 2022. *Sargassum* was incubated in seawater ("initial") for 24 h. Water was sampled ("24 h"), pooled and split into bottles for 24 h light and dark incubation.

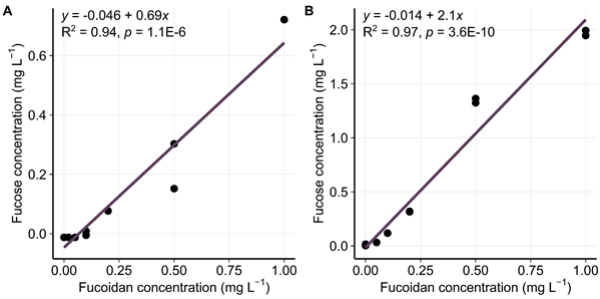

Figure 31: **Fucoidan purified from *Sargassum* biomass and processed with samples was used to calculate fucoidan concentrations from fucose concentrations.** Fucoidan was purified from biomass extracts by anion-exchange chromatography (AEX). It was then processed with hydrolyzed polysaccharide **(A)** and hydrolyzed AEX purified polysaccharides **(B)**. **(A)** Samples and fucoidan standards were dialysed with 1 kDa membranes against MilliQ-water, freeze-dried and acid hydrolyzed. Monosaccharides were quantified by HPAEC-PAD. **(B)** Samples and fucoidan standards were purified by AEX, then processing as in **(A)**.

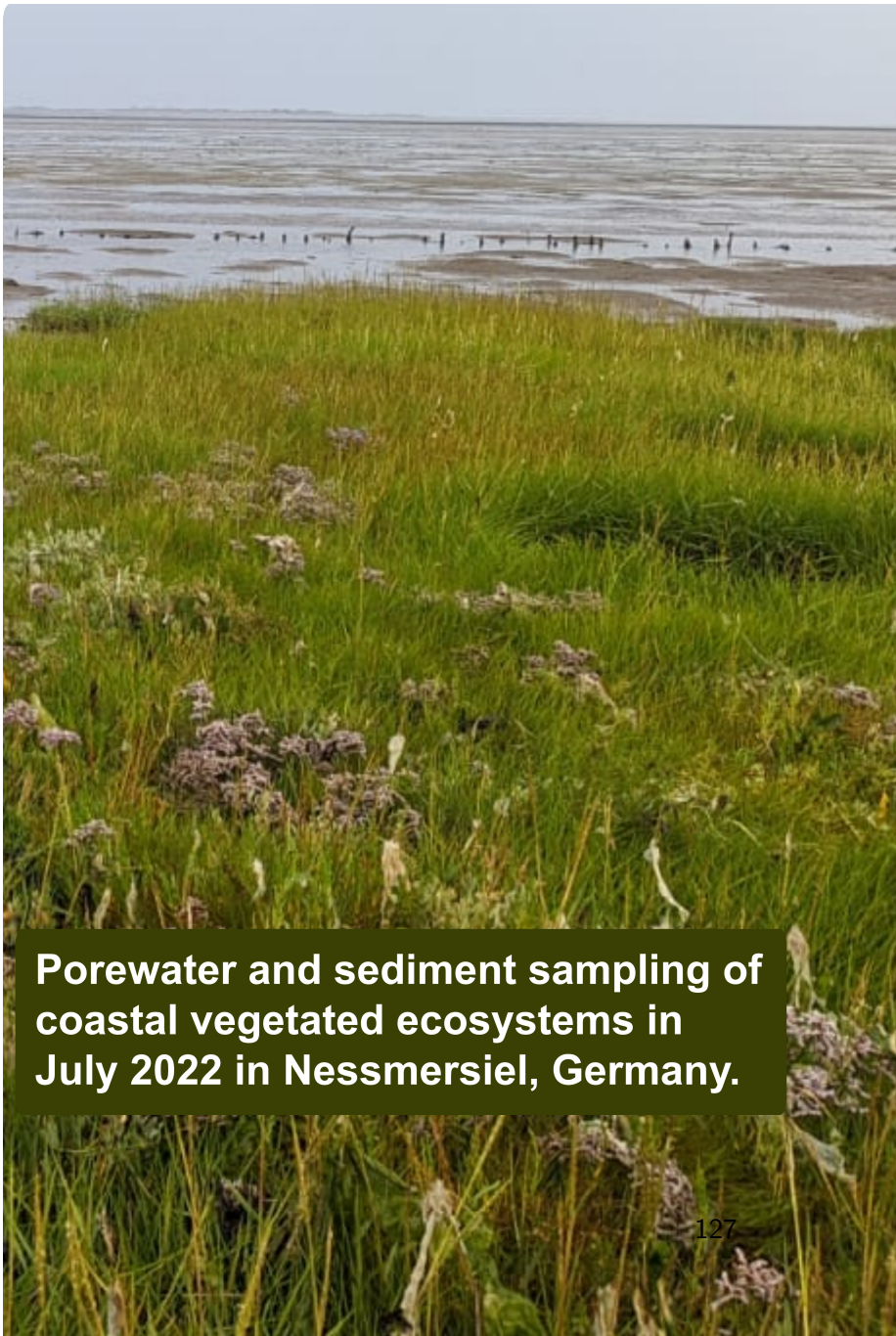

Porewater and sediment sampling of coastal vegetated ecosystems in July 2022 in Nessmersiel, Germany.

4 Roots of coastal plants stabilize carbon fixed by marine algae

4.1 Contribution to manuscript

Conceptualization: 70%
Field work: 50%; in detail: sampling in North and Baltic Sea
Laboratory work: 90%; in detail: carbohydrate extraction, quantification of total carbohydrates, monosaccharide analysis, ELISA antibody binding
Data analysis: 95%
Visualisation: 100%
Writing: 90%

submitted
preprint: DOI: 10.1101/2024.12.02.624615; [Hellige et al., 2024]

Authors: Inga Hellige, Aman Akeerath Mundanatt, Jana C. Massing and Jan-Hendrik Hehemann

Keywords: carbon dioxide removal | marine carbon sequestration | glycans | coastal vegetated ecosystems

4.2 Abstract

Coastal vegetated ecosystems are key-nature based solutions in climate change mitigations. Mangroves, seagrass meadows and saltmarshes contribute to carbon sequestration not only through the storage of biomass and sediments, but also through the secretion of dissolved organic carbon over their root system. Macro- and microalgae release most of their produced organic carbon as exudates, exported away from their origin, leading to underrepresentation of their contribution in blue carbon assessments. Here, we analysed 93 sediment cores of coastal vegetated ecosystems from temperate to tropical regions. We used polysaccharides as bioindicators of carbon sequestration to trace carbon from source to sink in different ecosystems. By binding of specific monoclonal antibodies, algal-derived polysaccharides were detected in sediments of coastal vegetated ecosystems. The relative abundance of the main building blocks of polysaccharides, monosaccharides was consistent across all 93 sediment cores, with no significant

differences, despite the varying ecosystems and locations. Our findings suggest that the restoration of plant ecosystems, fixing carbon, protecting coasts and enhance biodiversity should also be enumerated for the stored carbon from distant donors. Hence carbon sequestration is a collective or synergistic process of different photosynthetic organisms.

4.3 Significance statement

Coastal vegetated ecosystems are vital for climate change mitigation, sequestering carbon through biomass, sediments and the integration of organic carbon from external sources such as algae. By using polysaccharides as bioindicators, this study reveals that algal-derived carbon is preserved in sediment across diverse ecosystems, emphasizing the synergistic role of multiple photosynthetic organisms in carbon sequestration. This finding indicates that coastal vegetated ecosystems accept, accrete and stabilize carbon from different and distant donors and highlights the collective contribution of these ecosystems to global carbon storage.

4.4 Introduction

Coastal vegetated ecosystems, including mangroves, seagrass meadows, and saltmarshes, play a crucial role as carbon sinks, storing estimates of up to 0.7 Pg carbon year^{-1} [Temmink et al.,

2022]. With carbon sequestration rates up to 10 times greater than those of terrestrial forests [Mcleod et al., 2011], these ecosystems are increasingly recognized as nature-based climate solutions. This high carbon sequestration capacity, coupled with their abilities to protect coastlines, support biodiversity, and improve water quality, underscores their significance in carbon dioxide removal (CDR) strategies [Hagger et al., 2022, Mengis et al., 2023, Gattuso et al., 2018].

Mangroves, seagrass and saltmarshes sequester carbon through biomass and sediment storage and by releasing dissolved organic carbon (DOC) through their root system. Seagrass meadows were shown to be enriched in the sugar sucrose compared to unvegetated areas [Sogin et al., 2022]. In contrast, macro- and microalgae, which lack root systems, release most of their carbon as exudates, constituting between 1% and 35% of their net primary production [Abdullah and Fredriksen, 2004, Wada et al., 2007, Reed et al., 2015, Paine et al., 2021, Wada and Hama, 2013]. Due to the challenges in tracking algae's carbon storage potential from source to sink, they are often excluded from blue carbon strategies [Krause-Jensen et al., 2018, Krause-Jensen and Duarte, 2016].

Despite these challenges, algae contribute substantially to blue carbon pools. Macro- and microalgae have been shown to supply up to 50% of the carbon in seagrass sediments [Kennedy et al., 2010] and up to 60% of Red Sea mangrove sediments [Almahasheer et al., 2017], identifying algae as significant car-

bon donors [Krause-Jensen et al., 2018, Ortega et al., 2019]. However, once release into the environment, tracking algae-derived carbon becomes complex. While a portion of this carbon is remineralized, 10-60% can persist under environmental conditions, potentially forming long-term carbon sinks [Krause-Jensen and Duarte, 2016, Watanabe et al., 2020, Wada et al., 2008, Filbee-Dexter and Wernberg, 2020].

Further complicating this tracking process is the complexity of algae exudates. For instance, brown algae and diatoms secrete the complex and variable extracellular matrix polysaccharide fucoidan that might resist microbial degradation [Buck-Wiese et al., 2023, Vidal-Melgosa et al., 2021, Giljan et al., 2023, Arnosti et al., 2012, Lloyd et al., 2022]. These substances can assemble into particles [Vidal-Melgosa et al., 2021, Salmeán et al., 2022, Huang et al., 2021] that are carried by tides and currents before sinking to sediment [Vidal-Melgosa et al., 2022]. The extent of carbon transport and the composition of the stored organic carbon in coastal vegetated ecosystems remains understudied. Tracing carbon from source to sink is essential for understanding the potential for long-term carbon storage. Here, we hypothesized that specific polysaccharides can serve as bioindicators for algal carbon stored within coastal vegetated ecosystems, suggesting that blue carbon sequestration results from the collective carbon sequestration across ecological communities.

4.5 Results

4.5.1 *Global sediment analysis revealed similar monosaccharide abundance despite different ecosystems and locations*

To investigate the mono- and polysaccharides stored in sediments across coastal vegetated ecosystems, we analysed 93 sediment cores from the North Sea, Baltic Sea, Malaysia and Columbia. 50cm deep sediment cores were taken in saltmarsh, seagrass, mangroves and unvegetated areas (Fig. 32, A-C, Table 4). Up to 3 points per ecosystem were sampled along a transect (Fig. 32, D).

The major building blocks of polysaccharides, including fucose, galactose, glucose, mannose, xylose and galacturonic acid were found to be shared between all ecosystems and depths. Applying a non-metric multidimensional scaling (NMDS) analysis to the dataset of relative abundances of monosaccharides in each sample, we found no distinct clusters among the 93 sediment cores, indicating the composition of each sample remains unchanged with location and ecosystem (Fig. 32E). Diffusion mapping the dataset of relative abundances, revealed a reverse relationship between fucose and glucose, where high fucose abundances occur with low glucose abundances and vice versa (Fig. 32F-G).

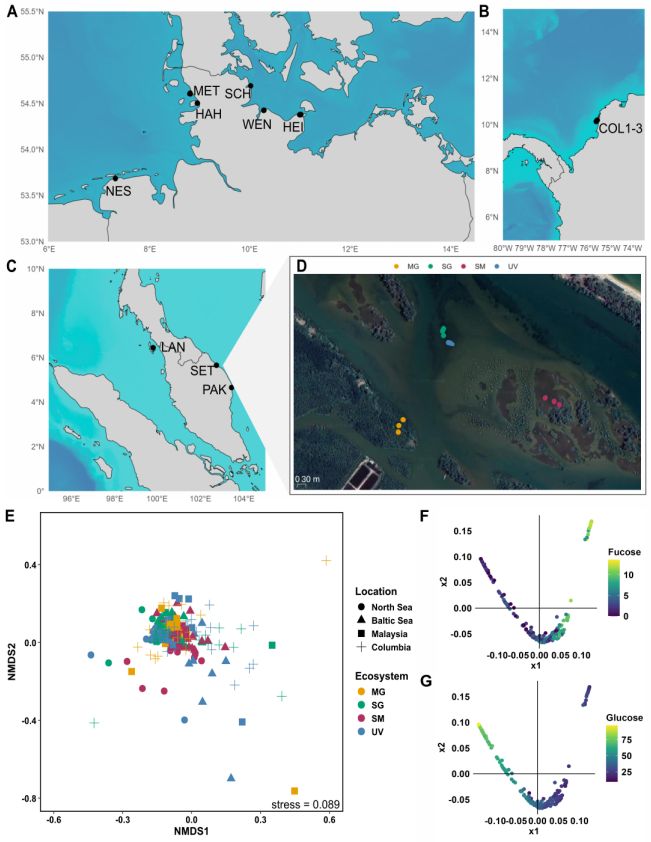

Figure 32: **93 analysed sediment cores from temperate to tropical regions revealed no major differences in monosaccharide abundances, despite ecosystems and locations. A-C)** Global sampling map of sediment cores of coastal vegetated ecosystems. Bathymetry is increasing with darker blue scale; bathymetry data is from NOAA (2022), plotted with R packages 'marmap' [Pante and Simon-Bouhet, 2013] and 'sf' [Bivand, 2021].

Figure 32: **A)** Sampling locations along the North and Baltic Sea, Germany. NES: Nessmersiel, HAH: Hamburger Hallig, MET: Mettgrund, SCH: Schleimünde, WEN: Wendtorf, HEI: Heiligenhafen, **B)** in Columbia: COL sites 1 to 3 and **C)** in Malaysia, LAN: Langkawi, SET: Setiu, PAK: Paka. **D)** Example transect map, plotted with QGIS, of analysed transect point in ecosystems sampled in Setiu, Malaysia: mangroves (yellow), seagrass (green), saltmarsh (maroon), unvegetated (blue). Further information on analysed sampling points with locations are shown in supplementary table 4. **E)** Non-metric multidimensional scaling (NMDS) plot, calculated by Bray-Curtis dissimilarity of monosaccharide composition of MilliQ-water and EDTA extracts across different sediment layers for four locations, North Sea and Baltic Sea in Germany, Malaysia and Columbia for four ecosystems, mangroves (MG, yellow), seagrass (SG, green), saltmarsh (SM, maroon) and unvegetated (UV, blue). NMDS stress level of 0.089. **F-G)** Diffusion maps of the relative abundances of monosaccharides identify new explanatory variables. X1 and x2 correspond to two new variables that identify the main dimensions of the data manifolds. Colouring the datapoints by relative abundance of fucose **(F)** and glucose **(G)** reveals an inverse relationship, where samples with high fucose levels tend to have low glucose levels, and vice versa.

The quantification of total carbohydrates across different ecosystems revealed the highest maximum mean concentrations of 1.67±0.23 mg g $_{\text{dry weight}}^{-1}$ in saltmarsh sediments. Mangroves and saltmarshes showed significant higher concentrations compared to seagrass and unvegetated areas ($p<0.001$)(Fig. 33A). Of the total carbohydrates, 10% could be attributed to total hydrolyzable carbohydrates. Except for mangroves, all ecosystems showed significant differences to each other ($p<0.001$, after Bonferroni correction, $\alpha=0.0083$) (Fig. 33B). Unvegetated areas ranging lowest in mean concentrations of 35.94±1.04 ug $_{\text{dry weight}}^{-1}$, followed by seagrass with 67.65±2.32 ug $g_{\text{dry weight}}^{-1}$ and saltmarsh (250.55±9.04 ug $_{\text{dry weight}}^{-1}$) areas. Mangroves recorded the highest mean concentrations of 494.08±45.51 ug $_{\text{dry weight}}^{-1}$, but also the greatest variations (Fig. 33B).
Fucose concentrations averaged 4.60 ±0.34 ug $_{\text{dry weight}}^{-1}$ across all samples (Fig. 33C). Significant differences were seen among concentrations between seagrass and unvegetated ($p= 0.0066$) and saltmarsh and unvegetated sediments ($p<0.001$, after Bonferroni correction, $\alpha= 0.0083$). Mean fucose concentrations were lowest in unvegetated areas with 2.57 ±0.46 ug $_{\text{dry weight}}^{-1}$, followed by seagrass with 3.88 ±0.40 $ug_{\text{dry weight}}^{-1}$, by mangroves with 4.35 ±0.67 and highest in saltmarshes with 7.67 ±0.88 $_{\text{dry weight}}^{-1}$ (Fig. 33C). An increasing trend (not significant) in the relative abundance of fucose was observed in seagrass meadows (ANOVA, $p = 0.0594$) comparing the sediment layer at the surface of each core to the deepest taken layer

(Fig. 33D). Fucose accounted for up to 10% of total hydrolyzable carbohydrates. It was significantly higher in seagrass and unvegetated areas compared to saltmarsh areas in the North Sea ($p = 0.0015$, $p = 0.0135$, respectively, Bonferroni correction, $\alpha = 0.0167$), as well as saltmarsh and mangrove areas in Malaysia ($p = 0.0032$, after Bonferroni correction, $\alpha = 0.0083$) (Fig. 33E).

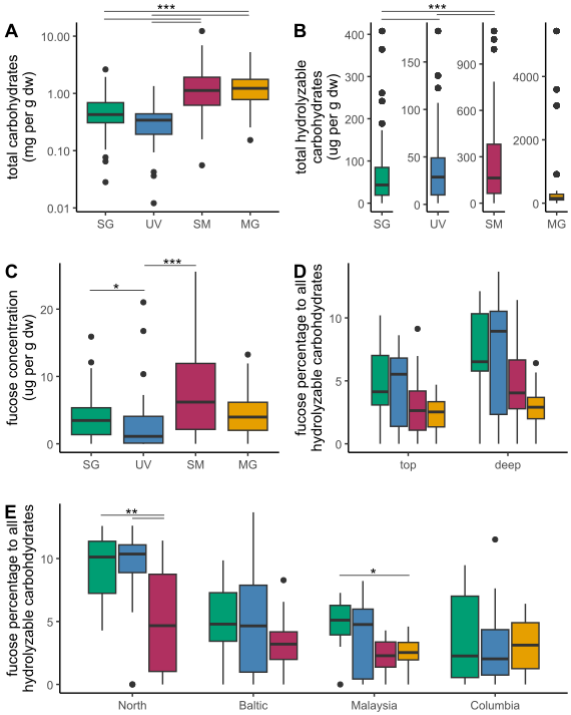

Figure 33: **Up to 10% of total hydrolyzable carbohydrates can be attributed to fucose. A)** Total carbohydrates, **B)** total hydrolyzable carbohydrates, **C)** fucose concentration in mg per g dry sediment from seagrass (SG; green), unvegetated (UV; blue), saltmarsh (SM; maroon) and mangroves (MG; yellow). **D)** Slight increase in relative fucose abundance comparing the surface layer of sediment cores to the deepest taken layer. **E)** Significantly higher fucose abundance in seagrass and unvegetated areas compared to saltmarsh sediment in the North Sea and in seagrass areas compared to mangroves in Malaysia.

4.5.2 *Specific antibody binding shows algae glycans in sediment cores under coastal vegetated ecosystems*

Structure specific monoclonal antibodies analysis indicate algae as a source of glycans in coastal vegetated ecosystems. Analysis of carbohydrate microarrays indicates the presence of alginate, pectin, fucoidan, arabinogalactan protein glycan, (1→3)-β-D-glucan and grass xylan (Fig. 36). Most signals were revealed for BAM7, indicative for alginate, fucoidan or pectin, across all ecosystems in Columbia and Germany. Further JIM13 indicative for arabinogalactan-protein glycans showed signal in saltmarsh and mangrove ecosystems. Notably, the upper layer of saltmarsh cores (0 up to 9.5 cm) in Heiligenhafen (HEI), Baltic Sea, revealed signal for grass xylan (LM27), not detected in further samples (Fig. 36). To confirm the presence of arabinogalactans and fucoidan the more sensitive antibody method ELISA was performed. Antibody binding to arabinogalactan protein glycan (JIM13) confirmed the signal in saltmarshes and mangroves, lower in seagrass sediments and close to no signal in unvegetated areas (Fig. 37). Monoclonal antibody BAM1, specific to algal polysaccharide fucoidan showed signal for all coastal vegetated ecosystems in all locations (Fig.34A). Relative signal appeared to be stronger in coastal vegetated ecosystems, enriched in sediments of saltmarshes, mangroves and seagrass, slightly lower in unvegetated areas. Fucoidan stored in

sediments of all coastal ecosystems was supported by the fucoidan antibody signal positively correlating with fucose concentration ($p<0.0001$ for seagrass, saltmarsh and unvegetated areas; mangroves: $p= 0.0022$) (Fig. 34B).

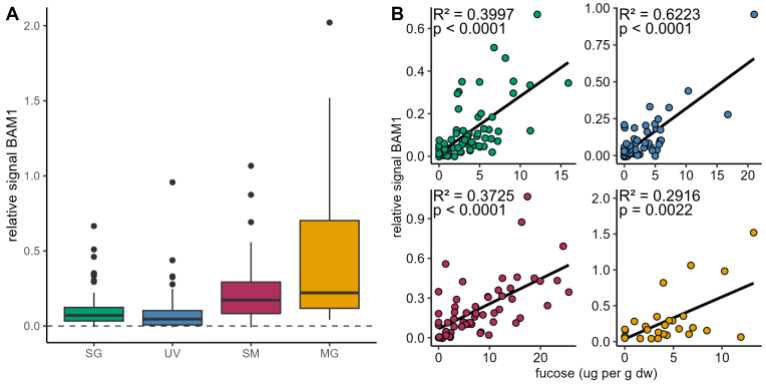

Figure 34: **Algal glycan fucoidan correlates with fucose concentrations in sediments. A)** Relative signal for antibody BAM1 (indicating presence of fucoidan) binding to sediment extracts from seagrass (SG; green), unvegetated (UV; blue), saltmarsh (SM; maroon) and mangrove areas (MG; yellow). Relative signal normalized to MilliQ-water blank shown by dashed line. **B)** Relative BAM1 signal correlates with fucose concentration derived from monosaccharide analysis in ug g_{dw}^{-1} (dw: dry weight).

The presence of the algal-derived glycan fucoidan was confirmed in porewater samples taken at depths of 30 to 50 cm along transects in North Sea sites (Table 5), using BAM1 antibody binding. The relative signal for fucoidan was notably higher beneath seagrass meadows compared to unvegetated areas. Similarly, strong signals were detected within the pioneer saltmarsh zone, relatively decreasing in within the low saltmarsh zone and being absent inside the high saltmarsh (Fig. 35A). These findings align with measured fucose concentrations of 46.98 $\pm$26.76 µg L^{-1} within the pioneer saltmarsh zone and 40.52 $\pm$10.85 µg L^{-1} beneath seagrass meadows. Concentrations were lower in the low saltmarsh zone (26.77 $\pm$11.72 µg L^{-1}) and unvegetated areas (14.56 $\pm$2.78 µg L^{-1}), with no detectable fucose in the high saltmarsh zone (Fig. 35A). These results indicate that dissolved algal-derived glycans, such as fucoidan, are secreted and transported into vegetated coastal ecosystems, which may act as acceptor systems. Algal-derived glycans carried by tidal waters may contribute to the enhancement and stabilization of sediment build-up within these ecosystems (Fig. 35B).

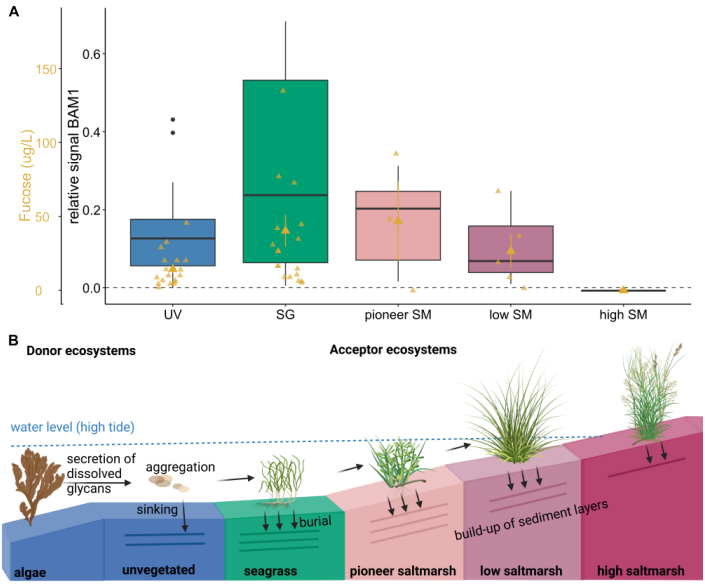

Figure 35: **Algal glycan fucoidan is stored in all coastal vegetated ecosystems. A)** Relative signal for antibody BAM1 (indicating presence of fucoidan) binding to porewater extracts from unvegetated (UV; blue), seagrass (SG; green), pioneer, low and high (SM; rose to maroon). Relative signal is normalized to signal of MilliQ-water blank (dashed line). Mean fucose concentration in ug L^{-1} (mean $\pm$s.e.m) for all ecosystems (yellow). **B)** Schematic view on storage of algal-derived glycans in coastal vegetated ecosystems, using BioRender [Hellige, 2024]. Donor ecosystems, such as algae secrete dissolved glycans, which may aggregate and being transported to coastal vegetated ecosystems. These acceptor ecosystems, reached by tidal waters may bury transported algal glycans and build-up of their sediment layers, accreting and storing their own and the carbon of donor ecosystems.

4.6 Discussion

This study revealed a similar monosaccharide abundance across different coastal ecosystems and study sites. We expected that dissolved organic carbon secreted by seagrass, saltmarshes and mangroves would show distinct carbohydrate profiles, according to the coastal ecosystem. However, the similarity in relative monosaccharide abundances underneath all sampled ecosystems (Fig. 32E) suggests a glycan continuum, as previously described in surface waters [Aluwihare et al., 1997, 2002]. The only differences seem to be driven by relative glucose and fucose abundances (Fig. 32F-G), indicating that fucose-rich oligosaccharides or polysaccharides might persist longer [Bligh et al., 2024].

Algal-derived polysaccharides, such as fucoidan can be used as bioindicators for algal carbon sequestration, tracing sources to sinks in different ecosystems. Polysaccharide screening revealed most binding to alginate, fucoidan and arabinogalactan (Fig.34, 36, 37). Arabinogalactan-protein glycan and fucoidan were shown to be exuded by algal species, in particular by brown algae [Koch et al., 2019]. Arabinogalactan-protein glycans can additionally stem from plant sources [Vidal-Melgosa et al., 2021, Koch et al., 2019]. Fucoidan was shown to be actively and continuously produced and secreted in the mucilage layer of brown algae and diatoms [Vidal-Melgosa et al., 2021, Buck-Wiese et al., 2023, Huang et al., 2021]. Contin-

uous fucoidan secretion and the resulting increase in dissolved organic matter might be followed by an increasing formation of particulate organic matter. These particles can be exported with other carbon-containing compounds through the biological carbon pump [Engel et al., 2004, Iversen, 2023]. We showed fucoidan and arabinogalactan-protein glycan signals in coastal vegetated ecosystems, suggesting its export to and storage in coastal sediments. The enhanced abundance in coastal vegetated ecosystems reached by tidal waters compared to unvegetated areas and high saltmarsh areas (Fig. 35) highlights the importance of algae as donor ecosystems to blue carbon [Krause-Jensen et al., 2018, Krause-Jensen and Duarte, 2016], while roots of plants stabilize carbon storage. However, the loss of at least around 7% of seagrass areas and up to 3% of saltmarsh and mangrove areas annually [Mcleod et al., 2011], reduces the potential for fucoidan and further algal-derived carbon sequestration in these ecosystems.

In conclusion, coastal vegetated ecosystems store carbon dioxide partially as glycans, from which some have the potential to sequester carbon as a long-term storage. Especially the interaction of ecosystems makes it difficult to track carbon compounds back to their origin, resulting in difficulties budgeting their individual climate storage potential. Fucoidan might serve as a bioindicator for algal carbon stored in different locations. Overall, this study highlights the interplay and the interconnectedness of various ecosystems in storing large amounts of

carbon. Together they function as a key-nature based solution for marine carbon dioxide removal.

4.7 Methods

50cm deep sediment cores were collected with a Russian peat corer (5cm diameter) in saltmarsh, seagrass, mangroves and unvegetated areas around the German Bight, Malaysia and Columbia (Fig. 32A-C). Up to 3 points per ecosystem were sampled along a transect (Fig. 32D), in total 93 cores were analysed (Table 4). Additionally, porewater samples were taken using lances or digging of holes. Samples were taken between 30 and 50 cm along 9 points per ecosystem at North Sea sites (Table 5). Samples were directly filtered over pre-combusted (450°C, 4.5h) GMF and GF/F filters and 200 ml of filtered porewater samples were frozen at -20°C for polysaccharide analysis.

Processing Cores were split visually according to physiochemical layers into up to 5 parts. Each layer was thoroughly homogenized by hand in a ziplock bag and stored at 4°C. Subsamples were frozen at -20°C prior to freeze drying with an Alpha 1-4 LSCbasic freeze dryer from Chris at -55°C until constant vacuum. Samples were pulverised with a ball mill (FRITSCH LLC Planeten-Mikromühle PULVERISETTE 7 premium line) at 500 rpm for 3 min. Sediment powder was stored at room temperature in the dark until further analysis.

Porewater samples were run over AMICON filtration device with 5kDa membrane (Biomax) to separate the polysaccharide fraction over 5 kDa, washed 2 times with 300 µL MilliQ and up-concentrated by a factor of 5 in MilliQ-water. Samples were freeze dried and resuspended at a final concentration factor of 100 times in MilliQ-water.

Carbohydrate extraction 90 mg of dried and pulverized material was sequentially extracted using MilliQ-water and 0.3 M EDTA. Sediment was mixed with 1.8 mL of MilliQ-water, vortexed and kept in an ultrasonic water bath for 1 hour. Extracts were centrifuged at 6000G for 15 min. The resulting supernatant was transferred into a new vial and the pellets were mixed with 1.8 mL of 0.3 M EDTA, vortexed and kept in an ultrasonic water bath for 1 hour. Extracts were centrifuged at 6000G for 15 min and the supernatant was again transferred into a new vial. Extracts were frozen at -20°C until further analysis.

Phenol-sulfuric assay The total carbohydrate content was determined by mixing 100 µL of resuspended samples or extracts with 100 µL of 5% phenol solution and 500 µL of concentrated sulfuric acid, incubated for 10 minutes at RT and afterwards for 20 min at 30°C. Absorbance at 490 nm was measured using Spectramax Id3 plate reader (Molecular Devices) against a

glucose standard curve.

Acid hydrolysis Polysaccharides were acid hydrolysed into quantifiable monosaccharides by adding 300 µL 2M HCl to 300 µL of the porewater extracts and MilliQ-sediment extracts and the 20x diluted EDTA extract in pre-combusted glass vials (450°C, 4.5 h). Glass vials were sealed and polysaccharides hydrolysed at 100°C for 24 h. The samples were transferred after hydrolysis to microtubes and dried in an acid-resistant vacuum concentrator (Martin Christ Gefriertrocknungsanlagen GmbH, Germany). Samples were resuspended in 300 µL MilliQ-water.

Monosaccharide quantification As previously described in two studies [Engel and Händel, 2011, Vidal-Melgosa et al., 2021], monosaccharides were quantified using anion exchange chromatography with pulsed amperometric detection (HPAEC-PAD). The sample analysis was conducted on a Dionex ICS-5000+ system, equipped with a CarboPac PA10 analytical column (2 x 250 mm) and a CarboPac PA10 guard column (2 x 50 mm). Neutral and amino sugars were separated applying an isocratic phase using 18 mM NaOH. A gradient reaching up to 200 mM NaCH3COO was applied to separate acidic monosaccharides.

Microarray MilliQ-water and EDTA sediment extracts were equally combined, 30 µL were transferred into wells of 384-microwell plates, where two consecutive two-fold dilutions were done in printing buffer (55.2% glycerol, 44% water, 0.8% Triton X-100), the microwell plates were centrifuged at 3500 x g for 10 min at 15 °C. Microarray printing and probing was performed as previously described in [Vidal-Melgosa et al., 2022].

ELISA Polysaccharides were detected using enzyme-linked immunosorbent assay (ELISA) as described in the following studies [Vidal-Melgosa et al., 2021, Cornuault et al., 2014]. In short, 100 µl of each combined extract and the porewater samples were pipetted into a pre-coated 96 well plate and incubated overnight at 4°C. Signal was developed using primary antibodies (BAM1 for porewaters samples and BAM1 and JIM13 for sediment samples) in skim milk PBS solution at a concentration of 1:10, followed by antibody anti-rat in skim milk PBS solution at a concentration of 1:1000. Absorbance after development was measured at 450 nm using Spectramax Id3 plate reader (Molecular Devices).

Statistical analysis All statistical analysis were carried out using R4.4.1 (R core team, [R Core Team, 2020]) and Julia [Bezanson et al., 2017]. The relative abundance of each monosaccharide was determined, all samples with a relative

abundance of acidic sugars of over 50% were excluded from calculations. Pairwise distances were calculated using the Bray-Curtis distance metric for non-metric multidimensional scaling, using the vegan package [Oksanen et al., 2018]. As NMDS can be quite sensitive to noise [Fahimipour and Gross, 2020], we also applied diffusion maps [Coifman et al., 2005] as a non-linear dimensionality reduction method for comparison using 1/Bray-Curtis distance to construct the similarity matrix and a threshold of 5. The eigenvectors corresponding to the smallest non-zero eigenvalues are the most interesting as they identify the directions of the largest variation, i.e. the main dimensions of the data manifolds.

To test for significant changes between ecosystems in the sum of MiliQ-water and EDTA extracts we applied the following statistical methods using the car package [Fox et al., 2019]. In case of no normal distribution, we performed the Kruskal-Wallis test, followed by the pairwise Wilcoxon test with α-correction according to Bonferroni to adjust for the inflation of type I error due to multiple testing. Bonferroni adjustment was performed as follows: $p = 0.05/k$, with k as the number of single hypotheses. Here, $k = 6$ was used for comparison among all 4 ecosystems and $k = 3$ for locations without mangroves. Therefore, $\alpha = 0.0083$ or $\alpha = 0.0167$ was considered statistically significant. When normality was met, we conducted an ANOVA, followed by a post-hoc Tukey test for pairwise comparisons.

4.8 Acknowledgements

The authors thank technicians at Max-Planck Institute for Marine Microbiology and Marum Centre for Environmental Research, University of Bremen, namely Tina Horstmann for assistance with carbohydrate microarray analysis, Katharina Föll for HPAEC-PAD measurements, as well as Theresa Fett and Mirco Wölfelschneider from Leibniz Centre for Tropical Marine Research (ZMT), Bremen, Germany for sampling of cores and processing of sediment cores. The authors thank Dariya Baiko and Michael Seidel from Institute for Chemistry and Biology of the Marine Environment (ICBM), Carl von Ossietzky University, Oldenburg and Jana Geuer and Tomasz Markowski from Max-Planck Institute for Marine Microbiology for sampling and processing of porewater. The authors thank José Ernesto Mancera-Pineda from Universidad Nacional de Colombia, Esteban Zarza González from Universidad del Sinú, Colombia, Jen Nie Lee from Faculty of Science and Marine Environment, Universiti Malaysia Terengganu and A. Aldrie Amir from Institute for Environment and Development (LESTARI), Universiti Kebangsaan Malaysia. Collections along the German North Sea coast in Lower Saxony and Schleswig-Holstein were made under the permit issued by the Lower Saxony Wadden Sea National Park Authority (Ref.no.: 01.2-22249-1-1.1 (60-8) / 2022) and the National Park Administration of the State Agency for Coastal Protection, National Park and Ma-

rine Conservation Schleswig-Holstein (Ref.no.: 3141-537.46) respectively. Collections along the German Baltic Sea coast near Massholm, Wendtorf, and Heiligenhafen were made under the permits issued by the
Schleswig-Flensburg District Department for Environment Section for Nature Conservation, the Plön District Administrator, Lower Nature Conservation Authority, Office for the Environment (Ref.no.: 3106-3/127/0161), and the District Administrator Department Nature and Soil (Ref.no.: 6.20.2-3117-IV-22-Fr) respectively. Collections from Colombia along the peninsula of Barú were made under the permit from the Sub-Directorate for Management and Administration of Protected Areas (Ref.no.: 20222000 120371). Collections from Malaysia were made under permit from the Ministry of Natural Resources, Environment and Climate Change (Access and benefit-sharing, Ref 974126). The permission to carry out research in Kilim Geoforest Park (Forest Reserve) in Kedah, Malaysia was obtained and approved by the Director-General of the Forestry Department of Peninsular Malaysia (Reference No.: JH/ 100 Jld. 33 (75)). The permit to enter Kilim Geoforest Park (Forest Reserve) in Kedah, Malaysia was obtained from the Langkawi District Forest Office (Permit No.: KL 72.2022). The authors acknowledge invaluable support from the Max-Planck-Society, the sea4SoCiety, CDRmare campaign in the German Marine Research Alliance.

4.9 Supplementary information

4.9.1 Supplementary tables

Table 4: **Sediment cores** taken in Germany, Malaysia and Columbia in all four ecosystems: SG (seagrass), UV (unvegetated), SM (saltmarsh) and MG (mangrove). Information on sampling location, date and time.

Country	Location	Ecosystem	Point	Longitude	Latitude	Date and time
Germany	NES	SG	P4	7.335864	53.686188	2022-08-16T08:43:00
Germany	NES	SG	P5	7.335658	53.686212	2022-08-16T08:59:00
Germany	NES	SG	P6	7.335419	53.686239	2022-08-16T09:13:00
Germany	NES	UV	P4	7.336820	53.685264	2022-08-17T07:02:00
Germany	NES	UV	P5	7.336531	53.685304	2022-08-17T07:13:00
Germany	NES	UV	P6	7.336299	53.685328	2022-08-17T07:26:00
Germany	NES	SM	P3	7.335585	53.684371	2022-08-15T10:46:00

Country	Location	Ecosystem	Point	Longitude	Latitude	Date and time
Germany	NES	SM	P6	7.335641	53.684276	2022-08-15T11:32:00
Germany	NES	SM	P8	7.335455	53.683768	2022-08-15T13:59:00
Germany	NES	SM	P9	7.335623	53.683454	2022-08-15T13:42:00
Germany	HAH	SG	P4	8.823788	54.612684	2021-11-09T09:31:03
Germany	HAH	SG	P6	8.823431	54.612663	2021-11-09T09:14:41
Germany	HAH	SG	P8	8.822986	54.612680	2021-11-09T09:01:44
Germany	HAH	UV	P4	8.811397	54.605695	2021-11-10T09:10:14
Germany	HAH	UV	P5	8.811318	54.605757	2021-11-10T09:20:28
Germany	HAH	UV	P6	8.811194	54.605855	2021-11-10T09:29:10
Germany	HAH	SM	P5	8.825151	54.604496	2021-11-08T14:20:59
Germany	HAH	SM	P7	8.824193	54.605339	2021-11-08T13:55:06
Germany	MET	SG	P4	8.967728	54.502967	2021-11-11T09:54:31

Country	Location	Ecosystem	Point	Longitude	Latitude	Date and time
Germany	MET	SG	P6	8.968376	54.502919	2021-11-11T09:41:19
Germany	MET	UV	P6	8.964934	54.503152	2021-11-11T12:17:11
Germany	MET	SM	P1	8.961645	54.503247	2021-11-10T15:01:18
Germany	MET	SM	P4	8.961963	54.503353	2021-11-10T14:30:54
Germany	SCH	SM	P4	10.024382	54.691559	2022-08-30T09:53:00
Germany	SCH	SM	P5	10.025295	54.691736	2022-08-30T09:54:00
Germany	SCH	SM	P6	10.026225	54.691997	2022-08-30T09:56:00
Germany	SCH	SM	P7	10.023244	54.692271	2022-08-30T10:43:00
Germany	WEN	SG	P5	10.287542	54.427274	2022-08-29T08:47:00
Germany	WEN	SG	P7	10.286985	54.427172	2022-08-29T08:25:00
Germany	WEN	SG	P9	10.286444	54.426960	2022-08-31T08:29:00
Germany	WEN	UV	P3	10.281737	54.425132	2022-08-26T10:31:00

Country	Location	Ecosystem	Point	Longitude	Latitude	Date and time
Germany	WEN	UV	P5	10.281203	54.424871	2022-08-26T10:26:00
Germany	WEN	UV	P7	10.280711	54.424579	2022-08-26T10:22:00
Germany	WEN	SM	P5	10.290692	54.425844	2022-08-26T08:21:00
Germany	WEN	SM	P7	10.291283	54.426592	2022-08-26T08:16:00
Germany	WEN	SM	P9	10.291536	54.427105	2022-08-26T08:11:00
Germany	HEI	SG	P3	11.024932	54.380240	2022-08-24T10:08:00
Germany	HEI	SG	P6	11.024368	54.380322	2022-08-24T10:04:00
Germany	HEI	SG	P8	11.024125	54.380358	2022-08-24T10:02:00
Germany	HEI	UV	P3	11.023301	54.381132	2022-08-25T09:01:00
Germany	HEI	UV	P5	11.022933	54.381358	2022-08-25T09:04:00
Germany	HEI	UV	P7	11.022446	54.381428	2022-08-25T09:06:00
Germany	HEI	SM	P1	11.021790	54.377104	2022-08-23T12:11:00

Country	Location	Ecosystem	Point	Longitude	Latitude	Date and time
Germany	HEI	SM	P3	11.020723	54.379271	2022-08-23T13:16:00
Germany	HEI	SM	P4	10.995120	54.377100	2022-08-24T07:49:00
Germany	HEI	SM	P9	10.998305	54.378869	2022-08-24T07:31:00
Malaysia	LAN	SG	P1	99.817006	6.447992	2022-09-29T00:26:00
Malaysia	LAN	SG	P3	99.817083	6.448251	2022-09-29T00:23:00
Malaysia	LAN	SG	P5	99.817260	6.448333	2022-09-29T00:19:00
Malaysia	LAN	UV	P1	99.819578	6.449959	2022-09-29T23:49:00
Malaysia	LAN	UV	P3	99.819896	6.450094	2022-09-29T23:54:00
Malaysia	LAN	UV	P5	99.820262	6.450287	2022-09-29T23:59:00
Malaysia	LAN	MG	P1	99.817696	6.448197	2022-09-24T02:47:00
Malaysia	LAN	MG	P5	99.818622	6.448140	2022-09-24T06:56:00
Malaysia	PAK	MG	P5	103.439177	4.660548	2022-10-11T04:51:00

Country	Location	Eco-system	Point	Longitude	Latitude	Date and time
Malaysia	PAK	MG	P9	103.439555	4.660660	2022-10-11T04:35:00
Malaysia	SET	SG	P1	102.740665	5.660896	2022-10-05T01:51:00
Malaysia	SET	SG	P2	102.740617	5.660790	2022-10-05T01:54:00
Malaysia	SET	SG	P4	102.740644	5.660663	2022-10-05T01:58:00
Malaysia	SET	UV	P1	102.740820	5.660473	2022-10-05T03:17:00
Malaysia	SET	UV	P2	102.740859	5.660461	2022-10-05T03:18:00
Malaysia	SET	UV	P3	102.740893	5.660429	2022-10-05T03:20:00
Malaysia	SET	MG	P2	102.739409	5.658089	2022-10-04T02:43:00
Malaysia	SET	MG	P5	102.739269	5.657932	2022-10-04T02:58:00
Malaysia	SET	MG	P8	102.739227	5.657740	2022-10-04T02:23:00
Malaysia	SET	SM	P1	102.743881	5.658787	2022-10-09T03:01:00
Malaysia	SET	SM	P3	102.744144	5.658643	2022-10-09T02:58:00

Country	Location	Ecosystem	Point	Longitude	Latitude	Date and time
Malaysia	SET	SM	P5	102.744319	5.658541	2022-10-09T02:55:00
Columbia1		SG	P3	-75.681974	10.136862	2022-05-03T16:47:00
Columbia1		SG	P4	-75.681995	10.136855	2022-05-03T16:48:00
Columbia1		SG	P8	-75.682115	10.137064	2022-05-03T16:53:00
Columbia1		UV	P2	-75.682109	10.137113	2022-05-03T16:57:00
Columbia1		UV	P3	-75.682165	10.137153	2022-05-03T16:56:00
Columbia1		UV	P4	-75.682178	10.137119	2022-05-03T16:55:00
Columbia1		MG	P7	-75.682718	10.136688	2022-05-01T14:44:00
Columbia1		MG	P8	-75.682815	10.136645	2022-05-01T14:45:00
Columbia1		MG	P9	-75.682996	10.136577	2022-05-01T14:46:00
Columbia2		SG	P3	-75.630319	10.192668	2022-05-05T15:43:00
Columbia2		SG	P4	-75.630338	10.192487	2022-05-05T15:39:00

Country	Location	Ecosystem	Point	Longitude	Latitude	Date and time
Columbia	2	SG	P5	-75.630355	10.192527	2022-05-05T15:41:00
Columbia	2	UV	P1	-75.630572	10.192642	2022-05-07T15:54:00
Columbia	2	UV	P2	-75.630508	10.192592	2022-05-07T15:53:00
Columbia	2	UV	P3	-75.630435	10.192557	2022-05-07T15:52:00
Columbia	2	MG	P6	-75.630144	10.191658	2022-05-04T15:44:00
Columbia	2	MG	P3	-75.629953	10.191859	2022-05-04T15:29:00
Columbia	2	MG	P2	-75.630129	10.192157	2022-05-04T14:26:00
Columbia	3	SG	P1	-75.655608	10.171513	2022-05-08T21:21:00
Columbia	3	SG	P6	-75.655606	10.171255	2022-05-08T21:17:00
Columbia	3	UV	P1	-75.655774	10.171481	2022-05-09T14:50:00
Columbia	3	UV	P2	-75.655756	10.171415	2022-05-09T14:57:00
Columbia	3	UV	P5	-75.655592	10.171073	2022-05-09T14:56:00

Country	Location	Ecosystem	Point	Longitude	Latitude	Date and time
Columbia	3	MG	P5	-75.655710	10.171036	2022-05-08T16:26:00
Columbia	3	MG	P6	-75.655767	10.170866	2022-05-08T16:21:00

Table 5: **Porewater samples** taken in North Sea, Germany; SG (seagrass), UV (unvegetated), SM (saltmarsh) and MG (mangrove). Information on sampling location, date and time.

Country	Location	Ecosystem	Point	Longitude	Latitude	Date and time
Germany	MET	UV	P8	8.965385	54.503093	2021-11-11T11:56:13
Germany	MET	UV	P7	8.965155	54.503122	2021-11-11T12:05:02
Germany	MET	UV	P6	8.964934	54.503152	2021-11-11T12:17:11
Germany	MET	UV	P5	8.964667	54.503183	2021-11-11T12:28:43
Germany	MET	UV	P4	8.964450	54.503218	2021-11-11T12:36:18

Country	Location	Eco-system	Point	Longitude	Latitude	Date and time
Germany	MET	UV	P2	8.964039	54.503253	2021-11-11T13:01:43
Germany	MET	UV	P1	8.963778	54.503281	2021-11-11T13:09:45
Germany	MET	SG	P7	8.968679	54.502892	2021-11-11T09:35:04
Germany	MET	SG	P6	8.968376	54.502919	2021-11-11T09:41:19
Germany	MET	SG	P5	8.968032	54.502951	2021-11-11T09:47:01
Germany	MET	SG	P3	8.967398	54.502991	2021-11-11T10:01:21
Germany	MET	SG	P2	8.967011	54.503010	2021-11-11T10:08:13
Germany	MET	SG	P1	8.966630	54.503043	2021-11-11T10:14:44
Germany	MET	SM	P9	8.962557	54.503675	2021-11-10T13:29:20
Germany	MET	SM	P7	8.962272	54.503539	2021-11-10T13:55:11
Germany	MET	SM	P4	8.961963	54.503353	2021-11-10T14:30:54
Germany	MET	SM	P3	8.961829	54.503302	2021-11-10T14:42:36

Country	Location	Ecosystem	Point	Longitude	Latitude	Date and time
Germany	NES	UV	P1	7.337581	53.685136	2022-08-17T06:15:00
Germany	NES	UV	P2	7.337332	53.685182	2022-08-17T06:33:00
Germany	NES	UV	P3	7.337112	53.685226	2022-08-17T06:48:00
Germany	NES	UV	P4	7.336820	53.685264	2022-08-17T07:02:00
Germany	NES	UV	P5	7.336531	53.685304	2022-08-17T07:13:00
Germany	NES	UV	P6	7.336299	53.685328	2022-08-17T07:26:00
Germany	NES	UV	P7	7.336025	53.685375	2022-08-17T07:39:00
Germany	NES	UV	P9	7.335574	53.685436	2022-08-17T07:50:00
Germany	NES	UV	P8	7.335799	53.685408	2022-08-17T08:03:00
Germany	NES	SG	P1	7.336522	53.686072	2022-08-16T07:34:00
Germany	NES	SG	P2	7.336250	53.686122	2022-08-16T07:49:00
Germany	NES	SG	P3	7.336035	53.686153	2022-08-16T08:26:00

Country	Location	Ecosystem	Point	Longitude	Latitude	Date and time
Germany	NES	SG	P4	7.335864	53.686188	2022-08-16T08:43:00
Germany	NES	SG	P5	7.335658	53.686212	2022-08-16T08:59:00
Germany	NES	SG	P6	7.335419	53.686239	2022-08-16T09:13:00
Germany	NES	SG	P7	7.335206	53.686254	2022-08-16T09:27:00
Germany	NES	SG	P8	7.335019	53.686274	2022-08-16T09:45:00
Germany	NES	SG	P9	7.334821	53.686297	2022-08-16T09:57:00
Germany	NES	SM	P1	7.334766	53.684303	2022-08-15T10:08:00
Germany	NES	SM	P2	7.335257	53.684291	2022-08-15T10:34:00
Germany	NES	SM	P5	7.335259	53.684215	2022-08-15T10:59:00
Germany	NES	SM	P6	7.335641	53.684276	2022-08-15T11:32:00

4.9.2 Supplementary figures

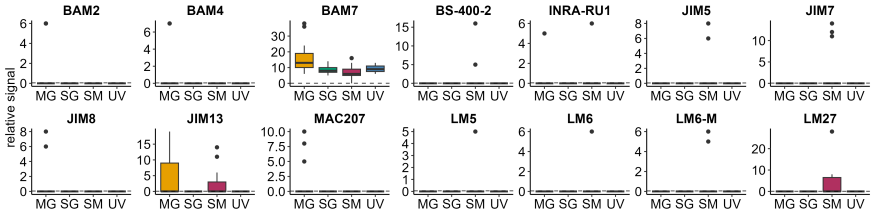

Figure 36: **Microarray antibody binding revealed presence of alginate, fucoidan, pectin, grass xylan and arabinogalactan.** Binding to BAM2 and BAM4 (sulfated epitope in sulfated fucan), BAM7 (alginate -pectin or fucoidan), BS-400-2 ((1→3)-β-D-glucan), INRA-RU1 (rhamnogalacturonan I backbone), JIM5 (partially methyl-esterified/de-esterified HG), JIM7 (methyl-esterified HG), JIM8, JIM13 and MAC207 (all arabinogalactan protein glycan), LM5 ((1→4)-β-D-galactan), LM6 ((1→5)-α-L-arabinan), LM6-M ((1→5)-α-L-arabinan), LM27 (grass-xylan).

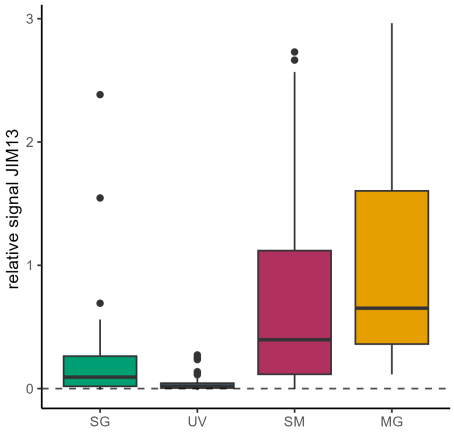

Figure 37: **Relative antibody signal of JIM13 normalized to MilliQ-blank, representing arabinogalactans.** Arabinogalactans (JIM13) found in saltmarsh (SM), mangrove (MG) and seagrass (SG) areas. No signal in unvegetated areas (UV).

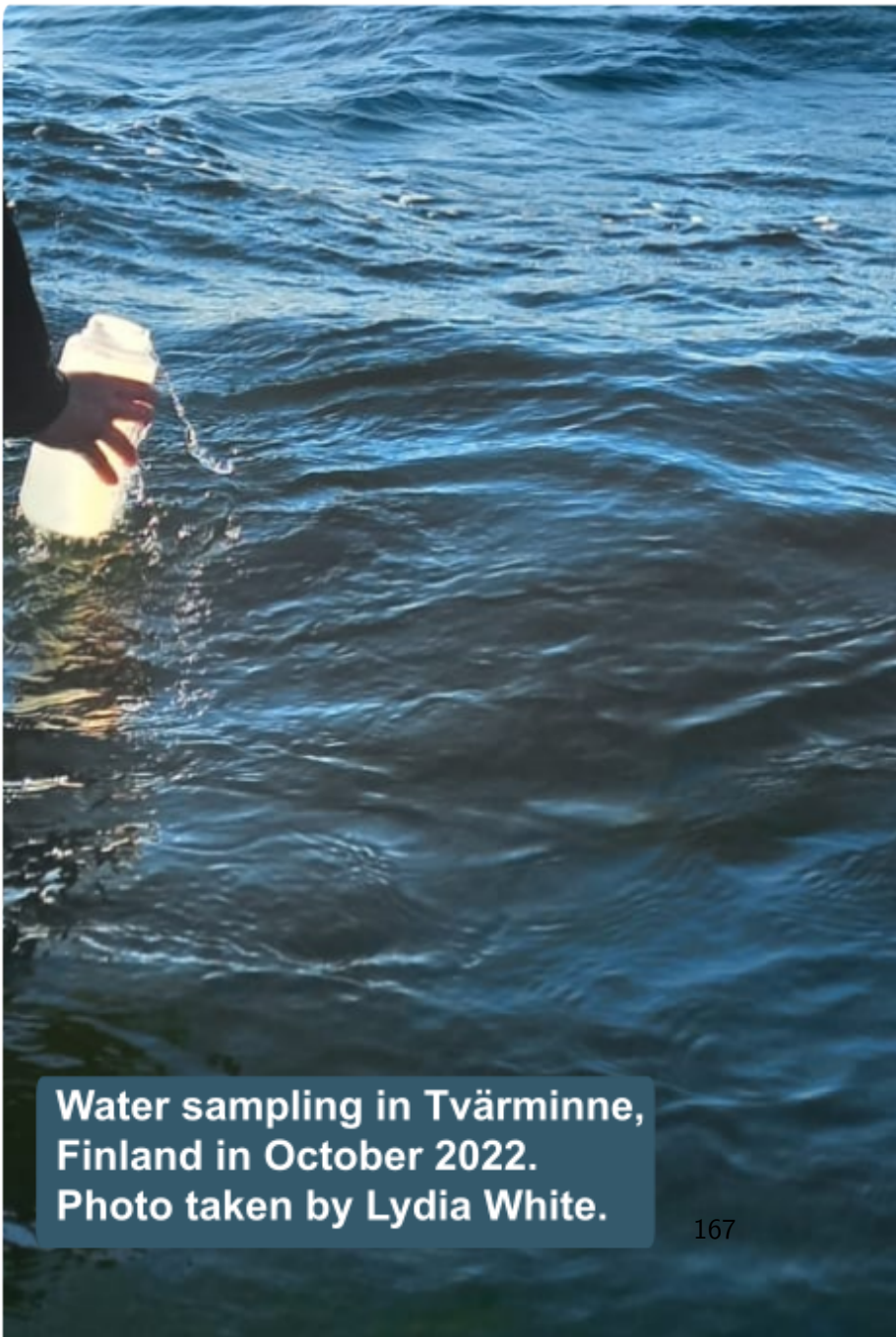

Water sampling in Tvärminne, Finland in October 2022. Photo taken by Lydia White.

5 Discussion

5.1 Summary of studies

This thesis revealed active secretion of the algal polysaccharide fucoidan by all six tested brown algae around the globe. Fucales and Laminariales species sourced dissolved fucoidan into surface waters. Fucoidan secretion was confirmed by analysis of total hydrolysed fucose and specifically after anion exchange chromatography, as well as confirmation by monoclonal antibody binding. Environmental transect data in proximity to brown algae detected the presence of fucoidan in surface waters (Manuscript I).

Fucoidan was shown to resist immediate microbial hydrolysis. Incubation of fluorescently labelled *Sargassum fluitans* fucoidan revealed no hydrolysis for 29 days under ocean water conditions, but revealed that bacteria had the enzymatic machinery to fragment *Sargassum* fucoidan when encountering high concentrations for a longer period of time. Bacteria started hydrolysing *Sargassum* fucoidan after six days of incubation with *Sargassum fluitans*, while fucoidan concentrations accumulated. Notably, close to no hydrolysis occurred in control tanks. Bacteria specifically targeted *Sargassum* fucoidan and not the further tested *Fucus vesiculosus* fucoidan, suggesting structure specificity. This study showed that fucoidan was resistant against complete hydrolysis under environmental occurring

concentrations (Manuscript II).

Resistance matched observed persistence of fucoidan in mesocosm waters for at least 12 days after removal of brown algae. After a year-long incubation in the dark dissolved fucose-polymers were still detectable. Relative persistence in the dissolved fraction and resistance against microbes suggests the possible transitioning from the dissolved to the particulate fraction. Fucoidan concentrations increased in the particulate fraction over the course of brown algae incubations. This concentration increase was quantified based on the fucose-hydrolysed fraction of GF/F filters and confirmed with antibody labelling and visual fucoidan aggregation after 9 months of incubation in the dark. The presence of fucoidan in sinking particles supported possible fucoidan sedimentation. Environmental POM data downstream of an algae farm in Northern Ireland revealed fucoidan transitioning into the particulate phase also under natural conditions (Manuscript I).

My research showed up to 0.1 Gt of fucoidan carbon is secreted per year globally. Secreted fucoidan does not equal sequestered fucoidan, but might be transported into coastal vegetated ecosystems. Sediment samples revealed no distinct relative monosaccharide abundance, despite varying locations and ecosystems. Up to 10% of total hydrolyzable mono- saccharides could be attributed to fucose, the main constituent monomer of fucoidan. Monoclonal antibody binding revealed the presence of fucoidan in all CVEs, including seagrass mead-

ows, saltmarsh areas and mangroves. The interaction of carbon storage in CVEs was shown to be essential for quantifying individual carbon storage potentials, suggesting a unified point of view on the carbon sequestration potential of all coastal ecosystems together (Manuscript III, [Hellige et al., 2024]) (Fig. 38).

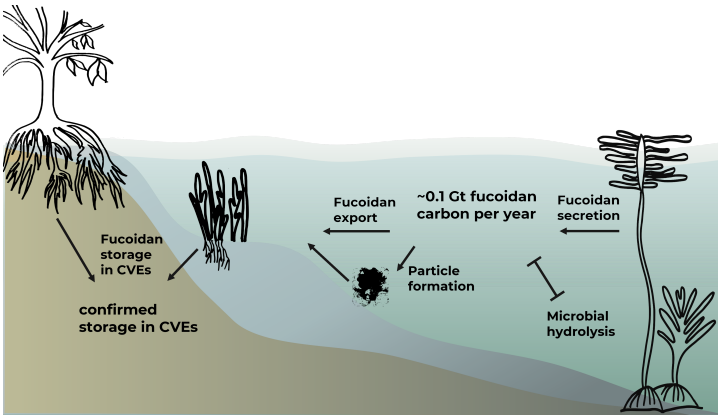

Figure 38: **Confirmed fucoidan carbon sequestration pathway.** Macroalgae exude up to 0.1 Gt fucoidan carbon per year globally, which resists direct microbial hydrolysis. Secreted fucoidan was shown to assemble into particles and being exported to coastal vegetated ecosystems (CVEs).

5.2 Discussion of combined studies

5.2.1 Fucoidan exudation as a carbon sequestration pathway

Algal fucoidan secretion is a carbon sequestration pathway. Gross fucoidan secretion accounted for 0.32-0.88 mg $g^{-1}_{\text{dry weight}}$ day^{-1}, based on the investigation of six macroalgae around the globe. The global potential of fucoidan secretion is still difficult to assess, but scales with biomass. Assuming an approximate kelp density of 0.5 kg dry biomass per m^2 [Filbee-Dexter and Wernberg, 2020] and a global kelp forest area of 1,965,227 km^2, excluding all holopelagic seaweed [Filbee-Dexter et al., 2024] this corresponds to 0.04 to 0.1 Gt fucoidan carbon secreted annually, accounting to 0.147 to 0.367 Gt carbon dioxide per year. In comparison to a global output of 36 to 40 Gt carbon dioxide per year [Gür, 2022, Masson-Delmotte et al., 2018], fucoidan carbon secretion, if completely sequestered offsets up to 1.02%. Notably, the global fucoidan carbon secretion is also impacted by the expanding holopelagic *Sargassum* spp. and microalgae blooms. Microalgae seemed to have an additive effect on fucoidan secretion and are not accounted for in the above calculation.

5.2.2 Enhancing brown algal biomass for afforestation, aquafarming and carbon capture

Increasing brown algae stocks is of interest for marine afforestation, and for aqua-farming for food and pharmaceutical industries and carbon capture. The increase in abundance and amount of biomass, along with their health state and photosynthetic activity, may directly influence the secretion of fucoidan. Changing environmental parameters are hard to foresee. Geographical distribution of brown macroalgae is shifting [Manca et al., 2024]. Multiple factors, such as marine heatwaves are threatening kelp forests, resulting in a decline of kelp forest worldwide [Filbee-Dexter et al., 2020]. Once lost, mostly turf algae take over, losing the kelp ecosystems completely [Filbee-Dexter and Wernberg, 2018]. Recent approaches, such as the green gravel project, restore kelp forest to help the ecosystem to survive and slowly adapt to changing conditions [Fredriksen et al., 2020]. Further, brown macroalgae were, have been and are estimated to expand poleward [Manca et al., 2024]. Notably, we also see increasing abundance of floating algae, such as *Sargassum* spp., expanding recently to the Great Atlantic *Sargassum* Belt [Wang et al., 2019, 2018]. Further expansion has been reported reaching from the Caribbean sea to West Africa [Wang et al., 2019, 2018]. Additionally to natural occurring increases, afforestation and reforestation, farming of macroalgae for food, pharmaceuticals or carbon storage, has in-

creased in recent years and can be further expanded [Froehlich et al., 2019, Duarte et al., 2017]. As fucoidan secretion scales with biomass, further increase in macroalgae biomass would result in increasing dissolved fucoidan concentrations, resulting in possibly higher carbon sequestration capacities.

It has been discussed that increasing algae stocks could deplete the water column of carbon dioxide if replenisment rates are below uptake rates [Warren, 2024, Bach et al., 2021]. Conversely, the direct uptake of CO_2 from the atmosphere, as well as the surrounding water is mostly not considered. Brown algae often have direct access to atmospheric CO_2 [Flores-Moya and Fernández, 1998]. Laminariales form kelp forests with specialized buoyant tissues enabling fronds to float at the surface [Bolton, 2010, Bringloe et al., 2020] (Fig. 21A,B in Manuscript I). Fucales predominantly inhabit the intertidal, where they are periodically exposed to air during low tide. Also many Fucales have buoyant tissues such as the planktonic *Sargassum fluitans*, which forms air-exposed floating rafts [Wang et al., 2019, Bringloe et al., 2020], all enabling the direct take-up of CO_2 (Fig. 21C,D in Manuscript I).

Aquafarming for carbon capture is discussed to be combined with baling and dumping of seaweed. In a theoretical study during my PhD (see Contributions to further manuscripts: CDR options for Germany; [Yao et al., 2024]), we calculated the need of sinking 9.75 Mt *Sargassum* biomass (dry weight) annually to sequester 10 Mt CO_2 $year^{-1}$. The value to sequester 10 Mt

CO_2 was chosen as it equals 8 to 22% of residual emissions in 2045 in Germany. For harvesting 9.75 Mt *Sargassum* dry weight biomass (around 57 Mt *Sargassum* biomass wet weight), we estimated the need of a standing stock of 4.63 Mt wet weight, equal to around 0.78 Mt (dry weight) *Sargassum* [Yao et al., 2024]. In comparison to the needed standing stock of 4.63 Mt wet weight, approximately 20 Mt *Sargassum*, this is around 5 times biomass than the amount that builds up annually in the Great Atlantic *Sargassum* belt [Wang et al., 2019, Smetacek et al., 2024]. The calculation of a standing stock of 0.78 Mt was only based on dumping biomass, not considering the sequestration potential in form of recalcitrant DOC, such as fucoidan. With the knowledge we gained through this thesis, we can calculate the approximate amount of secreted fucoidan. Based on *Sargassum* releasing between 0.42 and 0.75 mg fucoidan g_{dw}^{-1} d^{-1}, equal to 0.046 to 0.082 kg fucoidan C kg_{dw}^{-1} $year^{-1}$ and a standing stock of 0.78 Mt *Sargassum* biomass, this releases between 0.036 and 0.058 Mt fucoidan carbon $year^{-1}$. This equals between 0.13 and 0.21 Mt CO_2 $year^{-1}$ of fucoidan by an algae farm of the size of 1324 km^2 (approximately covering an area of the size of London). Dumping biomass has been discussed controversially and been described as unethical [Ricart et al., 2022]. Regarding its sequestration potential, large-scale dumping can sequester approximately 48 times more CO_2 compared to fucoidan carbon secretion with the same algae farm. Nevertheless, this theoretical calculation already shows the additional

ability to convert megatons of CO_2 $year^{-1}$ to secreted fucoidan with large algae farms, next to carbon storage in biomass. This highlights the opportunity of using the algae biomass with a different purpose to dumping, such as for food, pharmaceutical or energy industries.

5.2.3 Fucoidan removal via microbial hydrolysis and particle formation

Secretion of fucoidan does not equal sequestration, as multiple removal pathways are possible. Microbes have the potential and the adaptability to hydrolyse fucoidan. We showed that *Sargassum* fucoidan is resistant to hydrolysis by a natural community, but also the adaptability of fucoidan degraders when exposed to higher concentrations of fucoidan (Manuscript II). Most likely high enough fucoidan concentrations are only reached in very close proximity to the surface of brown algae, as well as possibly inside particles. Verrucomicrobia and Planctomycetes have been shown to be enriched on fucoidan-rich surface of brown algae [Bengtsson et al., 2011, Bengtsson and Ovreas, 2010]. The enzymatic hydrolysis capacity was increased in the particulate fractions [Arnosti et al., 2012, Lloyd et al., 2022, Reintjes et al., 2023]. Hydrolysis of fucoidan might be incomplete and might end with shorter oligosaccharides. This is supported by distinct patterns of fucose rich oligosaccha-

rides in deep ocean waters [Bligh et al., 2024]. This highlights the possible capacity of fucoidan or at least fucose-containing polysaccharides to escape complete microbial hydrolysis and form carbon sinks. Resistance of fucoidan towards hydrolysis versus microbial degradation might be a possible arms race. It is unclear how fast bacteria could turnover fucoidan inside an algae farm or patches of *Sargassum*, where they are exposed to high fucoidan concentrations. Evolution of bacteria and thus the turnover of fucoidan carbon back to CO_2, as well as changing fucoidan structures to challenge degradation need to be understood and considered in future assessments.

Nevertheless, a fraction of fucoidan might form aggregates before it can be degraded by microbes. Glycans are known to compose a gel like matrix, referred to as transparent exopolymer particles (TEP), which promote aggregation into larger particles [Verdugo, 2012, Busch et al., 2017, Engel, 2004]. We proved particulate fucoidan concentrations increase over the course of macroalgae incubations (Manuscript I). Here, the quantification of particulate fucoidan needs to be improved, as the bulk analysis was performed on glass fibre filter pieces. One option could be the sequential extraction of polysaccharides from filters prior to purification of the strongly anionic fraction to achieve a more conservative quantification approach for particulate fucoidan. Fucoidan aggregation was visually confirmed together with bacterial cells, highlighting the possibility of respiration inside the formed particles. Previous studies have

shown colonization of particles to happen in the upper water levels, and being transported through the water column [Legendre et al., 2015, Iversen, 2023, Martin et al., 1987, Jiao et al., 2020]. The scale of respiration of specific polysaccharides, such as fucoidan inside the particle remains unknown. The power-law function in the Martin Curve described mainly slow settling or labile particles being degraded, while degradation decreased with depth [Iversen, 2023, Martin et al., 1987]. A recent study [Bressac et al., 2024], determined microbes are responsible for 7 to 29% of flux attenuation inside particles until 300 m depths. The further fragmentation and ingestion of POC might be due to zooplankton grazing, which has been previously already described in e.g. Giering et al. [2014], Cavan et al. [2021].
Particle sinking is mainly dependent on the density of the aggregate. On average an aggregate is estimated to sink by 100 m day^{-1} [Iversen, 2023]. Considering that we found fucoidan present in sedimenting particles and in particles after one year of incubation (Manuscript I), this leads to the particles in theory having reached the deep ocean (below 1000m). Together with previously shown presence of fucoidan in deep sea sediment [Vidal-Melgosa et al., 2022] this indicates fucoidan sequestration through the biological carbon pump.

5.2.4 Fucoidan carbon storage in the environment

Complex glycans such as fucoidan are thought to resist degradation and thus might form a glycan background in the ocean. Fucoidan carbon storage depends on transportation through water currents and sedimentation. Previous studies have shown carbohydrates to constitute 15 to 35% of DOC [McCarthy et al., 1996, Pakulski and Benner, 1994], with similar monosaccharide profiles in surface waters [Aluwihare et al., 1997]. This continuity hints towards the same source, in which the same glycans resist. One of these molecules might be fucoidan as its abundance was confirmed in surface waters (Manuscript I). As deeper waters resembled blank concentrations, higher volumes of water should be analysed in future studies to track fucoidan in the environment. Notably, fucoidan concentrations inside an algae farm in Northern Ireland exceeded common fucoidan seawater concentrations, with even higher concentrations found in the particulate fraction (Manuscript I). This supports the idea that fucoidan carbon storage scales with algal biomass abundance. Further, with the current technologies we are not able to distinguish between microalgal or macroalgal fucoidan in the environment. Improvement and optimisation using a MALDI fingerprinting method [Reyes-Weiss et al., 2024] could result in the possibility to trace fucoidan presence back to its origin, helping to unravel the fate of glycans in the ocean.
Analysis of sediments of coastal vegetated ecosystems con-

firmed the presence of fucoidan (Manuscript III; [Hellige et al., 2024]). Previously, sediment cores from the Red Sea [Vidal-Melgosa et al., 2022] and the Koljö Fjord, Sweden [Salmeán et al., 2022] have shown the presence of fucoidan in centuries-old sediments. Together these results support that fucoidan settles in sediments and functions as a possible carbon sink in the ocean. Fucoidan carbon sedimentation can be estimated in coastal vegetated ecosystems. Herefore, sedimentation rates of carbon in ecosystems are estimated to account for 0.2 cm $year^{-1}$ in seagrass, 0.63 cm $year^{-1}$ in saltmarshes and 0.77 cm $year^{-1}$ in mangroves sediment, according to a recent study by Arias-Ortiz et al. [2018]. Sedimentation rates assuming similar fucose carbon concentrations throughout the core resulted in fucose estimates of 5.54 $\pm$0.58 ug C cm^{-3} in salt marshes, 3.77 $\pm$0.63 ug C cm^{-3} in mangroves and 3.80 $\pm$0.39 ug C cm^{-3} in seagrass. This resulted in highest fucose carbon sedimentation of 3.43 $\pm$0.36 in ug C cm^{-2} $year^{-1}$ in salt marshes. This equals fucoidan carbon estimates of around 116 mg C m^{-2} $year^{-1}$ for saltmarshes, 97 mg C m^{-2} $year^{-1}$ for mangroves and 25 mg C m^{-2} $year^{-1}$ for seagrass areas. These estimates do not account for potential compaction in deeper sediments and assume constant fucoidan concentrations throughout the core. Globally, fucoidan carbon sequestration across these coastal ecosystems, covering 22000-400000 km^2 for saltmarshes, 137760-152361 km^2 for mangroves and 177000-600000km^2 for seagrass areas [2], amounts to an estimate of 20 to 75 kilotons of fucoidan carbon sedimenting

per year in all three ecosystems together (Fig. 38). However, quantifying fucoidan in sediments is challenging, which could lead to either an underestimation or overestimation of fucoidan concentrations. Additionally, the loss of around 7% of seagrass areas and up to 3% of saltmarsh and mangrove areas annually [2], reduces the potential for fucoidan and further algal-derived carbon sequestration in these ecosystems.
Carbon estimates often try to separate CVEs to assess their carbon potential individually. The maximum carbon storage potential seems to be reached when all ecosystems are present and can collectively store carbon. Algal polysaccharides such as fucoidan might act as bioindicators for algal carbon stored in other ecosystems. Global budgeting of carbon sequestration in CVEs is important for protection, conservation and crediting of these ecosystems.

5.2.5 The missing piece

Amounts of global fucoidan carbon sequestration is not possible to state yet. Understanding fucoidan particle formation, drawing down not only fucoidan carbon but further carbon and microbial cells, but also understanding hydrolysis inside particles would give us a better idea on fucoidan sequestration rates. Substantial amounts of fucoidan carbon are proven to be stored in CVEs, as well as in unvegetated areas. Previous studies have

shown fucoidan signal in deep-sea sediments [Vidal-Melgosa et al., 2022]. It is important to note that methods for quantification of fucoidan from sediments are being improved and numbers for deep sea sediments are not known yet. Thus, the above given number on fucoidan carbon sequestration in sediments does not equal global fucoidan sequestration rates, but gives us insights on fucoidan stored in CVEs. Quantification of fucoidan carbon in sediments globally is essential to be able to calculate the percentage of secreted fucoidan being sequestered annually.

This research focuses on the algal polysaccharide fucoidan. Methods for complex glycan quantification are still being developed. Antibody signal has also revealed further presence of other glycans [Vidal-Melgosa et al., 2022], such as arabinogalactans (Manuscript III; [Hellige et al., 2024]), hinting towards fucoidan only being one of a range of different possible glyco-carbon sequestration molecules. Future studies should assess the potential of further glycans to describe the extent of glycan carbon sequestration globally. Improving methods for glycan analysis might allow us to quantify more specific glycans faster and more accurately.

Overall fucoidan carbon is a possible sequestration pathway, shown to store mega to gigatons of carbon dioxide in the form of one sugar. This makes fucoidan a promising candidate to focus on for climate change mitigation.

6 Conclusion and outlook

This study gives first numbers on global fucoidan secretion rates. It confirmed the pathway of fucoidan secretion *in situ* and in mesocosm experiments, aggregating into particles and transportation of fucoidan in coastal vegetated ecosystems. Future studies may focus on quantification of fucoidan in particles and in deep sea sediments, establishing rates of fucoidan sequestration. Monitoring of fucoidan secretion and fucoidan sequestration could allow carbon budgeting of fucoidan by macroalgae in the future. Joint approaches for all coastal vegetated ecosystems could allow national and international budgeting of carbon sequestration, using fucoidan as an identifier molecule for algal-derived carbon.

7 Contributions to further manuscripts

7.1 CDR options for Germany with storage or sequestration in the marine environment - The 10Mt CO_2 per year removal challenge

Authors: W. Yao., T. M. Morganti, J. Wu, M Borchers, R. Wollnik, A. Anschütz, M. Fink, F. Liu, F. Gasanzade, F. Havermann, A. Bhaumik, M. Ramasamy, J. M. Lencina-Avila, M. Jürchott, **I. Hellige**, F. Stahl, J. Kemper, I. Kremin, I. Diercks, S. Mathesius, N. Mehendale, I. Lange, T. Nagwekar, M. Philippi, L. Westmark, C. Spenger, L. Tank, H. Wey, H. T. T. Kalapurakkal, W. Bach, M. Liadova, M. Böttcher, L. Fricke, M. Fouqueray, M. Boersma, M. Wölfelschneider, M. Fernández-Méndez, S. Hoog, A. Kopf, N. Moosdorf, K. Bischof, L. Rupke, D. P. Keller, J. Geuer, G. J. Rehder, A. Oschlies, N. Szarka, M. Vorrath, and N. Mengis

under review
preprint: DOI: 10.22541/essoar.171650351.11778445/v1; [Yao et al., 2024]

Keywords: carbon dioxide removal (CDR), net-zero, ocean-based climate mitigation, natural C sink enhancement, artificial upwelling, seaweed farming, BECC(S), ocean alkalinity enhancement

Abstract: The implementation of carbon dioxide removal (CDR) options is necessary to counterbalance residual emissions to achieve net zero carbon dioxide or greenhouse gas emissions. The theoretical scalability of CDR options, however, depends on the technological maturity as well as context specific conditions including biophysical site characteristics, or availability of infrastructure and resources. Since the marine environment has a high theoretical CDR potential with less competition for resources like space, we here explore CDR options with storage or sequestration in the marine environment (mCDR).

We use the German context as a case study, and challenge mCDR options to remove a significant amount of 10 Mt CO_2 per year, if possible within the German boundaries. In total, we describe 11 mCDR options, three options employing geological off-shore storage, four options that aim at enhancing blue carbon sink capacity, and six options that aim to enhance the chemical carbon uptake of the ocean through alkalinity enhancement. For each option we assess if it would theoretically be able to reach the 10 Mt CO_2 yr^{-1} scale and describe the possible location, the necessary infrastructure, resource demands and biophysical conditions. Where possible expected cost estimates, environmental impacts and monitoring approaches are provided. Furthermore, we discuss main uncertainty factors and remaining research needs for the options.

Our results indicate that mCDR potential in Germany is not neglectable, but that not all options are available to Germany

within their own boundaries. The described 10 Mt CO_2 mCDR options should not be confused with actual implementation plans. Further studies are required to assess the socio-economic, legal, political and ethical aspects for such implementations.

7.2 Coral high molecular weight carbohydrates support opportunistic microbes in bacterioplankton from an algae-dominated reef

Authors: B. M. Thobor, A. F. Haas, C. Wild, C. E. Nelson, L. Wegley Kelly, J.-H. Hehemann, M. G. I. Arts, M. Boer, H. Buck-Wiese, N. P. Nguyen, **I. Hellige** and B. Mueller.

published by mSystems; [Thobor et al., 2024]

Abstract: High molecular weight (HMW, $>$ 1kDa) carbohydrates are a major component of dissolved organic matter (DOM) released by benthic primary producers. Despite shifts from coral- to algae-dominance on many reefs, little is known about the effects of exuded carbohydrates on bacterioplankton communities in reef waters. We compared the monosaccharide composition of HMW carbohydrates exuded by hard corals and brown macroalgae and investigated the response of the bacterioplankton community of an algae-dominated Caribbean reef to the respective HMW fractions. HMW coral exudates were compositionally distinct from the ambient, algae-dominated reef

waters and similar to coral mucus (high in arabinose). They further selected for opportunistic bacterioplankton taxa commonly associated with coral stress (i.e., Rhodobacteraceae, Phycisphaeraceae, Vibrionaceae, Flavobacteriales) and significantly increased the predicted energy-, amino acid-, and carbohydrate-metabolism by 28%, 44%, and 111%, respectively. In contrast, HMW carbohydrates exuded by algae were similar to those in algae tissue extracts and reef water (high in fucose) and did not significantly alter the composition and predicted metabolism of the bacterioplankton community. These results confirm earlier findings of coral exudates supporting efficient trophic transfer, while algae exudates may have stimulated microbial respiration instead of biomass production, thereby supporting the microbialization of reefs. In contrast to previous studies, HMW coral and not algal exudates selected for opportunistic microbes, suggesting that a shift in the prevalent DOM composition and not the exudate type (i.e., coral vs algae) per se, may induce the rise of opportunistic microbial taxa.

7.3 Selective preservation of fucose-rich oligosaccharides in the North Atlantic Ocean

Authors: M. Bligh and H. Buck-Wiese, A. Sichert, S. Bercovic, **I. Hellige**, H. Marchant, M. Iversen, U. Sauer, T. Dittmar, C. Arnosti, M. Liebeke, J.-H. Hehemann

submitted
preprint: DOI: 10.1101/2024.09.20.613644; [Bligh et al., 2024]

Abstract: The ocean has a substantial capacity to store carbon dioxide fixed via photosynthesis in dissolved organic molecules. An estimated 20% of the 660 Gt dissolved organic carbon in the ocean pool consists of structurally uncharacterized oligosaccharides, which appear to resist microbial degradation [Aluwihare et al., 1997]. Current technologies lack the sensitivity and molecular resolution to identify these oligosaccharides. Here, we adapted graphitized carbon chromatography to extract and separate marine oligosaccharides for liquid chromatography high resolution mass spectrometry analysis. Using a newly-developed *de novo* annotation tool, we found 110 oligosaccharide structures in surface and deep ocean seawater at two distant locations in the North Atlantic Ocean. One group of the detected oligosaccharides was found only in surface seawater and consisted of larger and more abundant molecules detected by our analysis. A second group of smaller, less abundant oligosaccharides was detected in both the surface and deep ocean seawater of both sampled locations. The composition of oligosaccharides differed between the surface and deep ocean, with deep ocean samples relatively enriched in hard-to metabolize deoxy-sugars, and xylose, amino sugars and uronic acids compared to simple hexoses. Notably the deoxy-sugar fucose constituted 35-40% of the monomers in deep-sea oligosaccharides, twice the per-

centage in surface ocean oligosaccharides. The ubiquity of deep ocean oligosaccharides indicates that they represent a preserved fraction of the carbohydrate pool. Their enrichment in specific monosaccharides suggests selective preservation of fucose-rich oligosaccharides in the deep ocean.

7.4 Silica based purification and desalting of fucoidan

Authors: M. Schultz-Johansen, J. Parnami, **I. Hellige**, J.-H. Hehemann

in preparation

Abstract: Algal fucoidans are promising molecules for carbon sequestration evaluation and have therapeutic potential due to their bioactive properties. The extraction, purification, characterization and quantification of fucoidan is important, both in biomedical as well as in environmental research. Common fucoidan purification methods require subsequent dialysis steps to remove salts prior to downstream analyses and applications. Here, we present a combined purification and desalting procedure for fucoidan, which is based on a solid-phase extraction principle using a silica containing column like those found in common DNA purification kits. Using a mini spin column from a commercial DNA kit we obtain milligram scale purification of

fucoidan with >95% recovery, while removing molar scale salts in a single step. Finally, we demonstrate that the method allows the extraction of fucoidan from seawater collected in North Sea kelp forests near the German island of Helgoland. The described method is a convenient tool for the purification and desalting of fucoidan from both preparative and environmental samples. In addition, the method also seems applicable to purify other anionic polysaccharides such as ulvan, pectin and carrageenans.

References

Mohammed I. Abdullah and Stein Fredriksen. Production, respiration and exudation of dissolved organic matter by the kelp laminaria hyperborea along the west coast of norway. *Journal of the Marine Biological Association of the United Kingdom*, 84(5):887–894, 2004. doi:10.1017/S002531540401015Xh.

Anne-Carlijn Alderkamp, Marion van Rijssel, and Henk Bolhuis. Characterization of marine bacteria and the activity of their enzyme systems involved in degradation of the algal storage glucan laminarin. *FEMS microbiology ecology*, 59(1):108–117, 2007. doi:10.1111/j.1574-6941.2006.00219.x.

Alice L. Alldredge, Uta Passow, and Bruce E. Logan. The abundance and significance of a class of large, transparent organic particles in the ocean. *Deep Sea Research*, (40): 1131–11440, 1993. doi:10.1016/0967-0637(93)90129-Q.

Hanan Almahasheer, Oscar Serrano, Carlos M. Duarte, Ariane Arias-Ortiz, Pere Masque, and Xabier Irigoien. Low carbon sink capacity of red sea mangroves. *Scientific reports*, 7(1): 9700, 2017. doi:10.1038/s41598-017-10424-9.

Lihini I. Aluwihare, Daniel J. Repeta, and Robert F. Chen. A major biopolymeric component to dissolved organic carbon in surface sea water. *Nature*, (387):166–169, 1997. doi:10.138/387166a0.

Lihini I. Aluwihare, Daniel J. Repeta, and Robert F. Chen. Chemical composition and cyclingof dissolved organic matter in the mid-atlantic bight. *Deep Sea Research*, (49):4421–4437, 2002. doi:10.1016/S0967-0645(02)00124-8.

Ariane Arias-Ortiz, Pere Masqué, Jordi Garcia-Orellana, Oscar Serrano, Inés Mazarrasa, Núria Marbà, Catherine E. Lovelock, Paul S. Lavery, and Carlos M. Duarte. Reviews and syntheses: 210pb-derived sediment and carbon accumulation rates in vegetated coastal ecosystems – setting the record straight. *Biogeosciences*, 15(22):6791–6818, 2018. doi:10.5194/bg-15-6791-2018.

Carol Arnosti. Substrate specificity in polysaccharide hydrolysis: Contrasts between bottom water and sediments. *Limnology and Oceanography*, 45(5):1112–1119, 2000. doi:10.4319/lo.2000.45.5.1112.

Carol Arnosti. Fluorescent derivatization of polysaccharides and carbohydrate-containing biopolymers for measurement of enzyme activities in complex media. *Journal of chromatography*, 793(1):181–191, 2003. doi:10.1016/s1570-0232(03)00375-1.

Carol Arnosti, Bernhard M. Fuchs, Rudolf Amann, and Uta Passow. Contrasting extracellular enzyme activities of particle-associated bacteria from distinct provinces of the north at-

lantic ocean. *Frontiers in microbiology*, 3:425, 2012. ISSN 1664-302X. doi:10.3389/fmicb.2012.00425.

Carol Arnosti, Matthias Wietz, Thorsten Brinkhoff, Jan-Hendrik Hehemann, David Probandt, Laura Zeugner, and Rudolf Amann. The biogeochemistry of marine polysaccharides: Sources, inventories, and bacterial drivers of the carbohydrate cycle. *Annual Review of Marine Science*, 13:81–108, 2021. doi:10.1146/annurev-marine-032020-012810.

Jorge Assis, Eliza Fragkopoulou, Duarte Frade, João Neiva, André Oliveira, David Abecasis, Sylvain Faugeron, and Ester A. Serrão. A fine-tuned global distribution dataset of marine forests. *Scientific data*, 7(1):119, 2020. doi:10.1038/s41597-020-0459-x.

Burak Avcı, Karen Krüger, Bernhard M. Fuchs, Hanno Teeling, and Rudolf I. Amann. Polysaccharide niche partitioning of distinct polaribacter clades during north sea spring algal blooms. *The ISME journal*, 14(6):1369–1383, 2020. doi:10.1038/s41396-020-0601-y.

Lennart T. Bach, Veronica Tamsitt, Jim Gower, Catriona L. Hurd, John A. Raven, and Philip W. Boyd. Testing the climate intervention potential of ocean afforestation using the great atlantic sargassum belt. *Nature communications*, 12(1):2556, 2021. doi:10.1038/s41467-021-22837-2.

Ulrike Baetz and Enrico Martinoia. Root exudates: the hidden part of plant defense. *Trends in plant science*, 19(2):90–98, 2014. doi:10.1016/j.tplants.2013.11.006.

Cristina Barron, Eugenia T. Apostolaki, and Carlos M. Duarte. Dissolved organic carbon fluxes by seagrass meadows and macroalgal beds. *Frontiers in Marine Science*, 1, 2014. doi:10.3389/fmars.2014.00042.

Marcus Bäumgen, Theresa Dutschei, and Uwe T. Bornscheuer. Marine polysaccharides: Occurrence, enzymatic degradation and utilization. *Chembiochem : a European journal of chemical biology*, 22(13):2247–2256, 2021. doi:10.1002/cbic.202100078.

Stefan Becker, André Scheffel, Martin F. Polz, and Jan-Hendrik Hehemann. Accurate quantification of laminarin in marine organic matter with enzymes from marine microbes. *Applied and environmental microbiology*, 83(9), 2017. doi:10.1128/AEM.03389-16.

Stefan Becker, Jan Tebben, Sarah Coffinet, Karen Wiltshire, Morten Hvitfeldt Iversen, Tilmann Harder, Kai-Uwe Hinrichs, and Jan-Hendrik Hehemann. Laminarin is a major molecule in the marine carbon cycle. *Proceedings of the National Academy of Sciences of the United States of America*, 117 (12):6599–6607, 2020. doi:10.1073/pnas.1917001117.

M. M. Bengtsson, K. Sjøtun, J. E. Storesund, and J. Øvreås. Utilization of kelp-derived carbon sources by kelp surface-associated bacteria. *Aquatic Microbial Ecology*, 62(2):191–199, 2011. doi:10.3354/ame01477.

Mia M. Bengtsson and Lise Ovreas. Planctomycetes dominate biofilms on surfaces of the kelp laminaria hyperborea. *BMC Microbiology*, (10):261, 2010. doi:10.1186/1471-2180-10-261.

Ronald Benner, J. Dean Pakulski, Matthew McCarthy, John I. Hedges, and Patrick G. Hatcher. Bulk chemical characteristics of dissolved organic matter in the ocean. *Science*, (255): 1561–1564, 1992. doi:10.1126/science.255.5051.1561.

J. Bezanson, A. Edelman, S. Karpinski, and V. B. Shah. Julia: A fresh approach to numerical computing. *SIAM Review*, (59):65–69, 2017.

Roger S. Bivand. Progress in the r ecosystem for representing and handling spatial data. *Journal of Geographical Systems*, 23(4):515–546, 2021. doi:10.1007/s10109-020-00336-0.

Margot Bligh, Nguyen Nguyen, Hagen Buck-Wiese, Silvia Vidal-Melgosa, and Jan-Hendrik Hehemann. Structures and functions of algal glycans shape their capacity to sequester carbon in the ocean. *Current opinion in chemical biology*, 71:102204, 2022. doi:10.1016/j.cbpa.2022.102204.

Margot Bligh, Hagen Buck-Wiese, Andreas Sichert, Sarah K. Bercovici, Inga Hellige, Hannah Marchant, Morten Iversen, Uwe Sauer, Thorsten Dittmar, Carol Arnosti, Manuel Liebeke, and Jan-Hendrik Hehemann. Selective preservation of fucose-rich oligosaccharides in the north atlantic ocean. *BioRxiv*, 2024. doi:10.1101/2024.09.20.613644.

John J. Bolton. The biogeography of kelps (laminariales, phaeophyceae): a global analysis with new insights from recent advances in molecular phylogenetics. *Helgoland Marine Research*, 64(4):263–279, 2010. doi:10.1007/s10152-010-0211-6.

M. Bressac, E. C. Laurenceau-Cornec, F. Kennedy, A. E. Santoro, N. L. Paul, N. Briggs, F. Carvalho, and P. W. Boyd. Decoding drivers of carbon flux attenuation in the oceanic biological pump. *Nature*, 2024. doi:10.1038/s41586-024-07850-x.

Trevor T. Bringloe, Samuel Starko, Rachael M. Wade, Christophe Vieira, Hiroshi Kawai, Olivier de Clerck, J. Mark Cock, Susana M. Coelho, Christophe Destombe, Myriam Valero, João Neiva, Gareth A. Pearson, Sylvain Faugeron, Ester A. Serrão, and Heroen Verbruggen. Phylogeny and evolution of the brown algae. *Critical Reviews in Plant Sciences*, 39(4):281–321, 2020. ISSN 0735-2689. doi:10.1080/07352689.2020.1787679.

Hagen Buck-Wiese, Mona A. Andskog, Nguyen P. Nguyen, Margot Bligh, Eero Asmala, Silvia Vidal-Melgosa, Manuel Liebeke, Camilla Gustafsson, and Jan-Hendrik Hehemann. Fucoid brown algae inject fucoidan carbon into the ocean. *Proceedings of the National Academy of Sciences of the United States of America*, 120(1):e2210561119, 2023. doi:10.1073/pnas.2210561119.

Kathrin Busch, Sonja Endres, Morten H. Iversen, Jan Michels, Eva-Maria Nöthig, and Anja Engel. Bacterial colonization and vertical distribution of marine gel particles (tep and csp) in the arctic fram strait. *Frontiers in Marine Science*, 4, 2017. doi:10.3389/fmars.2017.00166.

Craig A. Carlson and Dennis A. Hansell, editors. *Chapter 3 - DOM Sources, Sinks, Reactivity, and Budgets*. Biogeochemistry of Marine Dissolved Organic Matter. Academic Press, second edition, 2015. ISBN 9780124059405. doi:10.1016/B978-0-12-405940-5.00003-0.

E. L. Cavan, M. Trimmer, F. Shelley, and R. Sanders. Remineralization of particulate organic carbon in an ocean oxygen minimum zone. *Nature communications*, 8:14847, 2017. doi:10.1038/ncomms14847.

Emma L. Cavan, So Kawaguchi, and Philip W. Boyd. Implications for the mesopelagic microbial gardening hypothesis as determined by experimental fragmentation of antarctic krill

fecal pellets. *Ecology and evolution*, 11(2):1023–1036, 2021. ISSN 2045-7758. doi:10.1002/ece3.7119.

Siwang Chen, Kai Xu, Dehua Ji, Wenlei Wang, Yan Xu, Changsheng Chen, and Chaotian Xie. Release of dissolved and particulate organic matter by marine macroalgae and its biogeochemical implications. *Algal Research*, 52:102096, 2020. ISSN 22119264. doi:10.1016/j.algal.2020.102096.

Zhiyan Chen, Tianyi Nie, Xin Zhao, Jiwei Li, Bin Yang, Dongyang Cui, and Xinxin Li. Organic carbon remineralization rate in global marine sediments: A review. *Regional Studies in Marine Science*, 49:102112, 2022. ISSN 23524855. doi:10.1016/j.rsma.2021.102112.

Lionel Chevolot, Barbara Mulloy, Jacqueline Ratiskol, and Alain Foucault. A disaccharide repeat unit is the major structure in fucoidans from two species of brown algae. *Carbohydrate Research*, (330):529–535, 2001. doi:10.1016/S0008-6215(00)00314-1.

Soojeong Cho, Thi Le Thuy, Sangwon Ko, Yeonwoo Jeong, Sung Min Kang, Joon Sig Choi, and Woo Kyung Cho. Coordination-driven antifouling spray coating using a sulfated polysaccharide fucoidan. *Progress in Organic Coatings*, 169:106916, 2022. ISSN 03009440. doi:10.1016/j.porgcoat.2022.106916.

R. R. Coifman, S. Lafon, A. B. Lee, M. Maggioni, B. Nadler, F. Warner, and S. W. Zucker. Geometric diffusions as a tool for harmonic analysis and structure definition of data: Diffusion maps. *Proceedings of the National Academy of Sciences of the United States of America*, (102):7426–7431, 2005.

Valérie Cornuault, Iain W. Manfield, Marie-Christine Ralet, and J. Paul Knox. Epitope detection chromatography: a method to dissect the structural heterogeneity and interconnections of plant cell-wall matrix glycans. *The Plant journal: for cell and molecular biology*, 78(4):715–722, 2014. doi:10.1111/tpj.12504.

Estelle Deniaud-Bouët, Nelly Kervarec, Gurvan Michel, Thierry Tonon, Bernard Kloareg, and Cécile Hervé. Chemical and enzymatic fractionation of cell walls from fucales: insights into the structure of the extracellular matrix of brown algae. *Annals of botany*, 114(6):1203–1216, 2014. doi:10.1093/aob/mcu096.

Estelle Deniaud-Bouët, Kevin Hardouin, Philippe Potin, Bernard Kloareg, and Cécile Hervé. A review about brown algal cell walls and fucose-containing sulfated polysaccharides: Cell wall context, biomedical properties and key research challenges. *Carbohydrate polymers*, 175:395–408, 2017. doi:10.1016/j.carbpol.2017.07.082.

Carlos M. Duarte, Jiaping Wu, Xi Xiao, Annette Bruhn, and Dorte Krause-Jensen. Can seaweed farming play a role in climate change mitigation and adaptation? *Frontiers in Marine Science*, 4, 2017. doi:10.3389/fmars.2017.00100.

Carlos M. Duarte, Annette Bruhn, and Dorte Krause-Jensen. A seaweed aquaculture imperative to meet global sustainability targets. *Nature Sustainability*, 5(3):185–193, 2022a. doi:10.1038/s41893-021-00773-9.

Carlos M. Duarte, Jean-Pierre Gattuso, Kasper Hancke, Hege Gundersen, Karen Filbee-Dexter, Morten F. Pedersen, Jack J. Middelburg, Michael T. Burrows, Kira A. Krumhansl, Thomas Wernberg, Pippa Moore, Albert Pessarrodona, Sarah B. Ørberg, Isabel S. Pinto, Jorge Assis, Ana M. Queirós, Dan A. Smale, Trine Bekkby, Ester A. Serrão, and Dorte Krause-Jensen. Global estimates of the extent and production of macroalgal forests. *Global Ecology and Biogeography*, 31(7):1422–1439, 2022b. doi:10.1111/geb.13515.

M. Dubois, K. A. Gilles, J. K. Hamilton, P. A. Rebers, and F. Smith. A colorimetric method for the determination of sugars. *Analytical Chemistry*, (28):350–356, 1951. doi:10.1038/168167a0.

Hugh W. Ducklow, Deborah K. Steinberg, and Ken O. Buesseler. Upper ocean carbon export and the bi-

ological pump. *Oceanography*, (14):51–58, 2001. doi:10.5670/oceanog.2001.06.

Anja Engel. Distribution of transparent exopolymer particles (tep) in the northeast atlantic ocean and their potential significance for aggregation processes. *Deep Sea Research*, (51):83–82, 2004. doi:10.1016/j.dsr.2003.09.001.

Anja Engel and Nicole Händel. A novel protocol for determining the concentration and composition of sugars in particulate and in high molecular weight dissolved organic matter (hmw-dom) in seawater. *Marine Chemistry*, 127(1-4):180–191, 2011. doi:10.1016/j.marchem.2011.09.004.

Anja Engel, Silke Thoms, Ulf Riebesell, Emma Rochelle-Newall, and Ingrid Zondervan. Polysaccharide aggregation as a potential sink of marine dissolved organic carbon. *Nature*, 428 (6986):927–929, 2004. doi:10.1038/nature02506.

Ashkaan K. Fahimipour and Thilo Gross. Mapping the bacterial metabolic niche space. *Nature communications*, 11(1):4887, 2020. doi:10.1038/s41467-020-18695-z.

Sam Fankhauser, Stephen M. Smith, Myles Allen, Kaya Axelsson, Thomas Hale, Cameron Hepburn, J. Michael Kendall, Radhika Khosla, Javier Lezaun, Eli Mitchell-Larson, Michael Obersteiner, Lavanya Rajamani, Rosalind Rickaby, Nathalie Seddon, and Thom Wetzer. The meaning of net zero and

how to get it right. *Nature Climate Change*, 12(1):15–21, 2022. doi:10.1038/s41558-021-01245-w.

Elizabeth Ficko-Blean, Aurélie Préchoux, François Thomas, Tatiana Rochat, Robert Larocque, Yongtao Zhu, Mark Stam, Sabine Génicot, Murielle Jam, Alexandra Calteau, Benjamin Viart, David Ropartz, David Pérez-Pascual, Gaëlle Correc, Maria Matard-Mann, Keith A. Stubbs, Hélène Rogniaux, Alexandra Jeudy, Tristan Barbeyron, Claudine Médigue, Mirjam Czjzek, David Vallenet, Mark J. McBride, Eric Duchaud, and Gurvan Michel. Carrageenan catabolism is encoded by a complex regulon in marine heterotrophic bacteria. *Nature communications*, 8(1):1685, 2017. doi:10.1038/s41467-017-01832-6.

Karen Filbee-Dexter and Thomas Wernberg. Rise of turfs: A new battlefront for globally declining kelp forests. *BioScience*, 68(2):64–76, 2018. ISSN 0006-3568. doi:10.1093/biosci/bix147.

Karen Filbee-Dexter and Thomas Wernberg. Substantial blue carbon in overlooked australian kelp forests. *Scientific reports*, 10(1):12341, 2020. doi:10.1038/s41598-020-69258-7.

Karen Filbee-Dexter, Thomas Wernberg, Sean Grace, Jonas Thormar, Stein Fredriksen, Carla A. Narvaez, Colette Feehan, and Kjell Magnus Norderhaug. Marine heatwaves and the collapse of marginal north atlantic kelp forests. *Scientific*

reports, 10(1):13388, 2020. doi:10.1038/s41598-020-70273-x.

Karen Filbee-Dexter, Albert Pessarrodona, Morten F. Pedersen, Thomas Wernberg, Carlos M. Duarte, Jorge Assis, Trine Bekkby, Michael T. Burrows, Daniel F. Carlson, Jean-Pierre Gattuso, Hege Gundersen, Kasper Hancke, Kira A. Krumhansl, Tomohiro Kuwae, Jack J. Middelburg, Pippa J. Moore, Ana M. Queirós, Dan A. Smale, Isabel Sousa-Pinto, Nobuhiro Suzuki, and Dorte Krause-Jensen. Carbon export from seaweed forests to deep ocean sinks. *Nature Geoscience*, 17(6):552–559, 2024. doi:10.1038/s41561-024-01449-7.

H. R. Fletcher, P. Biller, A. B. Ross, and J.M.M. Adams. The seasonal variation of fucoidan within three species of brown macroalgae. *Algal Research*, 22:79–86, 2017. ISSN 22119264. doi:10.1016/j.algal.2016.10.015.

Antonio Flores-Moya and José A. Fernández. The role of external carbonic anhydrase in the photosynthetic use of inorganic carbon in the deep-water alga phyllariopsis purpurascens (laminariales, phaeophyta). *Planta*, (207):115–119, 1998. doi:10.1007/s004250050462.

John Fox, Sanford Weisberg, Brad Price, Daniel Adler, Douglas Bates, Gabriel Baud-Bovy, Ben Bolker, Steve Ellison, David Firth, Michael Friendly, Gregor Gorjanc, Spencer Graves, Richard Heiberger, Pacel Krivitsky, Rafael Laboissiere, Mar-

tin Maechler, Georges Monette, Duncan Murdoch, Henric Nilsson, Derek Ogle, Brian Ripley, Tom Short, William Venables, Steve Walker, David Winsemius, and Achim Zeileis. car: Companion to applied regression, 2019. URL `https://www.john-fox.ca/Companion/`.

Stein Fredriksen, Karen Filbee-Dexter, Kjell Magnus Norderhaug, Henning Steen, Torjan Bodvin, Melinda A. Coleman, Frithjof Moy, and Thomas Wernberg. Green gravel: a novel restoration tool to combat kelp forest decline. *Scientific reports*, 10(1):3983, 2020. doi:10.1038/s41598-020-60553-x.

Pierre Friedlingstein, Michael O'Sullivan, Matthew W. Jones, Robbie M. Andrew, Dorothee C. E. Bakker, Judith Hauck, Peter Landschützer, Corinne Le Quéré, Ingrid T. Luijkx, Glen P. Peters, Wouter Peters, Julia Pongratz, Clemens Schwingshackl, Stephen Sitch, Josep G. Canadell, Philippe Ciais, Robert B. Jackson, Simone R. Alin, Peter Anthoni, Leticia Barbero, Nicholas R. Bates, Meike Becker, Nicolas Bellouin, Bertrand Decharme, Laurent Bopp, Ida Bagus Mandhara Brasika, Patricia Cadule, Matthew A. Chamberlain, Naveen Chandra, Thi-Tuyet-Trang Chau, Frédéric Chevallier, Louise P. Chini, Margot Cronin, Xinyu Dou, Kazutaka Enyo, Wiley Evans, Stefanie Falk, Richard A. Feely, Liang Feng, Daniel J. Ford, Thomas Gasser, Josefine Ghattas, Thanos Gkritzalis, Giacomo Grassi, Luke Gregor, Nicolas Gruber, Özgür Gürses, Ian Harris, Matthew

Hefner, Jens Heinke, Richard A. Houghton, George C. Hurtt, Yosuke Iida, Tatiana Ilyina, Andrew R. Jacobson, Atul Jain, Tereza Jarníková, Annika Jersild, Fei Jiang, Zhe Jin, Fortunat Joos, Etsushi Kato, Ralph F. Keeling, Daniel Kennedy, Kees Klein Goldewijk, Jürgen Knauer, Jan Ivar Korsbakken, Arne Körtzinger, Xin Lan, Nathalie Lefèvre, Hongmei Li, Junjie Liu, Zhiqiang Liu, Lei Ma, Greg Marland, Nicolas Mayot, Patrick C. McGuire, Galen A. McKinley, Gesa Meyer, Eric J. Morgan, David R. Munro, Shin-Ichiro Nakaoka, Yosuke Niwa, Kevin M. O'Brien, Are Olsen, Abdirahman M. Omar, Tsuneo Ono, Melf Paulsen, Denis Pierrot, Katie Pocock, Benjamin Poulter, Carter M. Powis, Gregor Rehder, Laure Resplandy, Eddy Robertson, Christian Rödenbeck, Thais M. Rosan, Jörg Schwinger, Roland Séférian, T. Luke Smallman, Stephen M. Smith, Reinel Sospedra-Alfonso, Qing Sun, Adrienne J. Sutton, Colm Sweeney, Shintaro Takao, Pieter P. Tans, Hanqin Tian, Bronte Tilbrook, Hiroyuki Tsujino, Francesco Tubiello, Guido R. van der Werf, Erik van Ooijen, Rik Wanninkhof, Michio Watanabe, Cathy Wimart-Rousseau, Dongxu Yang, Xiaojuan Yang, Wenping Yuan, Xu Yue, Sönke Zaehle, Jiye Zeng, and Bo Zheng. Global carbon budget 2023. *Earth System Science Data*, 15(12): 5301–5369, 2023. doi:10.5194/essd-15-5301-2023.

Halley E. Froehlich, Jamie C. Afflerbach, Melanie Frazier, and Benjamin S. Halpern. Blue growth potential to mitigate cli-

mate change through seaweed offsetting. *Current biology*, 29(18):3087–3093.e3, 2019. doi:10.1016/j.cub.2019.07.041.

Sabine Fuss, Josep G. Canadell, Glen P. Peters, Massimo Tavoni, Robbie M. Andrew, Philippe Ciais, Robert B. Jackson, Chris D. Jones, Florian Kraxner, Nebosja Nakicenovic, Corinne Le Quéré, Michael R. Raupach, Ayyoob Sharifi, Pete Smith, and Yoshiki Yamagata. Betting on negative emissions. *Nature Climate Change*, (4):850–853. doi:10.1038/nclimate2392.

Jonah Gabry, Ben Goodrich, Martin Lysy, and Andrew Johnson. rstantools: Tools for developing r packages interfacing with 'stan', 2024. URL `https://mc-stan.org/rstantools/,https://discourse.mc-stan.org/`.

Jean-Pierre Gattuso, Alexandre K. Magnan, Laurent Bopp, William W. L. Cheung, Carlos M. Duarte, Jochen Hinkel, Elizabeth Mcleod, Fiorenza Micheli, Andreas Oschlies, Phillip Williamson, Raphaël Billé, Vasiliki I. Chalastani, Ruth D. Gates, Jean-Olivier Irisson, Jack J. Middelburg, Hans-Otto Pörtner, and Greg H. Rau. Ocean solutions to address climate change and its effects on marine ecosystems. *Frontiers in Marine Science*, 5, 2018. doi:10.3389/fmars.2018.00337.

Sarah L. C. Giering, Richard Sanders, Richard S. Lampitt, Thomas R. Anderson, Christian Tamburini, Mehdi Boutrif, Mikhail V. Zubkov, Chris M. Marsay, Stephanie A. Henson,

Kevin Saw, Kathryn Cook, and Daniel J. Mayor. Reconciliation of the carbon budget in the ocean's twilight zone. *Nature*, 507(7493):480–483, 2014. doi:10.1038/nature13123.

Greta Giljan, Sarah Brown, C. Chad Lloyd, Sherif Ghobrial, Rudolf Amann, and Carol Arnosti. Selfish bacteria are active throughout the water column of the ocean. *ISME communications*, 3(1):11, 2023. doi:10.1038/s43705-023-00219-7.

Espen Granum, Stale Kirkvold, and Sverre M. Myklestad. Cellular and extracellular porduction of carbohydrates and amino acids by the marine diatom skeletonema costatum: diel variations and effects of n depletion. *Marine Ecology Progess Series*, (242):83–94, 2002. doi:10.3354/meps242083.

Turgut M. Gür. Carbon dioxide emissions, capture, storage and utilization: Review of materials, processes and technologies. *Progress in Energy and Combustion Science*, 89:100965, 2022. ISSN 03601285. doi:10.1016/j.pecs.2021.100965.

Valerie Hagger, Nathan J. Waltham, and Catherine E. Lovelock. Opportunities for coastal wetland restoration for blue carbon with co-benefits for biodiversity, coastal fisheries, and water quality. *Ecosystem Services*, 55:101423, 2022. ISSN 22120416. doi:10.1016/j.ecoser.2022.101423.

Jack R. Hall, Gerli Albert, Isla M. Twigg, Federico Baltar, Christopher D. Hepburn, and Georg Martin. The

production of dissolved organic carbon by macroalgae and its consumption by marine bacteria: Implications for coastal ecosystems. *Frontiers in Marine Science*, 9, 2022. doi:10.3389/fmars.2022.934229.

Dennis A. Hansell. Recalcitrant dissolved organic carbon fractions. *Annual Review of Marine Science*, 5:421–445, 2013. doi:10.1146/annurev-marine-120710-100757.

Dennis A. Hansell and Craig A. Carlson. Deep-ocean gradients in the concentration of dissolved organic carbon. *Nature*, (395):263–266, 1998. doi:10.1038/26200.

B. G. Hatcher, A. R. O. Chapman, and K. H. Mann. An annual carbon budget for the kelp laminaria longicruris. *Marine Biology*, (44):85–96, 1977. doi:10.1007/BF00386909.

John I. Hedges. Why dissolved organics matter. 2002.

Jan-Hendrik Hehemann, Alisdair B. Boraston, and Mirjam Czjzek. A sweet new wave: structures and mechanisms of enzymes that digest polysaccharides from marine algae. *Current opinion in structural biology*, 28:77–86, 2014. doi:10.1016/j.sbi.2014.07.009.

Inga Hellige. Algal-derived carbon transported into coastal vegetated ecosystems. created in biorender., 2024. URL `https://BioRender.com/x10y435`.

Inga Hellige, Aman Akeerath Mundanatt, Jana C. Massing, and Jan-Hendrik Hehemann. *Roots of coastal plants stabilize carbon fixed by marine algae*. 2024. doi:10.1101/2024.12.02.624615.

Andrew G. Hettle, Chelsea J. Vickers, and Alisdair B. Boraston. Sulfatases: Critical enzymes for algal polysaccharide processing. *Frontiers in plant science*, 13:837636, 2022. ISSN 1664-462X. doi:10.3389/fpls.2022.837636.

Johanna Hofmann, Heung S. Hahm, Peter H. Seeberger, and Kevin Pagel. Identification of carbohydrate anomers using ion mobility-mass spectrometry. *Nature*, 526(7572):241–244, 2015. doi:10.1038/nature15388.

Andrea Désirée Holtkamp, Svenja Kelly, Roland Ulber, and Siegmund Lang. Fucoidans and fucoidanases–focus on techniques for molecular structure elucidation and modification of marine polysaccharides. *Applied microbiology and biotechnology*, 82(1):1–11, 2009. doi:10.1007/s00253-008-1790-x.

Chuanmin Hu, Mengqiu Wang, Brian E. Lapointe, Rachel A. Brewton, and Frank J. Hernandez. On the atlantic pelagic sargassum's role in carbon fixation and sequestration. *Science of The Total Environment*, 781:146801, 2021. ISSN 00489697. doi:10.1016/j.scitotenv.2021.146801.

Guoyin Huang, Silvia Vidal-Melgosa, Andreas Sichert, Stefan Becker, Yang Fang, Jutta Niggemann, Morten Hvitfeldt

Iversen, Yi Cao, and Jan-Hendrik Hehemann. Secretion of sulfated fucans by diatoms may contribute to marine aggregate formation. *Limnology and Oceanography*, 66(10): 3768–3782, 2021. doi:10.1002/lno.11917.

Chin-Chang Hung, Laodong Guo, Peter H. Santschi, Nicolas Alvarado-Quiroz, and Jennifer M. Haye. Distributions of carbohydrate species in the gulf of mexico. *Marine Chemistry*, 81(3-4):119–135, 2003. doi:10.1016/S0304-4203(03)00012-4.

Morten H. Iversen. Carbon export in teh ocean: A biologist's perspective. *Annual Reviews*, (15):357–381, 2023. doi:10.1146/annurev-marine-032122-035153.

Yeonwoo Jeong, Thi Le Thuy, So Hyun Ki, Sangwon Ko, Suyeob Kim, Woo Kyung Cho, Joon Sig Choi, and Sung Min Kang. Multipurpose antifouling coating of solid surfaces with the marine-derived polymer fucoidan. *Macromolecular bioscience*, 18(10):e1800137, 2018. doi:10.1002/mabi.201800137.

N. Jiao, C. Robinson, F. Azam, H. Thomas, F. Baltar, H. Dang, N. J. Hardman-Mountford, M. Johnson, D. L. Kirchman, B. P. Koch, L. Legendre, C. Li, J. Liu, T. Luo, Y.-W. Luo, A. Mitra, A. Romanou, K. Tang, X. Wang, C. Zhang, and R. Zhang. Mechanisms of microbial carbon sequestration in

the ocean – future research directions. *Biogeosciences*, 11 (19):5285–5306, 2014. doi:10.5194/bg-11-5285-2014.

N. Jiao, J. Liu, F. Jiao, Q. Chen, and X. Wang. Microbes mediated comprehensive carbon sequestration for negative emissions in the ocean. *Earth Sciences*, (7):1858–1860, 2020. doi:10.1093/nsr/nwaa171.

Charles D. Keeling, Robert B. Bacastow, Arnold E. Bainbridge, Carl A. Ekdahl, Peter R. Guenther, Lee S. Waterman, and John F. S. Chin. Atmospheric carbon dioxide variations at mauna loa observatory, hawaii. *Tellus*, 28(6):538–551, 1976. ISSN 00402826. doi:10.1111/j.2153-3490.1976.tb00701.x.

Hilary Kennedy, Jeff Beggins, Carlos M. Duarte, James W. Fourqurean, Marianne Holmer, Núria Marbà, and Jack J. Middelburg. Seagrass sediments as a global carbon sink: Isotopic constraints. *Global Biogeochemical Cycles*, 24(4), 2010. ISSN 0886-6236. doi:10.1029/2010GB003848.

D. L. Kirchman. Measuring bacterial biomass production and growth rates from leucine incorporation in natural aquatic environments. *Methods Microbiology*, (30):227–237, 2001. doi:10.1016/S0580-9517(01)30047-8.

Bernard Kloareg, Yacine Badis, J. Mark Cock, and Gurvan Michel. Role and evolution of the extracellular matrix in the acquisition of complex multicellularity in eu-

karyotes: A macroalgal perspective. *Genes*, 12(7), 2021. doi:10.3390/genes12071059.

Hanna Koch, Alexandra Dürwald, Thomas Schweder, Beatriz Noriega-Ortega, Silvia Vidal-Melgosa, Jan-Hendrik Hehemann, Thorsten Dittmar, Heike M. Freese, Dörte Becher, Meinhard Simon, and Matthias Wietz. Biphasic cellular adaptations and ecological implications of alteromonas macleodii degrading a mixture of algal polysaccharides. *The ISME journal*, 13(1):92–103, 2019. doi:10.1038/s41396-018-0252-4.

Georg Kopplin, Anne Mari Rokstad, Hugo Mélida, Vincent Bulone, Gudmund Skjåk-Bræk, and Finn Lillelund Aachmann. Structural characterization of fucoidan from laminaria hyperborea: Assessment of coagulation and inflammatory properties and their structure-function relationship. *ACS applied bio materials*, 1(6):1880–1892, 2018. doi:10.1021/acsabm.8b00436.

Dorte Krause-Jensen and Carlos M. Duarte. Substantial role of macroalgae in marine carbon sequestration. *Nature Geoscience*, 9(10):737–742, 2016. doi:10.1038/ngeo2790.

Dorte Krause-Jensen, Paul Lavery, Oscar Serrano, Núria Marbà, Pere Masque, and Carlos M. Duarte. Sequestration of macroalgal carbon: the elephant in the blue carbon room. *Biology letters*, 14(6), 2018. doi:10.1098/rsbl.2018.0236.

Karen Krüger, Meghan Chafee, T. Ben Francis, Tijana Del Glavina Rio, Dörte Becher, Thomas Schweder, Rudolf I. Amann, and Hanno Teeling. In marine bacteroidetes the bulk of glycan degradation during algae blooms is mediated by few clades using a restricted set of genes. *The ISME journal*, 13 (11):2800–2816, 2019. doi:10.1038/s41396-019-0476-y.

Dan Laffoley. Protecting and effectively managing blue carbon ecosystems to realise the full value to society- a sea of opportunities. an opinion piece by dan laffoley for wwf-uk. *WWF-UK*, 2020. URL `https://coilink.org/20.500.12592/45bd1b`.

Roger A. Laine. A calculation of all possible oligosaccharide isomers both branched and linear yields 1.05 x 1012 structures for a reducing hexasaccharide: the isomer barrier to development of single-method saccharide sequencing or synthesis systems. *Glyco-Forum section*, 1994. doi:10.1093/glycob/4.6.759.

Louis Legendre, Richard B. Rivkin, Markus G. Weinbauer, Lionel Guidi, and Julia Uitz. The microbial carbon pump concept: Potential biogeochemical significance in the globally changing ocean. *Progress in Oceanography*, 134:432–450, 2015. ISSN 00796611. doi:10.1016/j.pocean.2015.01.008.

C. Chad Lloyd, Sarah Brown, John Paul Balmonte, Adrienne Hoarfrost, Sherif Ghobrial, and Carol Arnosti. Particles

act as 'specialty centers' with expanded enzymatic function throughout the water column in the western north atlantic. *Frontiers in microbiology*, 13:882333, 2022. ISSN 1664-302X. doi:10.3389/fmicb.2022.882333.

C. Chad Lloyd, Sarah Brown, John Paul Balmonte, Adrienne Hoarfrost, Sherif Ghobrial, and Carol Arnosti. Links between regional and depth patterns of microbial communities and enzyme activities in the western north atlantic ocean. *Marine Chemistry*, 255:104299, 2023. doi:10.1016/j.marchem.2023.104299.

M. I. Lucas, R. C. Newell, and Velimirov B. Heterotrophic utilisation of mucilage released during fragmentation of kelp (ecklonia maxima and laminaria pallida). ii. differential utilisation of dissolved organic components from kelp mucilage. *Marine Ecology*, (4):43–55, 1981. doi:10.3354/meps004043.

Dieter Lüthi, Martine Le Floch, Bernhard Bereiter, Thomas Blunier, Jean-Marc Barnola, Urs Siegenthaler, Dominique Raynaud, Jean Jouzel, Hubertus Fischer, Kenji Kawamura, and Thomas F. Stocker. High-resolution carbon dioxide concentration record 650,000-800,000 years before present. *Nature*, 453(7193):379–382, 2008. doi:10.1038/nature06949.

Sibusiso Luthuli, Siya Wu, Yang Cheng, Xiaoli Zheng, Mingjiang Wu, and Haibin Tong. Therapeutic effects of fu-

coidan: A review on recent studies. *Marine drugs*, 17(9), 2019. doi:10.3390/md17090487.

Peter I. Macreadie, Andrea Anton, John A. Raven, Nicola Beaumont, Rod M. Connolly, Daniel A. Friess, Jeffrey J. Kelleway, Hilary Kennedy, Tomohiro Kuwae, Paul S. Lavery, Catherine E. Lovelock, Dan A. Smale, Eugenia T. Apostolaki, Trisha B. Atwood, Jeff Baldock, Thomas S. Bianchi, Gail L. Chmura, Bradley D. Eyre, James W. Fourqurean, Jason M. Hall-Spencer, Mark Huxham, Iris E. Hendriks, Dorte Krause-Jensen, Dan Laffoley, Tiziana Luisetti, Núria Marbà, Pere Masque, Karen J. McGlathery, J. Patrick Megonigal, Daniel Murdiyarso, Bayden D. Russell, Rui Santos, Oscar Serrano, Brian R. Silliman, Kenta Watanabe, and Carlos M. Duarte. The future of blue carbon science. *Nature communications*, 10(1):3998, 2019. doi:10.1038/s41467-019-11693-w.

Peter I. Macreadie, Micheli D. P. Costa, Trisha B. Atwood, Daniel A. Friess, Jeffrey J. Kelleway, Hilary Kennedy, Catherine E. Lovelock, Oscar Serrano, and Carlos M. Duarte. Blue carbon as a natural climate solution. *Nature Reviews Earth & Environment*, 2(12):826–839, 2021. doi:10.1038/s43017-021-00224-1.

Edén Magaña-Gallegos, Eva Villegas-Muñoz, Evelyn Raquel Salas-Acosta, M. Guadalupe Barba-Santos, Rodolfo Silva, and Brigitta I. van Tussenbroek. The effect of temperature

on the growth of holopelagic sargassum species. *Phycology*, 3(1):138–146, 2023. doi:10.3390/phycology3010009.

Federica Manca, Lisandro Benedetti-Cecchi, Corey J. A. Bradshaw, Mar Cabeza, Camilla Gustafsson, Alf M. Norkko, Tomas V. Roslin, David N. Thomas, Lydia White, and Giovanni Strona. Projected loss of brown macroalgae and seagrasses with global environmental change. *Nature communications*, 15(1):5344, 2024. doi:10.1038/s41467-024-48273-6.

John H. Martin, George A. Knauer, David M. Karl, and William W. Broenkow. Vertex: carbon cycling in the northeast pacific. *Deep Sea Research*, (34):267–285, 1987. doi:10.1016/0198-0149(87)90086-0.

Valérie Masson-Delmotte, Hans-Otto Pörtner, Jim Skea, Panmao Zhai, Debra Roberts, Priydarshi R. Shukla, Anna Pirani, Roz Pidcock, Yang Chen, Elisabeht Lonnoy, Wilfran Moufouma-Okia, Sarah Connors, Xiao Zhou, Tom Maycock, Melina Tignor, Clotilde Péan, J. B. Robin Matthews, Melissa I. Gomis, and Tim Waterfield. Global warming of 1.5°c - ipcc. 2018.

H. Damon Matthews, Nathan P. Gillett, Peter A. Stott, and Kirsten Zickfeld. The proportionality of global warming to cumulative carbon emissions. *Nature*, 459(7248):829–832, 2009. doi:10.1038/nature08047.

Matthew McCarthy, John Hedges, and Ronald Benner. Major biochemical composition of dissolved high molecular weight organic matter in seawater. *Marine Chemistry*, (55: 281-297), 1996. doi:10.1016/S0304-4203(96)00041-2.

Elizabeth Mcleod, Gail L. Chmura, Steven Bouillon, Rodney Salm, Mats Björk, Carlos M. Duarte, Catherine E. Lovelock, William H. Schlesinger, and Brian R. Silliman. A blueprint for blue carbon: toward an improved understanding of the role of vegetated coastal habitats in sequestering co 2. *Frontiers in Ecology and the Environment*, 9(10):552–560, 2011. doi:10.1890/110004.

Nadine Mengis, Allanah Paul, and Mar Fernández-Méndez. Counting (on) blue carbon - challenges and ways forward for carbon accounting of ecosystem-based carbon removal in marine environments. *PLOS Climate*, 2(8):e0000148, 2023. doi:10.1371/journal.pclm.0000148.

Gurvan Michel, Thierry Tonon, Delphine Scornet, J. Mark Cock, and Bernard Kloareg. The cell wall polysaccharide metabolism of the brown alga ectocarpus siliculosus. insights into the evolution of extracellular matrix polysaccharides in eukaryotes. *The New phytologist*, 188(1):82–97, 2010. doi:10.1111/j.1469-8137.2010.03374.x.

Kenneth Mopper, Jian Zhou, Konduru Sri Ramana, Uta Passow, Hans G. Dam, and David T. Drapeau. The role of

surface-active carbohydrates in the flocculation of diatom bloom in a mesocosm. *Deep Sea Research*, (42):47–73, 1995. doi:10.1016/0967-0645(95)00004-A.

Sverre M. Myklestad. Release of extracellular products by phytoplankton with special emphasis on polysaccharides. *The Science of the Total Environment*, (165):155–164, 1995. doi:10.1016/0048-9697(95)04549-G.

Masato Nagaoka, Hideyuki Shibata, Itsuko Kimura-Takagi, Shusuke Hashimoto, and Kazumasa Kimura. Structural study of fucoidan from cladosiphon okamuranus tokida. *Glycoconjugate Journal*, (16):19–26, 1999. doi:10.1023/a:1006945618657.

Didier Ndeh, Artur Rogowski, Alan Cartmell, Ana S. Luis, Arnaud Baslé, Joseph Gray, Immacolata Venditto, Jonathon Briggs, Xiaoyang Zhang, Aurore Labourel, Nicolas Terrapon, Fanny Buffetto, Sergey Nepogodiev, Yao Xiao, Robert A. Field, Yanping Zhu, Malcolm A. O'Neil, Breeana R. Urbanowicz, William S. York, Gideon J. Davies, D. Wade Abbott, Marie-Christine Ralet, Eric C. Martens, Bernard Henrissat, and Harry J. Gilbert. Complex pectin metabolism by gut bacteria reveals novel catalytic functions. *Nature*, 544 (7648):65–70, 2017. doi:10.1038/nature21725.

R. C. Newell, M. I. Lucas, Velimirov B., and L. J. Seiderer. Quantitative significance of dissolved organic losses

following fragmentation of kelp (ecklonia maxima and laminaria pallida). *Marine Ecology*, (2):45–49, 1980. doi:10.3354/meps002045.

Jari Oksanen, F. Guillaume Blanchet, Roeland Kindt, Pierre Legendre, Peter R. Minchin, R. B. O'Hara, Gavin L. Simpson, Peter Sólymos, M. Henry H. Stevens, and Helene Wagner. Vegan: community ecology package. r package version 2.5.3. https://cran.r-project.org/package=vegan. 2018. doi:10.32614/CRAN.package.vegan.

Luis H. Orellana, T. Ben Francis, Marcela Ferraro, Jan-Hendrik Hehemann, Bernhard M. Fuchs, and Rudolf I. Amann. Verrucomicrobiota are specialist consumers of sulfated methyl pentoses during diatom blooms. *The ISME journal*, 16(3): 630–641, 2022. doi:10.1038/s41396-021-01105-7.

Alejandra Ortega, Nathan R. Geraldi, Intikhab Alam, Allan A. Kamau, Silvia G. Acinas, Ramiro Logares, Josep M. Gasol, Ramon Massana, Dorte Krause-Jensen, and Carlos M. Duarte. Important contribution of macroalgae to oceanic carbon sequestration. *Nature Geoscience*, 12(9):748–754, 2019. doi:10.1038/s41561-019-0421-8.

Erin Ostrem Loss, Jaron Thompson, Pak Lun Kevin Cheung, Yili Qian, and Ophelia S. Venturelli. Carbohydrate complexity limits microbial growth and reduces the sensitivity of human gut communities to perturbations. *Nature Ecology*

and Evolution, 7(1):127–142, 2023. doi:10.1038/s41559-022-01930-9.

Ellie R. Paine, Matthias Schmid, Philip W. Boyd, Guillermo Diaz-Pulido, and Catriona L. Hurd. Rate and fate of dissolved organic carbon release by seaweeds: A missing link in the coastal ocean carbon cycle. *Journal of phycology*, 57(5): 1375–1391, 2021. doi:10.1111/jpy.13198.

J. Dean Pakulski and Ronald Benner. An improved method for the hydrolysis and mbth analysis of dissolved and particulate carbohydrates in seawater. *Marine Chemistry*, (40):143–160, 1992. doi:10.1016/0304-4203(92)90020-B.

J. Dean Pakulski and Ronald Benner. Abundance and distribution of carbohydrates in the ocean. *Limnology & Oceanography*, 39(4):930–940, 1994. doi:10.4319/lo.1994.39.4.0930.

Eric Pante and Benoit Simon-Bouhet. marmap: A package for importing, plotting and analyzing bathymetric and topographic data in r. *PloS one*, 8(9):e73051, 2013. doi:10.1371/journal.pone.0073051.

D. Pauly and V. Christensen. Primary production required to sustain global fisheries. *Nature*, 1995. doi:10.1038/376279b0.

Elizabeth Percival. The polysaccharides of green, red and brown seaweeds: Their basic structure, biosynthesis and function.

British Phycological Journal, 14(2):103–117, 1979. ISSN 0007-1617. doi:10.1080/00071617900650121.

Albert Pessarrodona, Rita M. Franco-Santos, Luka Seamus Wright, Mathew A. Vanderklift, Jennifer Howard, Emily Pidgeon, Thomas Wernberg, and Karen Filbee-Dexter. Carbon sequestration and climate change mitigation using macroalgae: a state of knowledge review. *Biological reviews of the Cambridge Philosophical Society*, 98(6):1945–1971, 2023. doi:10.1111/brv.12990.

Sammy Pontrelli, Rachelo Szabo, Shaul Pollak, Julia Schwartzman, Daniela Ledezma-Tejeida, Otto X. Cordero, and Uwe Sauer. Metabolic cross-feeding structures the assembly of polysaccharide degrading communities. *Science Advances*, (8), 2022. doi:10.1126/sciadv.abk3076.

Leanne C. Powers, Norbert Hertkorn, Natasha McDonald, Philippe Schmitt-Kopplin, Rossana Del Vecchio, Neil V. Blough, and Michael Gonsior. Sargassum sp. act as a large regional source of marine dissolved organic carbon and polyphenols. *Global Biogeochemical Cycles*, 33(11):1423–1439, 2019. ISSN 0886-6236. doi:10.1029/2019GB006225.

I. C. Prentice, G. D. Farquhar, M.J.R. Fasham, M. L. Goulden, M. Heimann, V. J. Jaramillo, H. S. Kheshgi, C. Le Quéré, R. J. Scholes, and D.W.R. Wallace, editors. *The carbon cycle and atmospheric carbon dioxide*. Climate Change 2001: The

Scientific Basis. Cambridge University Press, 2001. ISBN 0521807670.

Yanjun Qiu, Hong Jiang, Yueyang Dong, Yongzhen Wang, Hamed I. Hamouda, Mohamed A. Balah, and Xiangzhao Mao. Expression and biochemical characterization of a novel fucoidanase from flavobacteriumalgicola with the principal product of fucoidan-derived disaccharide. *Foods*, 11(7), 2022. doi:10.3390/foods11071025.

R Core Team. R: A language and environment for statistical computing., 2020.

John Raven. Blue carbon: past, present and future, with emphasis on macroalgae. *Biology letters*, 14(10), 2018. doi:10.1098/rsbl.2018.0336.

Daniel C. Reed, Craig A. Carlson, Elisa R. Halewood, J. Clinton Nelson, Shannon L. Harrer, Andrew Rassweiler, and Robert J. Miller. Patterns and controls of reef–scale production of dissolved organic carbon by giant kelp macrocystis pyrifera. *Limnology & Oceanography*, 60(6):1996–2008, 2015. doi:10.1002/lno.10154.

R. H. Reed and P. J. Wright. Release of mannitol from pilayella littoralis (phaeophyta. ectocarpales) in response to hypoosmotic stress. *Marine Ecology Progress Series*, 29:205–208, 1986. doi:10.3354/meps029205.

Greta Reintjes, Anneke Heins, Cheng Wang, and Rudolf Amann. Abundance and composition of particles and their attached microbiomes along an atlantic meridional transect. *Frontiers in Marine Science*, 10, 2023. doi:10.3389/fmars.2023.1051510.

Lukas Reisky, Aurélie Préchoux, Marie-Katherin Zühlke, Marcus Bäumgen, Craig S. Robb, Nadine Gerlach, Thomas Roret, Christian Stanetty, Robert Larocque, Gurvan Michel, Tao Song, Stephanie Markert, Frank Unfried, Marko D. Mihovilovic, Anke Trautwein-Schult, Dörte Becher, Thomas Schweder, Uwe T. Bornscheuer, and Jan-Hendrik Hehemann. A marine bacterial enzymatic cascade degrades the algal polysaccharide ulvan. *Nature chemical biology*, 15(8):803–812, 2019. doi:10.1038/s41589-019-0311-9.

Diego S. Reyes-Weiss, Margot Bligh, Nanna Rhein-Knudsen, Jan-Hendrik Hehemann, Manuel Liebeke, Bjørge Westereng, and Svein Jarle Horn. Application of maldi-ms for characterization of fucoidan hydrolysates and screening of endo-fucoidanase activity. *Carbohydrate polymers*, 340:122317, 2024. doi:10.1016/j.carbpol.2024.122317.

Aurora M. Ricart, Dorte Krause-Jensen, Kasper Hancke, Nichole N. Price, Pere Masqué, and Carlos M. Duarte. Sinking seaweed in the deep ocean for carbon neutrality is ahead of

science and beyond the ethics. *Environmental Research Letters*, 17(8):081003, 2022. doi:10.1088/1748-9326/ac82ff.

Joeri Rogelj, Alexander Popp, Katherine V. Calvin, Gunnar Luderer, Johannes Emmerling, David Gernaati, Shinichiro Fujimori, Jessic Strefler, Tomoko Hasegawa, Giacomo Marangoni, Volker Krey, Elmar Kriegler, Keywan Riahi, Detlef P. van Vuuren, Jonathan Doelman, Laurent Drouet, Jae Edmonds, Oliver Fricko, Mathijs Harmsen, Petr Havlík, Florian Humpenöder, Elke Stehfest, and Massimo Tavoni. Scenarios towards limiting global-mean temperature increase below 1.5°c. *Nature Climate Change*, (8):325–332, 2018. doi:10.1038/s41558-018-0091-3.

Artur Rogowski, Jonathon A. Briggs, Jennifer C. Mortimer, Theodora Tryfona, Nicolas Terrapon, Elisabeth C. Lowe, Arnaud Baslé, Carl Morland, Alison M. Day, Hongjun Zheng, Theresa E. Rogers, Paul Thompson, Alastair R. Hawkins, Madhav P. Yadav, Bernard Henrissat, Eric C. Martens, Paul Dupree, Harry J. Gilbert, and David N. Bolam. Glycan complexity dictates microbial resource allocation in the large intestine. *Nature communications*, 6:7481, 2015. doi:10.1038/ncomms8481.

Armando A. Salmeán, William George Tycho Willats, Sofia Ribeiro, Thorbjørn Joest Andersen, and Marianne Ellegaard. Over 100-year preservation and temporal fluctuations of

cell wall polysaccharides in marine sediments. *Frontiers in plant science*, 13(13):785902, 2022. ISSN 1664-462X. doi:10.3389/fpls.2022.785902.

W. Schramm, E. Gualberto, and C. Orosco. Release of dissolved organic matter from marine tropical reef plants: temperature and desiccation effects. *Botanica Marina*, (27):71–77, 1983. doi:10.1515/botm.1984.27.2.71.

Julia A. Schwartzman, Ali Ebrahimi, Grayson Chadwick, Yuya Sato, Benjamin R. K. Roller, Victoria J. Orphan, and Otto X. Cordero. Bacterial growth in multicellular aggregates leads to the emergence of complex life cycles. *Current biology*, 32 (14):3059–3069.e7, 2022. doi:10.1016/j.cub.2022.06.011.

Andreas Sichert and Otto X. Cordero. Polysaccharide-bacteria interactions from the lens of evolutionary ecology. *Frontiers in microbiology*, 12:705082, 2021. ISSN 1664-302X. doi:10.3389/fmicb.2021.705082.

Andreas Sichert, Christopher H. Corzett, Matthew S. Schechter, Frank Unfried, Stephanie Markert, Dörte Becher, Antonio Fernandez-Guerra, Manuel Liebeke, Thomas Schweder, Martin F. Polz, and Jan-Hendrik Hehemann. Verrucomicrobia use hundreds of enzymes to digest the algal polysaccharide fucoidan. *Nature microbiology*, 5(8):1026–1039, 2020. doi:10.1038/s41564-020-0720-2.

Chandni Sidhu, Inga V. Kirstein, Cédric L. Meunier, Johannes Rick, Vera Fofonova, Karen H. Wiltshire, Nicola Steinke, Silvia Vidal-Melgosa, Jan-Hendrik Hehemann, Bruno Huettel, Thomas Schweder, Bernhard M. Fuchs, Rudolf I. Amann, and Hanno Teeling. Dissolved storage glycans shaped the community composition of abundant bacterioplankton clades during a north sea spring phytoplankton bloom. *Microbiome*, 11(1):77, 2023. doi:10.1186/s40168-023-01517-x.

John McN. Sieburth. Studies on algal substances in the sea. *Biological ecology*, (3):290–309, 1969. doi:10.1016/0022-0981(69)90052-5.

David A. Siegel, Tim DeVries, Scott C. Doney, and Tom Bell. Assessing the sequestration time scales of some ocean-based carbon dioxide reduction strategies. *Environmental Research Letters*, 16(10):104003, 2021. doi:10.1088/1748-9326/ac0be0.

Artem S. Silchenko, Mikhail I. Kusaykin, Valeriya V. Kurilenko, Alexander M. Zakharenko, Vladimir V. Isakov, Tatyana S. Zaporozhets, Anna K. Gazha, and Tatyana N. Zvyagintseva. Hydrolysis of fucoidan by fucoidanase isolated from the marine bacterium, formosa algae. *Marine drugs*, 11(7):2413–2430, 2013. doi:10.3390/md11072413.

Victor Smetacek, Mar Fernández-Méndez, Franziska Pausch, and Jiajun Wu. Rectifying misinformation on the climate in-

tervention potential of ocean afforestation. *Nature communications*, 15(1):3012, 2024. doi:10.1038/s41467-024-47134-6.

SV. Smith. Marine macrophytes as a global carbon sink. *Science*, (211):838–840, 1981. doi:10.1126/ science.211.4484.838.

E. Maggie Sogin, Dolma Michellod, Harald R. Gruber-Vodicka, Patric Bourceau, Benedikt Geier, Dimitri V. Meier, Michael Seidel, Soeren Ahmerkamp, Sina Schorn, Grace D'Angelo, Gabriele Procaccini, Nicole Dubilier, and Manuel Liebeke. Sugars dominate the seagrass rhizosphere. *Nature ecology & evolution*, 6(7):866–877, 2022. doi:10.1038/s41559-022-01740-z.

Weizhi Song, Bernd Wemheuer, Peter D. Steinberg, Ezequiel M. Marzinelli, and Torsten Thomas. Contribution of horizontal gene transfer to the functionality of microbial biofilm on a macroalgae. *The ISME journal*, 15(3):807–817, 2021. doi:10.1038/s41396-020-00815-8.

Nicola Steinke, Silvia Vidal-Melgosa, Mikkel Schultz-Johansen, and Jan-Hendrik Hehemann. Biocatalytic quantification of alpha-glucan in marine particulate organic matter. *MicrobiologyOpen*, 11(3):e1289, 2022. doi:10.1002/mbo3.1289.

Andrew K. Swanson and Louis D. Druehl. Induction, exudation and the uv protective role of kelp phlorotannins.

Aquatic Botany, (73):241–253, 2002. doi:10.1016/S0304-3770(02)00035-9.

Taro Takahashi, Richard A. Feely, Ray F. Weiss, Rik H. Wanninkhof, David W. Chipman, Stewart C. Sutherland, and Timothy T. Takahashi. Global air sea flux of co2. *Proceedings of the National Academy of Sciences of the United States of America*, (94 (16)):8292–8299, 1997. doi:10.1073/pnas.94.16.8292.

Ralph J. M. Temmink, Leon P. M. Lamers, Christine Angelini, Tjeerd J. Bouma, Christian Fritz, Johan van de Koppel, Robin Lexmond, Max Rietkerk, Brian R. Silliman, Hans Joosten, and Tjisse van der Heide. Recovering wetland biogeomorphic feedbacks to restore the world's biotic carbon hotspots. *Science*, 376(6593):eabn1479, 2022. doi:10.1126/science.abn1479.

Bianca M. Thobor, Andreas F. Haas, Christian Wild, Craig E. Nelson, Linda Wegley Kelly, Jan-Hendrik Hehemann, Milou G. I. Arts, Meine Boer, Hagen Buck-Wiese, Nguyen P. Nguyen, Inga Hellige, and Benjamin Mueller. Coral high molecular weight carbohydrates support opportunistic microbes in bacterioplankton from an algae-dominated reef. *mSystems*, page e0083224, 2024. doi:10.1128/msystems.00832-24.

François Thomas, Philippe Bordron, Damien Eveillard, and

Gurvan Michel. Gene expression analysis of zobellia galactanivorans during the degradation of algal polysaccharides reveals both substrate-specific and shared transcriptome-wide responses. *Frontiers in microbiology*, 8:1808, 2017. ISSN 1664-302X. doi:10.3389/fmicb.2017.01808.

Thomas A. Torode, Susan E. Marcus, Murielle Jam, Thierry Tonon, Richard S. Blackburn, Cécile Hervé, and J. Paul Knox. Monoclonal antibodies directed to fucoidan preparations from brown algae. *PloS one*, 10(2):e0118366, 2015. doi:10.1371/journal.pone.0118366.

Thomas A. Torode, Amandine Siméon, Susan E. Marcus, Murielle Jam, Marie-Anne Le Moigne, Delphine Duffieux, J. Paul Knox, and Cécile Hervé. Dynamics of cell wall assembly during early embryogenesis in the brown alga fucus. *Journal of experimental botany*, 67(21):6089–6100, 2016. doi:10.1093/jxb/erw369.

Vo Thi Dieu Trang, Maria Dalgaard Mikkelsen, Marlene Vuillemin, Sebastian Meier, Hang Thi Thuy Cao, Jan Muschiol, Valentina Perna, Thuan Thi Nguyen, Vy Ha Nguyen Tran, Jesper Holck, Tran Thi Thanh Van, Huynh Hoang Nhu Khanh, and Anne S. Meyer. The endo-alpha(1,4) specific fucoidanase fhf2 from formosa haliotis releases highly sulfated fucoidan oligosaccharides. *Fron-*

tiers in plant science, 13:823668, 2022. ISSN 1664-462X. doi:10.3389/fpls.2022.823668.

M. Tsubo and S. Walker. Relationships between photosynthetically active radiation and clearness index at bloemfontein, south africa. *Theoretical and Applied Climatology*, 80(1): 17–25, 2005. doi:10.1007/s00704-004-0080-5.

Jefferson T. Turner. Zooplankton fecal pellets, marine snow, phytodetritus and the ocean's biological pump. *Progress in Oceanography*, 130:205–248, 2015. ISSN 00796611. doi:10.1016/j.pocean.2014.08.005.

Pedro Verdugo. Marine microgels. *Annual Review of Marine Science*, 4:375–400, 2012. doi:10.1146/annurev-marine-120709-142759.

Silvia Vidal-Melgosa, Andreas Sichert, T. Ben Francis, Daniel Bartosik, Jutta Niggemann, Antje Wichels, William G. T. Willats, Bernhard M. Fuchs, Hanno Teeling, Dörte Becher, Thomas Schweder, Rudolf Amann, and Jan-Hendrik Hehemann. Diatom fucan polysaccharide precipitates carbon during algal blooms. *Nature communications*, 12(1):1150, 2021. doi:10.1038/s41467-021-21009-6.

Silvia Vidal-Melgosa, Matija Lagator, Andreas Sichert, Taylor Priest, Jürgen Pätzold, and Jan-Hendrik Hehemann. Not digested: algal glycans move carbon dioxide into the deep-sea. *bioRxiv preprint*, 2022. doi:10.1101/2022.03.04.483023.

S. Wada, M. N. Aoki, A. Mikami, T. Komatsu, Y. Tsuchiya, T. Sato, H. Shinagawa, and T. Hama. Bioavailability of macroalgal dissolved organic matter in seawater. *Marine Ecology Progress Series*, 370:33–44, 2008. doi:10.3354/meps07645.

Shigeki Wada and Takeo Hama. The contribution of macroalgae to the coastal dissolved organic matter pool. *Estuarine, Coastal and Shelf Science*, 129:77–85, 2013. ISSN 02727714. doi:10.1016/j.ecss.2013.06.007.

Shigeki Wada, Masakazu N. Aoki, Yasutaka Tsuchiya, Toshihiko Sato, Hideo Shinagawa, and Takeo Hama. Quantitative and qualitative analyses of dissolved organic matter released from ecklonia cava kjellman, in oura bay, shimoda, izu peninsula, japan. *Journal of Experimental Marine Biology and Ecology*, 349(2):344–358, 2007. ISSN 00220981. doi:10.1016/j.jembe.2007.05.024.

Benjamin X. Wang, Chloe M. Wu, and Katharina Ribbeck. Home, sweet home: how mucus accommodates our microbiota. *The FEBS journal*, 288(6):1789–1799, 2021. doi:10.1111/febs.15504.

Mengqiu Wang, Chuanmin Hu, Jennifer Cannizzaro, David English, Xingxing Han, David Naar, Brian Lapointe, Rachel Brewton, and Frank Hernandez. Remote sensing of sargassum biomass, nutrients, and pigments. *Geophysi-*

cal Research Letters, 45(22), 2018. ISSN 0094-8276. doi:10.1029/2018GL078858.

Mengqiu Wang, Chuanmin Hu, Brian B. Barnes, Gary Mitchum, Brian Lapointe, and Joseph P. Montoya. The great atlantic sargassum belt. *Science*, 365(6448):83–87, 2019. doi:10.1126/science.aaw7912.

Cornwall Warren. Sinking seaweed: An ambitious strategy aims to cool the planet by dumping farmed seaweed on the sea floor. will it work? *Science Features*, 2024. doi:10.1126/science.zpxdfqh.

Kenta Watanabe, Goro Yoshida, Masakazu Hori, Yu Umezawa, Hirotada Moki, and Tomohiro Kuwae. Macroalgal metabolism and lateral carbon flows can create significant carbon sinks. *Biogeosciences*, 17(9):2425–2440, 2020. doi:10.5194/bg-17-2425-2020.

Carl Wunsch. What is the thermohaline circulation? Science's Compass, 2002. doi:10.1126/science.1079329.

Wanxuan Yao, Teresa Morganti, Jiajun Wu, Malgorzata Borchers, Anna-Adriana Anschütz, Lena-Katharina Bednarz, Amrita Bhaumik, Miranda Boettcher, Kremena Burkhard, Tony Cabus, Allison Sueyi Chua, Isabel Diercks, Esposito Mario, Michael Fink, Mondane Fouqueray, Firdovsi Gasanzade, Sonja Geilert, Judith Hauck, Felix Havermann, Inga

Hellige, Sven Hoog, Malte Jürchott, Habeeb Thanveer Kalapurakkal, Jost Kemper, Isabel Kremin, Isabel Lange, Jannine Marquez Lencina-Avila, Margarita Liadova, Feifei Liu, Sabine Mathesius, Neha Mehendale, Tanvi Nagwekar, Miriam Philippi, Gustavo Leite Neves Da Luz, Murugan Ramasamy, Florian Stahl, Lukas Tank, Maria-Elena Vorrath, Lennart Westmark, Hao-Wei Wey, Ronja Wollnik, Mirco Wölfelschneider, Wolfgang Bach, Kai Bischof, maarten boersma, Ute Daewel, Mar Fernández-Méndez, Jana Geuer, David Peter Keller, Achim J. Kopf, Christine Merk, Nils Moosdorf, Natascha Maria Oppelt, Andreas Oschlies, Julia Pongratz, Alexander Proelss, Gregor Rehder, Lars Helmuth Rüpke, Nora Szarka, Daniela Thrän, Klaus Wallmann, and Nadine Mengis. Exploring site-specific carbon dioxide removal options with storage or sequestration in the marine environment - the 10 mt co2 yr-1 removal challenge for germany. *preprint ESS open archive*, 2024. doi:10.22541/essoar.171650351.11778445/v1.

Acknowledgements

This thesis would not have been possible without many people contributing to this work. First of all, I would like to thank Jan-Hendrik Hehemann for giving me the opportunity to work in the Carbon Sequestration and Glycobiochemistry Group and for his continuous support and supervision. Further, I would like to thank all members of my examination committee! A huge thank you goes to Katia Föll for her never ending support with the HPAEC-PAD, as well as Tina Horstmann and Bruno Stahl for their general support in the lab and for microarray analysis of hundreds of samples. Thanks to Astrid Stierle for administrative support. I would like to thank the whole working group, as well as students Mohammad Shahin, Carla Knappik, Hussein Awwad and Daria Gulenko for all your help. I would further like to thank my project partners in Sea4soCiety, especially Dariya Baiko and Jana Geuer, working during daily sampling and late-night lab shifts. To all the partners around the world who made the algae incubations possible, from setting up the experiments to sample transport and post-work efforts, a huge thank you! Further, I would like to thank my thesis committee members, Naomi Levine, Francois Thomas and Luis Humberto Orellana for their supervision and support. A special thank you to Margot Bligh and Hagen Buck-Wiese, without the two of you this would have not been possible. Finally, I would like to thank my family and Janis for their patience and support!

Appendix

Anlage 1 zur Promotionsordnung

Versicherung an Eides Statt

Ich,

versichere an Eides Statt durch meine Unterschrift, dass ich die vorstehende Arbeit selbstständig und ohne fremde Hilfe angefertigt und alle Stellen, die ich wörtlich dem Sinne nach aus Veröffentlichungen entnommen habe, als solche kenntlich gemacht habe, mich auch keiner anderen als der angegebenen Literatur oder sonstiger Hilfsmittel bedient habe.
Ich versichere an Eides Statt, dass ich die vorgenannten Angaben nach bestem Wissen und Gewissen gemacht habe und dass die Angaben der Wahrheit entsprechen und ich nichts verschwiegen habe.
Die Strafbarkeit einer falschen eidesstattlichen Versicherung ist mir bekannt, namentlich die Strafandrohung gemäß § 156 StGB bis zu drei Jahren Freiheitsstrafe oder Geldstrafe bei vorsätzlicher Begehung der Tat bzw. gemäß § 161 Abs. 1 STGB bis zu einem Jahr Freiheitsstrafe oder Geldstrafe bei fahrlässiger Begehung.

Ort, Datum, Unterschrift

Anlage 2 zur Promotionsordnung

Erklärung zur elektronischen Version und zur Überprüfung einer Dissertation

Hiermit betätige ich gemäß §7, Abs.7, Punkt 4, dass die zu Prüfungszwecken beigelegte elektronische Version meiner Dissertation identisch ist mit der abgegebenen gedruckten Version. Ich bin mit der Überprüfung meiner Dissertation gemäß §6 Abs.2, Punkt 5 mit qualifizierter Software im Rahmen der Untersuchung von Plagiatsvorwürfen einverstanden.

Ort, Datum, Unterschrift